Tréhu, A.M., Bohrmann, G., Rack, F.R., Torres, M.E., et al., 2003
Proceedings of the Ocean Drilling Program, Initial Reports Volume 204

2. EXPLANATORY NOTES[1]

Shipboard Scientific Party[2]

INTRODUCTION

Information assembled in this chapter will help the reader understand the basis for our preliminary conclusions and also enable the interested investigator to select samples for further analysis. This information concerns only shipboard operations and analyses described in the site reports in the *Initial Reports* volume of the Leg 204 *Proceedings of the Ocean Drilling Program*. Methods used by various investigators for shore-based analyses of Leg 204 data will be described in the individual contributions published in the *Scientific Results* volume and in publications in various professional journals.

Authorship of Site Chapters

The separate sections of the site chapters were written by the following shipboard scientists (authors are listed in alphabetical order; no seniority is implied):

Leg Summary and Principal Results: Shipboard Party
Background and Objectives: Bohrmann, Tréhu
Operations: Rack, Schultheiss, Storms, Torres
Lithostratigraphy: Gracia, Johnson, Teichert, Weinberger, Xu
Biostratigraphy: Watanabe, Xu
Microbiology: Delwiche, Holland
Interstitial Water Geochemistry: Borowski, Tomaru, Torres
Organic Geochemistry: Claypool, Lee, Milkov
Physical Properties: Liu, Long, Riedel, Schultheiss
Downhole Tools and Pressure Coring: Milkov, Schroeder, Schultheiss, Tréhu
Downhole Logging: Barr, Collett, Guèrin
Underway Geophysics: Tréhu

[1]Examples of how to reference the whole or part of this volume.
[2]Shipboard Scientific Party addresses.

Ms 204IR-102

Site Planning Based on Three-Dimensional Seismic Data

The three-dimensional (3-D) seismic reflection data, collected before the cruise, imaged a 4 km × 11 km volume recorded to 3 s two-way traveltime (Tréhu and Bangs, 2001). The survey used a differential GPS navigation system provided by RACAL Geodetic. Four base stations (Vancouver, British Columbia, Canada; Washington state; northern California; and San Diego, California) provided differential corrections at 1 Hz. Fixes were smoothed with a 15-s running average filter to eliminate ship's motion and determine shot locations in real time. The single 600-m streamer was navigated with compass readings at 150-m intervals along the streamer. Streamer configuration was constructed from compass data for each shot. Tests of navigation accuracy conducted in port show that the ship's position fell within a 2-m radius 95% of the time. During the experiment, the streamer was located by reconstructing the streamer position from the compass readings. Locations are better in the direction parallel to the streamer than perpendicular to it, but both are probably within 5 m of uncertainty.

Horizontal and vertical resolution of the 3-D seismic images is dependent on the frequency content of the data, which becomes lower and more bandwidth limited with depth of penetration. The Hydrate Ridge 3-D seismic data have an approximate bandwidth of 25–200 Hz and a dominant frequency of 125 Hz at the seafloor. The vertical resolution of these data is therefore 3 m based on resolving distinctions of one-quarter of the dominant frequency's wavelength. The common midpoint spacing of 10 m in the in-line and 25 m in the cross-line direction effectively integrates the seismic acoustic impedance data over an estimated first Fresnel zone radius of ~75 m at the seafloor. First-order depth conversions of the seismic reflection data were calculated using velocities obtained from ocean-bottom seismometer data acquired with the 3-D data (Arsenault et al., 2001). These were further refined during the cruise using major seismic horizons correlated to the core and logging data and through velocities obtained from the wireline and core data.

Navigation

During Leg 204, surface navigation consisted of dynamic positioning at the surface relative to an acoustic beacon placed on the seafloor at each drill site. A Global Positioning System (GPS) was used after the selective availability signal was removed, thereby providing the accuracy of P-code GPS. There is no navigation information for the bottom of the drill string; therefore, its exact position relative to the ship's position is unknown. We assume that the hole's position is directly below the rig floor. During previous drilling, deviation of the hole from the ship's position was determined from cores recovered at shallow depths by the advanced piston corer (APC). Little significant deviation from the vertical was noted.

Drilling Operations

Three standard coring systems were used during Leg 204: the APC, the extended core barrel (XCB), and the rotary core barrel (RCB). These standard coring systems and their characteristics are summarized in the "Explanatory Notes" chapters of various *Initial Reports* volumes as well

as in Graber et al. (2002). Most cored intervals were ~9.6-m long, which is the length of a standard core barrel. In other cases, the drill string was "washed ahead" without recovering sediments in order to advance the drill bit to a target depth where core recovery needed to be resumed. In addition to these conventional coring tools several pressure coring systems (PCS) were used (see **"Downhole Tools and Pressure Coring,"** p. 34). In situ temperature and pressure were measured at ~10 depths in each hole (see **"Downhole Tools and Pressure Coring,"** p. 34). Logs of geophysical and geochemical parameters were obtained during logging while drilling (LWD) and using wireline tools (see **"Downhole Logging,"** p. 43).

Drilled intervals are referred to in meters below rig floor (mbrf), which are measured from the kelly bushing on the rig floor to the bottom of the drill pipe, and meters below seafloor (mbsf), which are calculated. When sediments of substantial thickness cover the seafloor, the mbrf depth of the seafloor is determined with a mudline core, assuming 100% recovery for the cored interval in the first core. Water depth is calculated by subtracting the distance from the rig floor to sea level from the mudline measurement in mbrf. This water depth usually differs from precision depth recorder measurements by a few to several meters. The mbsf depths of core tops are determined by subtracting the seafloor depth (mbrf) from the core top depth (mbrf). The resulting core top data in mbsf are the ultimate reference for any further depth calculation procedures.

Drilling Deformation

When cores are split, many show signs of significant sediment disturbance, including the concave-downward appearance of originally horizontal bedding, haphazard mixing of lumps of different lithologies (mainly at the tops of cores), fluidization, and flow-in. Core deformation may also occur during retrieval because of changes in pressure and temperature as the core is raised and during cutting and core handling on deck. These changes were particularly important during Leg 204 because temperature and pressure variations induce exsolution of gas from interstitial waters (IWs) and dissociation of gas hydrate, which also releases large amounts of gas. The "Lithostratigraphy" section in each site chapter discuss characteristics of cores that indicate this type of disturbance and can, therefore, serve as proxies for the presence of gas hydrates in situ.

Curatorial Procedures and Sample Depth Calculations

Numbering of sites, holes, cores, and samples follows the standard Ocean Drilling Program (ODP) procedure (Fig. **F1**). A full curatorial identifier for a sample consists of the leg, site, hole, core number, core type, section number, and interval in centimeters measured from the top of the core section. For example, a sample identification of 204-1244A-1H-1, 10–12 cm, represents a sample removed from the interval between 10 and 12 cm below the top of Section 1. Core 1 (H designates that this core was taken with the APC system) of Hole 1244A during Leg 204. Cored intervals are also referred to in "curatorial" mbsf. The mbsf of a sample is calculated by adding the depth of the sample below the section top and the lengths of all higher sections in the core to the core top datum measured with the drill string.

F1. Example of coring and depth intervals, p. 68.

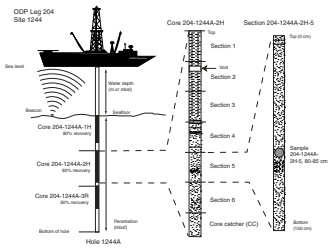

A sediment core from less than a few hundred mbsf may, in some cases, expand upon recovery (typically 10% in the upper 300 mbsf), and its length may not necessarily match the drilled interval. In addition, a coring gap is typically present between cores. Thus, a discrepancy may exist between the drilling mbsf and the curatorial mbsf. For instance, the curatorial mbsf of a sample taken from the bottom of a core may be larger than that of a sample from the top of the subsequent core, where the latter corresponds to the drilled core top datum.

If a core has incomplete recovery, all cored material is assumed to originate from the top of the drilled interval as a continuous section for curation purposes. The true depth interval within the cored interval is not known. This should be considered as a sampling uncertainty in age-depth analysis and correlation of core facies with downhole log signals.

Core Handling and Analysis

Cores were generally handled according to the ODP standard core-handling procedures as described in previous *Initial Reports* volumes and the *Shipboard Scientist's Handbook,* with modifications required to quickly identify intervals containing gas hydrates and to maintain approximately sterile conditions for microbiological sampling. Precautions were also taken to identify and safely deal with hydrogen sulfide.

To identify gas hydrates, cores were scanned with both handheld and track-mounted infrared (IR) cameras. Intervals with significant thermal anomalies were marked with magic marker, and whole-round cores were removed and stored in liquid nitrogen or pressure vessels. This is explained further in **"Physical Properties,"** p. 22, and in individual site chapters. Some suspected gas hydrate–bearing intervals were cut and immediately dropped into liquid nitrogen–filled dewars on the catwalk. Others were rapidly frozen. Others were placed in pressure chambers. Others were allowed to dissociate for various shipboard IR calibration experiments or geochemical analyses.

Certain cores were identified ahead of time as being candidates for microbiological sampling and tagged with tracers (see **"Microbiology,"** p. 18). When these cores were brought on board, appropriate sections for microbiological study were identified by the microbiologist on shift and taken immediately to the microbiology laboratory, which was located in a refrigerated van aft of the drilling floor.

Gas samples for routine shipboard safety and pollution-prevention samples were collected on the catwalk (see **"Organic Geochemistry,"** p. 16). Whole rounds (10 to 20 m long) were taken for IW analysis (see **"Interstitial Water Geochemistry,"** p. 13). The cores were then compressed with a plunger to remove large voids and cut into nominally 1.5-m sections. The remaining cut sections were transferred to the core laboratory for further processing.

Whole-round core sections not used for microbiological sampling were run through the multisensor track (MST), and thermal conductivity measurements were performed (see **"Physical Properties,"** p. 22). The cores were then split into working and archive halves (from bottom to top). Investigators should be aware that older material may have been transported upward on the split face of each section.

Visual core descriptions (VCDs) were prepared of the archive halves augmented by smear slides and thin sections (see **"Lithostratigraphy,"** p. 5). The archive halves were photographed with both black-and-white and color film. In addition, close-up photographs were taken of particular features for illustrations in site chapters, as requested by individual

scientists. All sections of core not removed for microbiological sampling were additionally imaged using a digital imaging track system equipped with a line-scan camera. A few cores of special interest were measured for color reflectance and high-resolution magnetic susceptibility (MS) using the archive multisensor track (AMST) (see "Lithostratigraphy," p. 5), but this was not standard procedure for most cores because of time limitations. No paleomagnetic studies were done on board because of limited personnel. Moreover, shipboard biostratigraphy indicates that most cores were too young for magnetostratigraphy to have provided significant temporal resolution.

The working half was sampled both for shipboard analysis, such as physical properties, carbonate, and bulk X-ray diffraction (XRD) mineralogy and for shore-based studies (see "Physical Properties," p. 22). Both halves of the core were then put into labeled plastic tubes, sealed, and placed in cold storage space aboard the ship. At the end of the leg, the cores were transferred from the ship into refrigerated containers and shipped to the ODP Gulf Coast Core Repository in College Station, Texas.

LITHOSTRATIGRAPHY

The techniques and procedures used to describe, analyze, and name the lithologies recovered during Leg 204 are detailed below. These include VCDs, smear slide and thin section descriptions, XRD analyses, color spectrophotometry, and high-resolution digital color imaging. Any significant deviations from the procedures outlined in this section are discussed in the individual site chapters.

Sediment Classification

The naming conventions adopted during Leg 204 follow the ODP sediment-classification scheme of Mazzullo et al. (1988). Principal names were assigned to sediments based on composition, texture, and degree of lithification as determined primarily from visual description and smear slide analyses. Modifiers to the principal name were determined based on both the abundance and type of the nonprincipal component or components (e.g., siliciclastic or biogenic). Total calcium carbonate content of the sediments (see "Carbonate Carbon and Carbonate," p. 17, in "Organic Geochemistry") was also used to aid in classification. Major modifiers, those components that compose >25% of the sediment, precede the principle name and are listed in order of increasing abundance. Genetic terms, such as pelagic, neritic, and debris flow, were not used in classifying the sediments and are used only in geologic interpretations of the sedimentary sequence. Additionally, the conventions used here apply only to granular sediments, as chemical sediments were only encountered as accessory minerals and nodules.

Siliciclastic Sediments

For sediments and rocks composed of >60% siliciclastic components, the principal name was determined by the texture of the grains. Textural names were derived from the Udden-Wentworth grain-size scale (Wentworth, 1922) (Fig. F2). In this classification scheme, the term clay is independent of mineralogy and refers to all siliciclastic grains <3.9

F2. Grain-size classification diagram for siliciclastic sediments, p. 69.

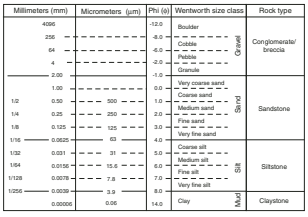

µm in size, regardless of composition. The relative proportion of different grain sizes was determined by visual percentage estimation using the comparison chart of Terry and Chilingarian (1955). Once the relative proportions were determined, a modified Shepard (1954) classification scheme was used to assign the principal name (Fig. F3). Clay, silt, and sand are the principal names in the Shepard diagram. If any component exceeds 25% of the total siliciclastic grains, it becomes a modifier to the principal name. For example, sediment composed of 10% clay and 90% silt is simply a silt, whereas sediment composed of 30% clay and 70% silt is a clayey silt.

Where diagnostic minerals (e.g., glauconite) or unusual components (e.g., volcanic glass) compose ≥5% of the sediment, the naming conventions of biogenic and mixed sediments were adopted. Thus, if the mineral component represents 5%–10% of the sediment, it is hyphenated with the suffix "-bearing" and precedes the major siliciclastic component name. If the component is 10%–40% of the sediment, it is hyphenated with the suffix "-rich," instead. For example, sediment composed of 15% glauconite sand grains, 30% silt, and 55% clay is called a glauconite-rich silty clay. Where volcanic glass composed >40% of the sedimentary components, the name volcanic ash was used.

F3. Classification scheme for siliciclastic sediment components, p. 70.

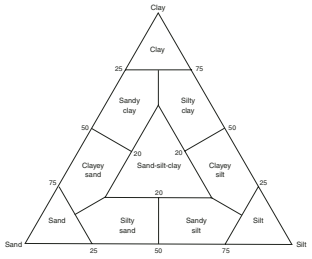

Biogenic Sediments

Unlike siliciclastic sediments, biogenic sediments, defined as containing >60% biogenic components, are not described based on texture. Rather, the principal name for all biogenic sediments is ooze. If the siliciclastic component represents 5%–40% of a sediment, the naming conventions using "-rich" and "-bearing" described above are followed. Thus, a sediment composed of 30% siliciclastic clay and 70% sand-sized foraminifers is called a clay-rich foraminifer ooze, not a clay-rich foraminifer sand.

Mixed Sediments

Subequal mixtures of biogenic and nonbiogenic material, where the biogenic content is 40%–60%, are termed "mixed sediments" in the ODP classification (Mazzullo and Graham, 1988). The name of a mixed sediment consists of a major modifier(s) consisting of the name(s) of the major fossil group(s), with the least common fossil listed first, followed by the principal name appropriate for the siliciclastic components (e.g., foraminifer clay). The same naming conventions for using "-bearing" and "-rich" apply to mixed sediments as described above. An unconsolidated sediment containing 5% foraminifers, 40% nannofossils, and 55% silt is, thus, called a foraminifer-bearing nannofossil silt. Sediment containing 5% diatoms, 40% clay, and 55% nannofossils is called a diatom-bearing nannofossil clay.

Firmness

The definition of Gealy et al. (1971) was used to identify the firmness of recovered sediments. Siliceous sediments and rocks are divided into two classes of firmness:

1. Soft sediments, which are composed of gravels, sands, silts, and clays (sediment core can be split with a wire cutter), and

2. Hard sediments, which are composed of conglomerates, sandstones, siltstones, and claystones (sediment core must be cut by a band or diamond saw).

Calcareous sediments and rocks are divided into three classes of firmness:

1. Unlithified: soft sediments that readily deform under the pressure of a fingernail or spatula;
2. Partly lithified: firm but friable sediments that can be scratched with a fingernail or the edge of a spatula; and
3. Lithified: hard, nonfriable cemented rocks that are difficult or impossible to scratch with a fingernail or the edge of a spatula.

Special Rock Types

The definitions and nomenclatures of special rock types were adopted and modified from ODP Legs 112 and 138 (Suess, von Huene, et al., 1988; Mayer, Pisias, Janacek, et al., 1992) and adhere as closely as possible to conventional terminology. One special rock type, authigenic carbonate, was particularly important during Leg 204.

Carbonates

Authigenic carbonates (aragonite, calcite, and dolomite) are present in various morphologies, as nodules or irregular precipitates, and are designated as "C" in the "Diagenesis" column of the core description forms ("barrel sheets") (Figs. F4, F5). In cases where it was possible to clearly identify the carbonate mineralogy, symbols for the respective carbonate minerals were used (see Fig. F3). The degree of lithification is noted in the core description as "friable" (the rock showed only partial lithification) or "lithified" (the rock is fully cemented).

Visual Core Descriptions

Detailed sedimentologic observations and descriptions were recorded manually for each core section on VCD sheets. A wide variety of features that characterize the sediments were recorded, including lithology, sedimentary structures, color, diagenetic precipitates, and core disturbance. Compositional data were obtained from smear slides. The color (hue and chroma) of the sediments was determined by both color spectrophotometry and, more often, by visual comparison with the Munsell soil color chart (Munsell Color Co., 1975). This information was synthesized for each core in the AppleCORE software (version 8.1m), which generates a simplified one-page graphical description of each core, or barrel sheet (Fig. F4). Barrel sheet symbols used during Leg 204 are described in Figure F5. For more detailed information on sedimentary features, VCD forms are available from ODP upon request.

Of particular interest during Leg 204 were the visual indications of disruption to the sediment caused by the dissociation of gas hydrate in the recovered sediment. Massive hydrate was removed on the catwalk prior to core description, but sampled intervals were noted in the barrel sheets. The two primary textures identified as resulting from the dissociation of gas hydrate are soupy and mousselike. Soupy sediments are watery, homogeneous, and fluidized (Fig. F6). These sediments are often associated with void spaces in the core because they are able to flow

F4. Example of VCDs, p. 71.

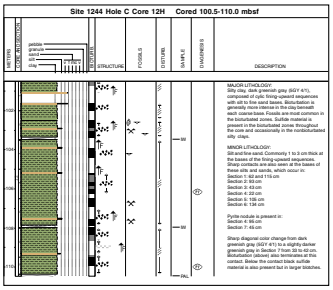

F5. Key to patterns and symbols used on barrel sheets, p. 72.

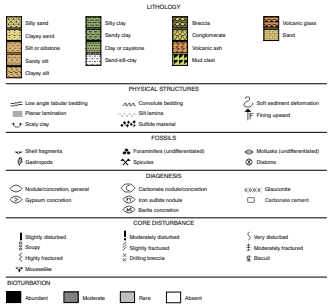

F6. Example of "soupy" sediment texture, p. 73.

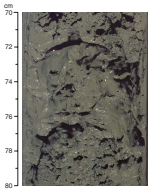

from their original position during core recovery and therefore retain no original sedimentary structures. Sediments containing mousselike textures can be divided into two descriptive types based on water content. Wet, watery mousselike sediment texture is soft and deforms plastically under slight pressure from one finger (Fig. F7). Mousselike texture can also occur in drier sediments that are stiffer and tend to form brittle flakes, which break off under the pressure of one finger (Fig. F8). These drier, stiffer sediments often appear foliated when split by the core cutter wire. Both types of mousselike texture contain gas vesicles and obscures primary sedimentary structures.

Mousselike and soupy textures related to the dissociation of hydrate not sampled prior to description were observed at all sites and noted on the barrel sheets. Remarks made on barrel sheets for each core describe any additional potential indications of gas hydrate near the sampled intervals, including the presence of dry, flaky sediment that may have been dewatered by the formation of hydrate nearby.

F7. Example of wet, watery, mousselike sediment texture associated with hydrate dissociation, p. 74.

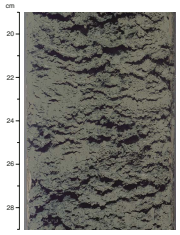

F8. Example of "flaky" mousselike texture associated with hydrate dissociation, p. 75.

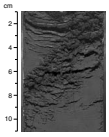

Lithology and Grain Size

The lithology and grain size of the described sediments are represented graphically in a column of the barrel sheets using the symbols illustrated in Figure F5. A maximum of three different lithologies (for interbedded sediments) or three different components (for mixed sediments) can be represented within the same core interval. Intervals that are a few centimeters or greater in thickness can be portrayed accurately in the lithology column. Percentages are rounded to the nearest 10%, and lithologies that constitute <10% of the core are generally not shown but are listed in the "Description" column.

Bioturbation

Visible bioturbation was classified into four intensity levels based on the degree of disturbance of the physical sedimentary structures:

1. Absent = no bioturbation; all physical sedimentary structures are preserved.
2. Rare = isolated trace fossils; up to 10% of physical sedimentary structures are disrupted.
3. Moderate = ~10%–40% disrupted physical sedimentary structures; burrows are generally isolated but may overlap locally.
4. Abundant = bedding completely disturbed; burrows are still intact in places.

These categories are based on the ichnofossil indices of Droser and Bottjer (1986) and are illustrated with graphic symbols in the "Bioturbation" column on the barrel sheets. Visual recognition of bioturbation was often limited in homogeneous sediments, particularly in hemipelagic clay zones without sulfide material.

Sedimentary Structures

Each type of sedimentary structure and its exact location are displayed in the "Structure" column of the barrel sheet. Symbols are used to note the wide variety of sedimentary structures encountered throughout Leg 204, and these are listed in the legend for the barrel sheets. Some of the more common structures observed were parallel

bedding, fining-upward sequences, and the mottled appearance of sulfide-rich layers.

Fossils

The presence of macroscopic fossils (including aggregates of sponge spicules, large diatoms [~1 mm], shell fragments, preserved whole shells, and gastropods) is displayed in a separate column on the barrel sheets.

Sediment Disturbance

Drilling-related sediment disturbance that persists over intervals of ~20 cm or more is recorded in the "Disturbance" column. Separate terms are used to describe the degree of drilling disturbance in soft and firm sediments:

1. Slightly disturbed = bedding contacts are slightly deformed.
2. Moderately disturbed = bedding contacts have undergone extreme bowing.
3. Highly disturbed = bedding is completely deformed as flow-in, coring/drilling slough, and other soft sediment stretching and/or compressional shearing structures attributed to coring/drilling (e.g., gas expansion).
4. Soupy = intervals are water saturated and have lost all primary sedimentary structures.

The degree of fracturing in indurated sediments and igneous rocks is described using the following categories:

1. Slightly fractured = core pieces in place and broken.
2. Moderately fractured = core pieces are in place or partly displaced, but original orientation is preserved or recognizable.
3. Highly fractured = core pieces are probably in correct stratigraphic sequence (although they may not represent the entire sequence), but original orientations are lost.
4. Drilling breccia = core pieces (small and angular pieces) have lost their original orientation and stratigraphic position and may be mixed with drilling slurry.
5. Drilling biscuits = drilling slurry surrounding an intact or slightly fractured drilling biscuit.

Cores recovered from gas and gas hydrate–bearing sediments are often disturbed by gas expansion and fracturing. In cases where it is possible to distinguish between disturbance of the core resulting from drilling and disturbance resulting from gas expansion, notes were made in the comments section of the barrel sheets listing the depths at which gas fracturing was observed.

Samples

The position of whole-round samples, as well as smear slides and samples taken to support and verify the observations of the smear slide and thin section analyses, are indicated in the "Sample" column on the barrel sheets. The abbreviations used are as follows: smear slide (SS), in-

terstitial water (IW), microbiology (MBI), gas hydrate (HYD), personal sample (PS), and micropaleontology (PAL).

Diagenesis

The relative position of features that are related to diagenesis are displayed in the "Diagenesis" column on the barrel sheets. These are mineral precipitates (e.g., pyrite, gypsum, and carbonate).

Analysis of Smear Slides and Thin Sections

Smear slides were prepared from the archive halves of the cores. With a toothpick, a small amount of sediment was taken and put on a 1 in × 3 in glass slide, homogenized, and dispersed over the slide with a drop of deionized water. The sample was then dried on a hot plate at the lowest effective temperature. A drop of Norland optical adhesive and a 1 in × 1 in cover glass were added. The smear slide was fixed in an ultraviolet light box. With a transmitted light petrographic microscope, both the grain size and abundance of dominant components in a sample were determined. Abundance was estimated with the help of a comparison chart for visual percentage estimation (after Terry and Chilingarian, 1955). Note that smear slide analyses tend to underestimate the amount of sand-sized and larger grains because these grains are difficult to incorporate into the slide. Table **T1** is an example of data obtained from smear slide analyses and was generated using the spreadsheet program SLIDERS. This table includes information about the location of samples, their grain-size distribution, and whether the sample represents the dominant (D) or the minor (M) lithology in the core. Additionally, it provides estimates of the major mineralogical and biological components from the examination of each smear slide. The presence of authigenic minerals, such as manganese oxides, iron sulfides, or carbonates, as well as the presence of rare trace minerals, was noted in the "Comments" column. The mineralogy of the major smear slide components was also validated by XRD analyses, and the relative proportion of carbonate and noncarbonate material was validated by chemical analysis of the sediments (see **"Carbonate Carbon and Carbonate,"** p. 17, in "Organic Geochemistry").

T1. Sample spreadsheet for smear slide and thin section analyses, p. 95.

Thin sections were taken from several authigenic carbonate precipitates and from a few well-indurated sediments. Tables summarizing thin section data, such as grain size and relative abundance of sedimentary components, were also generated using SLIDERS. A Zeiss Axioplan microscope equipped with a digital camera was used to obtain images of the thin sections on board. Digital photomicrographs were obtained and stored as TIFF (.tif) files. Thin section results were used to complement the VCDs and as a substitute for smear slides when sediments were well indurated.

X-Ray Diffraction Analyses

XRD analyses were used to support and verify the smear slide and thin section descriptions. Each sample was freeze-dried, ground, and mounted with a random orientation into an aluminum sample holder. For these measurements, a Philips PW-1729 X-ray diffractometer with a CuK_α source (40 kV and 35 mA) and a Ni filter was used. Peak intensities were converted to values appropriate for a fixed slit width. The goniometer scan was performed from 2° to 70° (2θ), at a scan rate of 1.2°/min

(steps = 0.01° and count time = 0.5 s). Diffractograms were peak corrected to match the (100) quartz peak at 4.26 Å. Common minerals were identified based on their peak position and relative intensities in the diffractogram using the interactive software package MacDiff 4.1.1 (Petschick, 2000).

Color Reflectance Spectrophotometry

In addition to visual estimates of the color, reflectance of visible light from soft sediment cores was often measured using a Minolta Spectrophotometer (model CM-2002) mounted on the AMST. The AMST measures the archive half of each core section and provides a high-resolution record of downcore color variations for the visible wavelengths (400–700 nm). Freshly split cores were covered with clear plastic wrap and placed on the AMST. Measurements were taken at 2.0 cm spacing. The AMST skips empty intervals and intervals where the core surface is well below the level of the core liner but does not recognize relatively small cracks or disturbed areas of core. Thus, AMST data may contain spurious measurements that should, to the extent possible, be edited out of the data set before use. Each measurement recorded consists of 31 separate determinations of reflectance in 10-nm-wide spectral bands from 400 to 700 nm. Additional detailed information about the measurement and interpretation of spectral data with the Minolta spectrophotometer can be found in Balsam et al. (1997, 1998) and Balsam and Damuth (2000). When sediment color became uniform, use of the Minolta system was discontinued.

Digital Color Imaging

All core sections were imaged using the Geotek X-Y digital imaging system (DIS) immediately after being split and scraped. We found it particularly useful to scrape the cores immediately prior to imaging in order to capture the ephemeral nature of some sedimentary features, particularly sulfide precipitates, which become oxidized within minutes of core splitting. It is worth noting that this fresh scraping did not occur prior to the regular photo imaging, which can take place between 30 and 60 min after scraping. Consequently, some of the sedimentary details may be lost using the more conventional archive-core table photographs. For this reason, cores were scraped before close-up photographs were taken. For digital imaging, core sections were routinely loaded into each imaging tray as soon as the previous sections were imaged so that the imaging system ran continuously during section loading and unloading. Some problems were encountered with occasional system crashes, however, which were probably a result of automated network uploading of files during image transfer from the camera hardware to the local computer.

In the core section dialogue box, we set the subbottom depth (SBD) of section at zero for Section 1 and let it automatically increment down the remaining sections for each core. All images were acquired at a crosscore and downcore resolution of 100 pixels/cm. At the beginning of Leg 204, the acquisition aperture was varied in an attempt to maximize the dynamic range captured. However, after Site 1244, we found it more expedient to fix the aperture at a value that would image most cores without the need for further adjustment. It was, therefore, normally set to f4.7, which maximized the dynamic range for most of the core sections, but it had to be decreased when bright ash-rich or car-

bonate layers were imaged to prevent image saturation. To prevent saturation of the bar-code label (placed at the end of each section) and of the polystyrene inserts (e.g., for voids and whole-round samples), we placed pieces of dark overhead-transparency film over them to reduce the brightness. This was a satisfactory but inelegant solution that would be improved with some high-quality gray translucent overlays. Care was taken to ensure that the system was correctly calibrated using the "white tile" procedure and that the camera position was correctly set up. If the image field is incorrectly set such that the ruler on the left side of the core is in the camera's field of view, then horizontal stripes, caused by pixel blooming, occur on the resulting image, which results in relatively dark cores. This is caused by the bright nature of the lettering on the ruler and could be prevented by having darker lettering (gray instead of white). Output from the DIS includes an uncompressed TIFF file (available upon request) and a compressed Mr.Sid (.sid) file (available in the Janus database) for each scanned section. Red-green-blue (RGB) profiles for all images were also automatically saved (available upon request) but were generally not used on board. Additional post-processing of the color imagery was done to achieve a "medium"-resolution JPEG (.jpg) image of each section and a composite PDF (.pdf) image of each core. The PDF full-core color images were useful for quick reference at sea, particularly when writing the site chapters.

BIOSTRATIGRAPHY

During Leg 204, diatoms and calcareous nannofossils were studied to assign preliminary ages to core catcher samples. Samples from within the cores were examined when a more refined age determination was necessary. The timescale of Berggren et al. (1995a, 1995b) was used. The biostratigraphic zones of calcareous nannofossils and diatoms are summarized in Figure F9.

F9. Correlation of the GPTS and biostratigraphic zonations, p. 76.

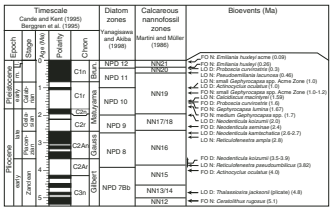

Diatoms

During Leg 204, we used the Neogene diatom zonations and code number of the North Pacific Diatom Zone (NPD) by Yanagisawa and Akiba (1998) (Fig. F9).

Diatom bioevents that define the zones used in Leg 204 are summarized in Figure F9. Ages for the events are based on Barron (1992), Barron and Gladenkov (1995), Koizumi (1992), Koizumi and Tanimura (1985), and Yanagisawa and Akiba (1998).

Smear slides were prepared for each sample using Pleulax as a mounting medium. The slides were examined on a light microscope at magnifications of 400×, 630×, and 1000×. The abundance of diatoms was estimated based on the number of specimens observed per field of view, with a magnification of 630× and the following definitions:

A = abundant; five or more valves per field of view.
C = common; one to five valves per field of view.
F = few; more than five valves per each vertical traverse but less than one specimen per field of view.
R = rare; more than one valve per two vertical traverses but less than five valves per each vertical traverse.
T = trace; for sparser occurrences.
B = barren; no valves observed on the slide.

The quantitative estimation of preservation of diatoms was recorded as follows:

G = good; both thinly silicified forms and heavy robust forms are present, and no alteration of the frustules was observed.
M = moderate; thinly silicified forms are present but exhibit some alteration.
P = poor; thinly silicified forms are rare or absent, and robust forms dominate the assemblage.

Calcareous Nannofossils

During Leg 204, calcareous nannofossils were studied to obtain biostratigraphic constraints for the sediments recovered on Hydrate Ridge. Ages for calcareous nannofossil events in the Pliocene and Pleistocene follow the geomagnetic polarity timescale (GPTS) of Cande and Kent (1995). We employed the nannofossil zonations of Martini and Müller (1986) for late Cenozoic sediments. Numerical ages used are those compiled by Berggren et al. (1995a, 1995b) (Fig. F9) to facilitate easy comparison with other studies.

Calcareous nannofossil assemblages were examined using smear slides prepared from each core catcher sample and from additional core samples. Standard smear slides were made for all samples using Norland Optical Adhesive as a mounting medium. Examination was performed with a light microscope. Unless otherwise noted, we followed taxonomic concepts summarized in Perch-Nielsen (1985).

INTERSTITIAL WATER GEOCHEMISTRY

The biogeochemistry program of Leg 204 had three major objectives: (1) to explore the relationship between fluid flow and gas hydrate dynamics at Hydrate Ridge, (2) to constrain the role of microbial communities in methane generation and consumption, and (3) to use carbonate and sulfide minerals as potential indicators of past events of hydrate formation and dissociation. The distribution of dissolved constituents in IW has proven to be a powerful tool for quantifying hydrogeochemical and geological processes within sediments. The sampling, processing, and preservation protocol for IW samples during this leg were designed to provide the data needed to address these biogeochemical objectives.

Dissolved chloride content of the pore fluids has been widely used to constrain estimates of hydrate concentration in marine sediments (e.g., Froelich et al., 1995; Kastner et al., 1995; Paull, Matsumoto, Wallace, et al., 1996; Hesse, 2003). These estimates are based on the concept that dissolved ions are excluded from the hydrate cages during gas hydrate formation, such that the gas hydrate lattice contains little or no salt. This process causes the pore water to become saltier, and over time, the excluded ions are removed from the zones of hydrate formation by advection or diffusion. Gas hydrate dissociation during core recovery results in freshening of the pore fluids by the addition of water sequestered by gas hydrate prior to recovery (Hesse and Harrison, 1981). Thus, negative chloride anomalies relative to in situ chloride concentration should be proportional to the amount of gas hydrate in a sediment sample. During Leg 204, high-resolution profiles of dissolved chloride were used to generate first-order estimates of the amount of hydrate in

sediment. Uncertainties in these estimates arise from a paucity of information on (1) the in situ chlorinity values of pore water; (2) the amount of chloride potentially trapped within the gas hydrate internal structure, such as micropores or veins; (3) the spatial sampling bias; and (4) fluid transport and diffusion rates. Shore-based isotopic characterization of the pore fluids will provide additional constraints on physical transport (e.g., $\delta^{37}Cl$ and ^{129}I) as well as hydrate formation and dissociation ($\delta^{18}O$ and D/H) processes in this environment.

Methane hydrate formation depends on pressure, temperature, pore water salinity, and a sufficient amount of methane. Methane inventory is highly dependent on rates of microbial methanogenesis, microbial methane oxidation, and physical transport processes. The dissolved sulfate distribution in marine pore fluids can be used to estimate methane flux toward the seafloor in certain situations, which, in turn, depends on the methane inventory below (Borowski et al., 1996). The distribution of dissolved sulfate in Leg 204 IW samples has been used to provide constraints on methane fluxes on Hydrate Ridge. Shore-based isotopic characterization of dissolved carbon, nitrogen, and sulfur species as well as data on microbial communities and metabolic rates will further constrain preliminary shipboard estimates.

Interstitial Water Collection

The majority of shipboard IW samples were obtained on 5- to 20-cm-long whole-round cores that were cut according to two general procedures. Routine samples at each site were collected at a frequency of approximately two sections per core in the upper 150 m of the sediment section, followed by a sampling resolution of one whole-round sample per core in the deeper sequences. These whole-round samples were cut on the catwalk, capped, and taken to the laboratory for immediate processing. At most sites, samples within the anaerobic methane oxidation (AMO) zone were taken at higher resolution (approximately two samples per section) in a coordinated program with the shipboard microbiologists. Samples from the end of each section were cut on the catwalk, and the samples from the middle intervals of each section were cut from microbiology whole-round sections that were subsampled in the walk-in refrigerator. During high-resolution sampling, when there were too many IW cores to process immediately, capped whole-round core sections were stored in a refrigerator until they were squeezed, which occurred no later than 12 hr after core retrieval.

After extrusion from the core liner, the surface of each whole-round IW core sample was carefully scraped with an acid-washed (10% HCl) plastic spatula to remove potential contamination from seawater and sediment smearing in the borehole. In APC cores, ~0.5 cm from the outer diameter, top and bottom faces were removed; whereas in the XCB cores, where borehole contamination is higher, as much as two-thirds of the sediment was removed from each whole round. Approximately 2 cm^3 of uncontaminated sediment was saved for grain-size analyses. The remaining sediment (~150–300 cm^3) was placed into a titanium squeezer, modified after the stainless-steel squeezer of Manheim and Sayles (1974). Gauge pressures up to 15 MPa were applied using a laboratory hydraulic press to extract pore water. IW was passed through a prewashed Whatman No. 1 filter fitted above a titanium screen, filtered through a 0.45-µm Gelman polysulfone disposable filter, and subsequently extruded into a precleaned (10% HCl) 50-mL plastic syringe attached to the bottom of the squeezer assembly. In most cases, 25–40

cm^3 of pore water was collected from each sample, which required squeezing the sediment for 20–40 min. To prevent loss of ephemeral constituents, IW subsamples were collected in a 10-mL syringe attached to the squeezer assembly and the 50-mL syringe via a three-way valve (D'Hondt, Jørgensen, Miller, et al., 2003). IW emerging from the disposable filter at the bottom of the squeezer assembly was directed into one or the other syringes, as necessary, for rapid and appropriate dispensing of aliquots. Use of the 10-mL syringe also avoided air bubbles, minimized contamination of this fraction of the IW by dissolved oxygen, and allowed for efficient subsampling during the sediment squeezing process (D'Hondt, Jørgensen, Miller, et al., 2003).

In addition to the whole-round IW samples, we collected 10-cm^3 samples from the working half of the cores within 90 min after core retrieval at Sites 1245 and 1249. To construct a high-resolution chloride distribution relative to a discrete gas hydrate layer, we collected samples from the hydrate and at various distances from it in Core 204-1245C-7H. To further evaluate the effect of heterogeneous gas hydrate distribution and to recover sediments that showed minimum disturbance from gas hydrate dissociation, we collected paired samples from consolidated and mousselike sediments from Cores 204-1249F-3H and 7H. These samples were squeezed following the same procedures as described for the whole-round samples, but the amount of fluid collected (<5 cm^3) was only enough for analyses of dissolved chloride (shipboard) and characterization of the isotopic composition of the water (shore based).

Collection of Subsamples for Shore-Based Analyses

Subsamples were collected from the whole-round IW samples for shore-based isotopic characterization of the water (oxygen and deuterium) and dissolved metabolites (bicarbonate, sulfate, sulfide, and ammonium). These subsamples were preserved with mercuric chloride or cadmium acetate and were flame sealed in glass ampoules. In addition, subsamples were collected for analyses of dissolved volatile fatty acids (in glass vials and frozen), halogens (including $\delta^{37}Cl$ and ^{129}I), and minor and trace metal constituents (acidified with ultrapure nitric acid). Dissolved sulfide (ΣHS^-) within pore water was fixed by pipetting a 1-mL IW subsample into a vial containing 1.0 mL of 1-M cadmium acetate solution (20 g ZnAc per 100-mL solution) and will be measured onshore using the methylene blue method of Cline (1969).

Shipboard Interstitial Water Analyses

IW samples were analyzed for routine shipboard measurements according to standard procedures (Gieskes et al., 1991). Salinity was measured as total dissolved solids using a Goldberg optical handheld refractometer. The pH was determined by ion-selective electrode. Alkalinity was determined by Gran titration with a Metrohm autotitrator. Sulfate (SO_4^{2-}) concentration was measured using a Dionex DX-120 ion chromatograph. High-precision chloride concentrations were determined by titration using silver nitrate ($AgNO_3$), and the values were corrected for the presence of the other halogens assuming seawater ratios, as detailed by Gieskes et al. (1991). International Association of Physical Sciences organization (IAPSO) standard seawater was used for calibrating sulfate and chloride techniques. Dissolved phosphate (PO_4^{3-}) and ammonium (NH_4^+) concentration were determined by spectrophotometric

methods using a Milton Roy Spectronic 301 spectrophotometer, with a "Mr. Sipper" sample-introduction system (Gieskes et al., 1991). During Leg 201, a method was developed to semiquantify the pore water color. To provide a comparison to the Peru margin sites, a selected set of samples from Site 1244 was analyzed for yellowness relative to the JWBL standard used during Leg 201 (D'Hondt, Jørgensen, Miller, et al., 2003). The procedure involves a one to three dilution of pore water samples with deionized water and measurement of absorbance at 325 nm using the Milton Ray Spectronic 301 spectrophotometer.

Dissolved organic carbon (OC) analyses were conducted in a Shimadzu TOC-5000A total carbon analyzer. Approximately 1–5 mL of IW, depending on sample volume available, was placed in TOC vials, which had been prewashed with 10% HCL and combusted at 450°C for 4 hr. Samples were acidified to a pH of ~2 with 2-N HCL and placed in the ASI-5000A autosampler that was set up to purge the sample with purified air for 3 min prior to analysis. Triplicate injections of 25 µL were introduced to the combustion tube and heated to 680°C in the presence of a catalyst. The resulting CO_2 was detected in a nondispersive IR gas analyzer (NDIR). Detector output was calibrated against potassium phthalate standard solutions covering a range of 0–49 ppm carbon.

Sodium and potassium were measured using a Dionex DX-120 ion chromatograph; whereas magnesium and calcium were measured by ICP-AES using a Jobin Yvon JY2000 spectrometer with yttrium as an internal standard (Mix, Tiedemann, Blum, et al., 2003). For all major cations, we used dilutions of IAPSO standard seawater as calibration standards. ICP-AES techniques were also used for the minor elements Mn^{2+}, Fe^{2+}, B, Sr^{2+}, Ba^{2+}, and Li^{+} (modified from Murray et al., 2000) by preparing calibration standards in an acidified (2.5% HNO_3 by volume) sodium chloride matrix (35 g NaCl per liter). In addition, a 2.5% HNO_3 matrix solution with yttrium at 10 ppm (1:10) served as an internal standard to dilute standards and acidified IW samples (Mix, Tiedemann, Blum, et al., 2003).

The reproducibility of techniques, expressed as 1-σ relative standard deviations of means, was evaluated by replicate analyses of calibration standards, of IAPSO, and/or of samples both within a given analytical run and in different analytical runs (Table T2). Chemical data for IW are reported in molar concentration units.

T2. Techniques, standards, and typical reproducibility for IW analyses, p. 96.

ORGANIC GEOCHEMISTRY

The shipboard organic geochemistry program for Leg 204 included four routine sets of analyses: (1) analysis for volatile hydrocarbons in cores as required by ODP safety regulations; (2) measurement of carbonate carbon (IC) content of the sediments; (3) elemental analyses of total carbon (TC), total nitrogen (TN), and total sulfur (TS) content of sediment; and (4) characterization of organic matter by Rock-Eval pyrolysis. Procedures and instruments used during Leg 204 are described by Pimmel and Claypool (2001) and are generally the same as those used during most recent ODP legs. Brief comments on routine sampling and deviations from standard practice are noted below.

Hydrocarbon Gases

For pollution prevention and safety, composition of gases in sediment typically was determined at least once every core. Two sampling

methods were employed: headspace (HS) sampling and syringe or vacutainer (VAC) sampling. Headspace gas was collected after heating a nominal 5-cm^3 plug of sediment at 70°C for 30 min in an airtight vial. VAC gas samples were collected from gas pockets, bubbles, or voids in the core by piercing the core liner and allowing gas to expand into a 60-cm^3 syringe connected to the penetration tool.

Gas obtained by either method was analyzed by one of two gas chromatography systems: a Hewlett Packard 5890 Series II (GC3) or a Hewlett-Packard 5890A natural gas analyzer (NGA). The first system determines concentrations of C_1–C_3 hydrocarbons with a flame ionization detector (FID); the latter system measures concentrations of C_1–C_7 hydrocarbons with an FID as well as N_2, O_2, CO_2, and H_2S with a thermal conductivity detector (TCD). For both systems, chromatographic response was calibrated to six different gas standards, with variable quantities of low molecular weight hydrocarbons, N_2, O_2, CO_2, H_2S, Ar, and He.

In both the HS and VAC analyses, the gas composition is expressed as component parts per million by volume (ppmv) relative to the analyzed gas. To the extent that sampling procedures are uniform, the differences in the HS results reflect differences in the amount of gas remaining in the cores. Major variation in the C_1 ppmv results for the VAC samples reflects dilution of the gas void samples with air. The HS results were recalculated to adjust for sample size variability and to express the result on a more meaningful concentration basis, at least for lower concentration ranges. HS samples were weighed, and net sample weights were calculated by subtracting an average vial weight (15.6 g). Wet bulk density of the corresponding depth in the core was used to convert sample weight to sample volume. Porosity at the depth of the sample was used to estimate the volume of water in the sample. Accordingly, the methane concentration can be expressed as millimoles per liter of pore water,

$$CH_4\ (mM) = CH_4\ (ppmv) \times (21/[\text{sample weight/density}] - 1) \times (1/[\text{porosity} \times 22{,}400]), \quad (1)$$

where density and fractional porosity are taken from average depth trends presented in the "Physical Properties" section of each site chapter.

Carbonate Carbon and Carbonate

IC content of sediment samples was determined by coulometry. Carbonate content of sediment (in weight percent) was calculated from IC by assuming all carbonate is present as calcium carbonate:

$$CaCO_3 = IC \times 8.33. \quad (2)$$

Elemental Analyses

TC, TN, and TS contents of sediment samples were determined with a Carlo Erba NCS analyzer. TOC content was calculated as the difference between TC and IC:

$$TOC = TC - IC. \quad (3)$$

Organic Matter Characterization

The type and quantity of organic matter in sediment were evaluated by Rock-Eval pyrolysis. In this procedure, volatile hydrocarbon content (in milligrams per gram) released at 300°C for 3 min is S_1. The hydrocarbon quantity (in milligrams per gram) released as the temperature is increased from 300° to 600°C at 2°C/min is S_2. The nominal temperature of the maximum rate of hydrocarbon yield during S_2 analysis is defined as T_{max}. TOC content was independently measured, and the carbon-normalized hydrogen index (HI), in milligrams of hydrocarbon per gram of carbon (mg HC/g C), was calculated from the pyrolysis assay as

$$HI = (100 \times S_2 \text{ [in milligrams per gram]/TOC [in weight percent]}). \quad (4)$$

MICROBIOLOGY

Microorganisms are the kinetic controls on both methane production and consumption. Their distribution and activity must, therefore, be estimated in order to model the dynamics of the gas hydrate system. Target zones of interest include (1) the top of the sediment column, where microbial sulfate reduction and microbial methane oxidation are coupled; (2) the base of the gas hydrate stability zone (GHSZ), which was a region of increased microbial numbers at Blake Ridge (Wellsbury et al., 2000); and (3) sediments hosting massive and disseminated hydrates, which may also host distinct microbial communities.

Because good microbiology samples can only be taken when the cores are fresh, the shipboard microbiologists focused on getting the best samples possible for future investigations. In addition to processing cores to accommodate sample requests, a whole-round sample from every section sampled for microbiology was frozen as an ODP archive sample. Cores were sampled for microbiology at Sites 1244, 1245, 1249, 1250, and 1251 and may be identified in the ODP database query "Hole, Core" summaries by the notation "Tracer/Whirl-Pac."

Core Handling and Sampling

Core Collection and Retrieval

Because of the need to monitor contamination and control core temperature, cores for microbiological sampling were specified prior to core collection. Two types of tracers were used to monitor seawater infiltration into these cores: soluble perfluorocarbons and fluorescent microparticles. The perfluoro(methylcyclohexane) tracer was pumped into the drilling fluid (surface seawater) by a variable-speed, high-pressure liquid chromatography pump connected to the mud-pump system. The tracer pump operated at a fixed rate relative to the mud-pump speed so that the concentration of tracer was always 1 ppm (v/v). The pump was started for each designated microbiology core immediately after recovery of the previous core so that tracer would be "washed down" with the core barrel and arrive at the drill bit before coring began. The tracer pump was then run continuously until the core had been completely cut. The fluorescent microspheres were delivered in a plastic bag (designed to rupture on contact with the sediment) attached to the core catcher (see **"Contamination Tests,"** p. 20, in "Shipboard Microbiological Procedures and Protocols").

Core temperature is an important consideration when taking microbiological samples. Ideally, cores should be maintained as close to in situ temperatures as possible; in practice, cooling cores below in situ temperatures is acceptable, whereas warming cores above in situ temperatures can yield disastrous results. Our goal was to maintain core temperature at or below in situ temperatures at all times. Shallow cores at Hydrate Ridge have in situ temperatures below the temperature of the surface seawater (12°C), which is used as drilling fluid and through which the cores must travel to reach the rig floor. Cores with in situ temperatures <10°C that warmed to >10°C were rejected for microbiological sampling. To keep warming to a minimum, microbiology cores were retrieved and sent to the catwalk using the expedited core-retrieval protocol implemented during Leg 201 (see the "Introduction" in "Microbiology" in the "Explanatory Notes" chapter of D'Hondt, Jørgensen, Miller, et al., 2003). When a core barrel was retrieved, the core was immediately removed from the barrel and sent to the catwalk. Once the core was completely in the hands of the core technicians, the drilling crew sent the next core barrel down the wireline. This core-handling protocol increased the coring time but was necessary to keep core temperatures <10°C. Temperatures were monitored using the IR camera on freshly cut core ends.

Core Section Subsampling

Core sections were cut on the catwalk as usual, but no acetone was used to seal the end caps. Most sections that were sampled for microbiology had whole rounds for IW removed from the bottom end. A refrigerated cargo van (provided by Dr. Scott Dallimore of the Geologic Survey of Canada [GSC] Pacific for use during this cruise) mounted on the port side of the ship, aft of the rig floor, was maintained at 4°C and used as a microbiological laboratory space. All cores for microbiological study were transported directly from the catwalk to the van, where they were subsampled and packaged.

APC core sections sampled for microbiology were generally intact and undisturbed. Whole-round samples were removed from these sections in the refrigerated van by first cutting the liner with the rotary knife cutter (as normally used on the catwalk) and then fracturing, rather than cutting, the sediment. The whole rounds were dropped into Whirl-Pak bags (Nasco) or the Fisher equivalent and frozen, refrigerated, or further subsampled. Although this method leaves most samples in contact with contaminated material near the core liner, a decision was made that, in view of the very slow nature of the diffusion process and of the low storage temperatures involved, such treatment was preferable to additional processing under adverse shipboard conditions.

XCB core sections were processed by splitting the liner, but not the core itself, on the core cutting table. In the refrigerated van, the top of the liner was removed to expose the core and individual biscuits were removed and repeatedly pared on fresh sterile sheets of aluminum foil. Pared biscuits were placed in Whirl-Pak bags and frozen, refrigerated, or subsampled. Although we removed the contaminated material from XCB core samples to the best of our ability, they should be pared again in a sterile environment.

Whole-round samples or pared biscuits were subsampled with sterile, truncated 5-mL syringes or alcohol-flamed spatulas. Subsamples were placed in preservative solutions for direct microscopic counts, fluorescent in situ hybridization (FISH) with nucleic acid probes, and micro-

sphere enumeration. Whole-round samples, biscuits, or subsamples that were stored unpreserved at 4°C were sealed in nitrogen-flushed triple-ply Mylar heat-seal bags (Kapak Corp., Minneapolis, Minnesota) to maintain an anoxic environment. Samples to be frozen were stored at –80°C.

A glove bag (Coy, Grass Lake, Michigan) containing a nitrogen atmosphere with 5% CO_2 and 5% H_2 was used for anaerobic handling of core sections to inoculate growth media selective for methane-producing organisms and iron- and manganese-reducing microorganisms. Subcores were brought into the glove bag in nitrogen-filled jars, maintained cold on blue ice, and work was performed quickly to minimize warming. All media and sterile tools were also precooled and kept on blue ice during processing. Hydrogen is present to combine with residual oxygen in a reaction catalyzed by palladium pellets maintained within the bag. The bag was maintained regularly, and several hours before each use was flushed with a gas mixture and provided with freshly baked (140°C) catalyst. As an additional precaution to minimize oxygen contamination, tools and glassware to be used for manipulation and storage of samples for strict anaerobic work were stored within the glove bag.

Although cores were processed as quickly and as carefully as possible, shipboard handling should not be simply accepted as aseptic. We recommend that investigators receiving samples treat them as potentially contaminated and subsample accordingly whenever possible. Microsphere enumerations, summarized in the relevant site chapters, and additional microsphere evaluations performed postcruise at individual laboratories should be used to evaluate the quality of individual samples.

Shipboard Microbiological Procedures and Protocols

Contamination Tests

The greatest challenge for subsurface microbiological investigations is verification that observed populations and activities are authigenic and not the result of introduced contaminants. Chemical (perfluorocarbon) and particulate (latex microsphere) tracers were used during microbiological coring to check for the potential intrusion of drilling fluid (surface seawater) and confirm the suitability of the core material for microbiological research. The presence or absence of these two tracers also acts as a quality assurance check on core-handling methods. These tracer techniques were used during Leg 201 and are described in ODP *Technical Note,* 28 (Smith et al., 2000b). Freshly collected cores were also examined through the transparent core liner for signs of drilling disturbance (shearing or slurrying). Core sections observed to be disturbed before or during subsampling were considered unsuitable for further study and were discarded.

Perfluorocarbon Tracer

Perfluorocarbon tracer (PFT) was continuously fed into the drilling fluid at a concentration close to the limit of solubility (1 µg/g) and well above the detection limit for gas chromatographic analysis (1 pg/g) of that material. Samples for PFT analysis were taken from all cores intended for microbiological studies. Syringe subcores were taken from the interior (to monitor intrusion) and exterior (to verify delivery) of a freshly broken core or biscuit surface, extruded into headspace vials,

and sealed with Teflon septa. Air samples were occasionally taken to monitor the background (blank) level of PFT in the refrigerated van. Samples were kept at –80°C until ready for analysis by gas chromatography (GC). Methods described in Smith et al. (2000b) were used for PFT analysis, with minor modifications. The same GC setup was used, but the instrument was modified by installation of a 1-cm^3 sample loop and injector valve to standardize injection volumes.

Fluorescent Microparticle Tracer

Latex fluorescent microspheres (Polysciences, Inc., Warrington, Pennsylvania) (YG; 0.5 µm diameter) were used as a particulate tracer complementary to the volatile PFT. A 2-mL aliquot of microsphere stock (2.69% solids) was diluted with 40-mL distilled water, sonicated for 2 min, and heat sealed into a 4-oz Whirl-Pak bag. The bag was then attached as described in Smith et al. (2000a, 2000b) to the inside of the core catcher and positioned to rupture upon impact of the core tube with bottom sediments, where the microspheres will mix with seawater and coat the outside of the core as it is pushed into the liner. During core processing, subsamples of sediments were collected from outer and inner layers for microscopic examination. Weighed samples were mixed thoroughly with saturated sodium chloride solution to extract microspheres. The slurry was then centrifuged to separate the liquid phase (Marathon 21K; 5 min; 1000 relative centrifugal force), the supernatant was filtered onto a black polycarbonate filter (Millipore; 0.2-µm pore size), and the filter was mounted on a clean slide for microscopic examination. Microspheres in slide preparations were counted using a Zeiss Axioplan fluorescence microscope equipped with the Zeiss No. 9 filter set (BP 450-490; LP 520), and the number of spheres observed was used to quantify contamination in spheres per gram of sample. Comparison of microsphere numbers between paired samples from inner and outer core layers provides a relative measure of fluid intrusion. A sample with many spheres in outer layers and few or none within may be considered "higher quality" than one with very few spheres in the outer layers and few or none within.

Enrichment Cultures

Liquid-culture enrichments were begun for methanogenic organisms that use either hydrogen or acetate as an energy source and for organisms or consortia capable of dissimilatory iron or manganese reduction coupled with either acetate or formate oxidation. Media, as described in Boone et al. (1989) and Lovley and Phillips (1988), were prepared at Idaho National Energy and Environmental Laboratories (INEEL) prior to the voyage.

Samples for enrichments were taken from cores that had been maintained at low temperature and placed in oxygen-free conditions as quickly as possible. For sediment transfers, subcores were brought into the glove bag in nitrogen-filled jars and insulated on blue ice; work was performed quickly to minimize warming. All media and sterile tools were also precooled and kept on blue ice during processing. One to two grams of sediment were aseptically transferred to culture tubes containing 10 mL of selective medium. Tubes were opened only briefly for the transfer and immediately resealed. Methanogen enrichments were serially diluted as a first step in isolating novel organisms. The tubes containing 2 g of sediment were vigorously mixed with a vortexer and seri-

ally diluted 10-, 100-, and 1000-fold by transferring with a syringe into sealed culture tubes containing 10 mL of medium. Inoculated tubes were then placed in a 10°C incubator until shipment, at the end of the voyage, to INEEL for long-term enrichment and isolation study.

Summary of Sampling for Shore-Based Studies

The bulk of the samples taken were for shore-based investigations. Whole-round samples were taken for lipid analysis, adenosine triphosphate (ATP) analysis, and deoxyribonucleic acid (DNA) extraction and stored double-bagged in Whirl-Pak bags at –80°C. Subsamples were preserved for direct counts (stored in 0.2-µm-filtered artificial seawater containing 2% formaldehyde) and FISH with nucleic acid probes as well as FISH–secondary ion mass spectroscopy (both stored in a 1:1 solution of ethanol and phosphate-buffered saline); all of these samples were stored at 4°C. Cores to be used for culture-based analyses and for methods that require living cells as starting material (e.g., rate measurements) were stored under nitrogen either in triple-ply Mylar heat-seal bags or in Whirl-Pak bags inside canning jars that were flushed with nitrogen before sealing.

PHYSICAL PROPERTIES

A suite of physical property measurements was made to complement the other data sets taken on board and to support the main scientific objectives of Leg 204. Physical characteristics of the subsurface environment play an important role in determining the nature of fluid and gas migration, which, in turn, affect the nature of microbial communities and gas hydrate formation.

Sediment physical properties were routinely measured using the MST on whole-round cores and using discrete samples to measure bulk density, porosity, grain density, compressional wave (*P*-wave) velocity (V_P), and magnetic susceptibility (MS). In addition, thermal conductivity was measured on whole cores.

Core handling was done routinely following ODP standards (i.e., after sectioning the core on the catwalk, the core sections were stored inside the laboratory to equilibrate to ambient room temperatures). This took, on average, 4 hr. After temperature equilibration, MST measurements were conducted on whole-round core, followed by measurements of thermal conductivity. The core sections were then split for discrete sampling for moisture and density (MAD) as well as for measurements of shear strength and V_P with the Hamilton Frame velocimeter.

Brief summaries of each of the physical property measurement procedures used during Leg 204 are presented below, but the reader is referred to Blum (1997) for more detail. Apart from these routine measurements, which are made during most ODP legs, some special procedures and specific measurements related to hydrates were used during Leg 204. In particular, we collected IR images of the cores on the catwalk to identify and quantify the presence of gas hydrate. These measurements were supplemented by the use of handheld IR cameras and by self-logging temperature-probe measurements made both on the catwalk and in the core laboratory. We also used a Vertical Multi Sensor Core Logger (V-MSCL) on pressurized and repressurized cores in an at-

tempt to help characterize the in situ properties of gas hydrate–bearing lithologies (see "Downhole Tools and Pressure Coring," p. 34).

Infrared Thermal Imaging

IR thermal imaging of the surface of the core liner was fully implemented during Leg 204. The initial development of the technique was accomplished during Leg 201, where IR imaging was shown to successfully identify thermal anomalies associated with gas hydrate and voids.

Thermal anomalies in marine sediment cores on short length scales (less than a few meters) could result from (1) adiabatic gas expansion, (2) gas exsolution from pore water, or (3) gas hydrate dissociation. All of these processes cool cores (Ussler et al., unpubl. data). However, discrete, strong cold anomalies in Leg 204 cores were shown to be directly associated spatially with gas hydrate. These negative temperature anomalies developed, for the most part, in response to gas hydrate dissociation after the core arrived on deck. Variations in heat capacity also impact core temperatures, but generally differences in thermal conductivity or density are relatively small and do not result in large enough heat capacity differences to cause discrete, negative thermal anomalies.

IR imaging on Leg 204 also confirms earlier thermistor measurements that show variations in thermal structure along entire cores, which are typically warmer at the bottom and cooler at the top (Ussler et al., unpubl. data). Gas expansion and gas exsolution may account for the observed gradient along cores. If so, the thermal structure developed principally during ascent of the core through the upper part of the water column. Alternatively, the thermal structure along entire cores may reflect differences in frictional heating during coring, creating warmer temperatures near the core barrel shoe (APC) or bit (XCB) and cooler temperatures near the core top. Analysis of data from the advanced piston corer methane (APCM) tool from Leg 204 is expected to help determine the origin of temperature gradients typically observed along each core. Regardless of the origin of the overall thermal structure of cores, the discrete, negative thermal anomalies associated with gas hydrate are superimposed on the broader gradient, providing a robust proxy for the location and abundance of gas hydrate in cores. Gas shows up as warm anomalies because of the low heat capacity of gas voids compared to sediment and in spite of the cooling effect of gas expansion.

The primary benefits of using IR cameras (rather than running a hand down the length of the core) include the following: (1) more precise identification of thermal anomalies, (2) the estimation of hydrate volume in processed images, and (3) determinations of shapes of gas hydrate. The IR camera is also quicker and simpler to use and has a much higher spatial resolution than an array of thermistors. Hydrate veins or lenses, hydrate nodules, and disseminated gas hydrate were all identified. The resolution of thermal anomalies observed indicates that the camera can detect small volumes of gas hydrate if they are adjacent to the core liner. Determining precise, quantitative volumetric estimates of gas hydrate in cores was an objective during Leg 204, but realizing this objective will require further postcruise analysis of collected data. IR images were used to do the following:

1. Rapid identification of gas hydrate in cores from temperature anomalies on the surface of the core liner for immediate sampling of gas hydrate;

2. Preliminary assessment of the abundance of gas hydrate in cores based on the volume of core that shows thermal anomalies of varying ΔTs;
3. Quantification of the relative proportions of different gas hydrate textures;
4. Estimation of the cross-sectional temperature gradient in cores prior to sampling for microbiology;
5. Assessment of the thermal structure of entire cores and the differences in thermal structure between APC and XCB cores.

Methodology

Two ThermaCam SC 2000 cameras (FLIR Systems) and an AVIO Neo Thermo model TVS-610 (Nippon Avionics Co., Ltd.) were used to map temperature variations along core. The FLIR Systems cameras provide temperature-calibrated images over a temperature range from –40° to ≥1500°C. For shipboard measurements, the cameras were set to record a more limited range of temperatures from –40° to ≥120°C (Range 1). To perform the critical task of rapid identification of gas hydrate within the core on the catwalk, one of the FLIR Systems IR cameras was mounted on a track above the catwalk and driven automatically by a stepper motor controlled by a LabView software program. The camera was mounted in such a way that a 20-cm field of view along the core was obtained with the camera lens located 55 cm from the top of the surface of the core liner. To minimize the effect of external IR radiation reflecting off the core-liner surface, the camera was enclosed within a cardboard sheath covered on the outside with aluminized Mylar and lined on the inside with black felt (Fig. **F10**). After operations at Site 1244 were complete, the catwalk was also shaded with cardboard and the camera enclosure was extended to minimize ambient IR reflections from the core liner.

F10. FLIR SC-2000 camera, p. 77.

Images and data for each core were acquired immediately after the core liner was wiped dry. The mounted camera was moved down the core in 20-cm increments, starting 10 cm from the core top. Each image was saved with a unique identifier (header file) that included information about the position of the center of the image. Initially, all images were automatically saved over the shipboard computer network. Network slowdowns early in the cruise necessitated modification of the system to save images for a single core directly on the computer controlling the camera. Images were then manually transferred over the network to a laptop computer dedicated to processing of the IR images. Camera span and level parameters were automatically adjusted to optimize visual contrast on the computer screen for the expected downcore temperature variation. A physical properties scientist or technician observed the scan results visually, either by following the camera-mounted monitor or by looking at the monitor connected to the computer controlling the scan. As soon as each scan was completed, scientists typically examined the scan results on the laptop computer running ThermaCam Researcher software in the core laboratory. The locations of thermal anomalies were marked on the core and whole-round samples (e.g., hydrate and microbiology samples) were collected as defined by the core-sampling plan for the hole. After catwalk sampling, the cores were cut into 1.5-m sections and many cores were reimaged to provide an image sequence matching the length of the curated core sections.

The track-mounted IR imaging camera was supplemented on most cores by discrete imaging using a second FLIR Systems camera or an AVIO Neo Thermo camera in a handheld mode (Fig. F10). In this mode, a physical properties scientist walked along the catwalk with the IR camera pointed perpendicular to the core liner, usually just after the track scan was completed. This approach provided immediate confirmation of temperature anomalies from a viewpoint rotated 90° from the orientation of the track scan. If anomalies were detected, they were marked on the core, stored on the camera's memory card, and logged on a log sheet; later, the files were transferred to the ship's computer network for storage, analysis, and archiving. Temperature anomalies detected with the handheld camera were compared with the track scans, and decisions were made to guide the sampling of any gas hydrate present.

In some instances, subtle thermal anomalies or observations of gas escaping from holes drilled into the core liner triggered the decision to perform an additional track scan. Results from successive scans could then be directly compared; typical results show the spatial expansion of cold zones over time periods of only a few minutes.

Image Processing

To develop downcore profiles of temperature anomalies, the following procedures were established, building on the experience from Leg 201:

1. ThermaCam Researcher software was embedded as an object into a Microsoft Excel spreadsheet. The folder containing sequential images from the core scan was selected and opened in Researcher.
2. An analysis box was used to extract temperature data from the central part of the core image.
3. In Microsoft Excel, a macro was written to extract the pixel-by-pixel temperature values as ASCII data.
4. These ASCII data were then transferred to a UNIX workstation to extract the pixel-by-pixel temperature values from the analysis box imbedded in each image as well as the depth of the center of each image. Depths were then calculated and assigned to each pixel in successive images from a given core.

Following this process, the data files were combined to provide profiles of downhole temperature anomalies. Where core recovery was >100%, the overlapping depth interval was manually edited and the data were deleted from the resulting profile.

Extraction of Thermal Anomaly Data

Downcore thermal profiles and IR images were used to extract individual negative thermal anomalies (cold zones on the core liner). Parameters obtained were (1) core and section (if available); (2) depth interval on uncut liner (top and bottom); (3) ΔT (peak anomaly temperature–background temperature); and (4) gas hydrate texture or shape description and other comments on anomaly shape. A unique identifier was assigned to each IR anomaly for reference in text and figures. Results were tabulated for each site. Thermal anomalies were identified from the downcore temperature profiles derived from the images

as described in the previous section. An analysis of thermal data on board showed that ΔT values indicative of hydrate were insensitive to ambient catwalk temperature and illumination conditions. The ΔT values provide an approximate measure of hydrate abundance, albeit influenced by the proximity of hydrate to the core liner. Gas hydrate undergoing dissociation and directly in contact with the core liner produces a larger ΔT than hydrate insulated from the liner by sediment.

It is important to note that depth measurements were recorded on uncut core liners before sectioning and removal of gas voids. Hence, depth assignments do not precisely match the curated depths of core sections; typically depth differences are <1 m. Hydrate samples are included on IR anomaly tables and provide specific data on curated and uncut core-liner depth discrepancies.

Comparison of Thermal Anomaly Data with S_w

Extracted thermal anomalies were plotted as a function of depth and, for many sites, compared with pore water saturation (S_w) derived from resistivity logs using Archie's Relation (see **"Downhole Logging,"** p. 43). The visual comparison of the two data sets provided a useful means of assessing the overall similarity of the two methods in detecting differences in gas hydrate abundance as a function of depth. Calculation of S_w is ordinarily used to estimate volume fraction of pore space occupied by pore water in a homogeneous media as opposed to a more resistive fluid such as gas or liquid hydrocarbons. In the GHSZ, it is assumed that the resistive material is gas hydrate, which may be present in veins that are very heterogeneous. This heterogeneity may cause large errors when calculating S_w in a hydrate-bearing sediment and hence should be used with caution. S_w estimates from Hydrate Ridge typically range from 1.0 to 0.5 (usually 1.0 to 0.85), but in some cases (Site 1249) values as low as ~0.1 were obtained. These values are interpreted as

$$1 - S_w = \text{volume fraction of hydrate}, \quad (5)$$

including all hydrate regardless of size of hydrate features (not just pore scale hydrate). IR anomalies and S_w were plotted back-to-back with depth on the ordinate, ΔT increasing to the left, and S_w increasing to the right on the abscissa. The position of the S_w plot extending to the right from the abscissa provides a visual depiction of the estimated hydrate concentration for direct comparison with the IR thermal anomalies. Values >1 (physically impossible) are truncated in this and other plots of S_w in this volume.

Definition of Terms for Hydrate Shapes

A variety of gas hydrate shapes were observed during the leg, providing significant new insight into how those shapes and textures are distributed in marine sediments. Usage of terms for describing hydrate shapes evolved during the leg as sites were drilled. Defining terms used is particularly important for hydrate studies because of the ephemeral nature of gas hydrates. Gas hydrates must be either described within minutes after sampling and prior to dissociation or they must be preserved in pressure vessels or liquid nitrogen where, for the most part, they are not available for further description shipboard. However, IR imaging provided permanent information on hydrate shapes to a reso-

lution of ~0.5 cm. These IR images together with visual observations and photographs of gas hydrate form the basis for the terms described below to define terms defining macroscopic (scales approximately ≥0.5 cm) geometries of gas hydrates:

Layer: tabular gas hydrate feature that transects the core conformable to bedding. Its apparent thickness is, typically, on the order of a few centimeters. Layers thicker than ~10 cm are generally considered massive hydrate (interval 204-1250C-11H-3, 94–95 cm). See Figure **F11F.**

Lens: a hydrate layer or other feature with tapering margins. Many hydrate layers may be lenses on a scale larger than the core diameter. See Figure **F11.**

Vein: tabular gas hydrate feature that transects the core at an angle to bedding. Its apparent thickness is, typically, on the order of a few centimeters. Veins thicker than ~10 cm are generally considered massive hydrate (interval 204-1244C-8H-1, 47–52 cm). See Figure **F11D.**

Veinlet: thin, tabular hydrates ~1 mm thick or less, commonly present adjacent to veins or layers and oriented in mutually orthogonal directions. Veinlets are visible by eye or with the aid of a hand lens but were commonly the smallest macroscopic hydrate features observed during Leg 204. See Figure **F8C,** p. 43, in the "Site 1249" chapter.

Nodular: spherical to oblate features typically 1–5 cm in diameter. Two-dimensional circular shapes in IR images on core liners are usually described as nodular, recognizing that 3-D shapes may actually be blades or rods. Shipboard examination of liquid nitrogen–preserved cores clearly shows that some nodular IR features are, in fact, nearly spherical in shape, whereas others are rod or blade shaped with long dimensions significantly greater than the core diameter (interval 204-1244C-10H-2, 70–103 cm). See Figure **F11B.**

Disseminated: hydrate grains less than ~3 mm distributed throughout the sediment matrix. This includes grain size ranging from ~3 mm to pore scale and produces IR anomalies that have diffuse boundaries. IR data typically cannot distinguish between disseminated hydrate and a single hydrate nodule in the center of the core. Any distributed form of hydrate with a small dimension <3 mm may be described as disseminated (interval 204-1249C-2H-1, 108–140 cm). See Figure **F11A.**

Massive: the presence of hydrate in core greater than ~10 cm in thickness and with less than ~ 25% intercalated sediment (Section 204-1249C-1H-CC). See Figure **F11C.**

F11. Typical gas hydrate shapes observed, p. 78.

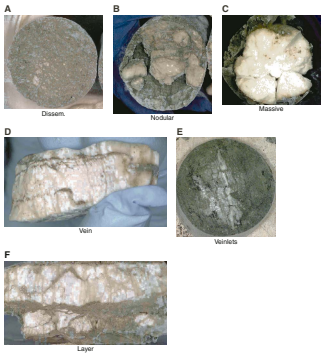

Multisensor Track Measurements

The MST has four physical property sensors mounted on an automated track that sequentially measure MS, gamma ray attenuation (GRA) density, V_P, and natural gamma emissions on intact whole-round core sections. We concluded that at low count times the natural gamma data would not contribute to the leg objectives. Therefore, we did not run the natural gamma system during Leg 204. However, we did have the opportunity to test the new Geotek Non Contact Resistivity (NCR) system.

Whole-core MST measurements are nondestructive to sediment fabric and can be used as proxies for other data as well as for facilitating core-to-core correlation between adjacent holes at the same site or among different sites. These correlations between holes can be used to construct composite stratigraphic sections at a single site and to correlate core data with measurements made by downhole tools. Each device has an intrinsic downcore spatial resolution determined by its design specifications (see discussion of each measurement below). Data quality is a function of both core quality and sensor precision. Optimal MST measurements require a completely filled core liner with minimal drilling disturbance. Precision is a function of measurement time for MS and GRA density but not for V_P. The spatial interval used for all sensors was generally set at 2.5 cm.

At the end of Hole 1251B operations, we discovered, while checking the new position of the NCR system, that the positions of the other sensors on the track as entered into the configuration set up in the controlling computer had a small error. The positions are measured from the end of the water check sample to the sensor. Table T3 shows the original positions (for Hole 1251B; before 29 July 2002 at 2235 hr) that are in error, the actual measured position, and the new positions as entered (for Hole 1251B; before 29 July at 2235 hr).

T3. MST sensors, p. 97.

Prior to the adjustment and including data from previous legs, we concluded that offsets between MST data and core position are in error by 1.3 cm, whereas after the change, the error was reduced to 0.5 cm.

Magnetic Susceptibility

Whole-core volume MS was measured using a Bartington MS2 meter coupled to a MS2C sensor coil with a diameter of 8.8 cm operating at 565 Hz. The measurement resolution of the MS2C sensor is a function of many factors but is generally taken to be around 3–4 cm. The instrument has two fixed integration periods of ~1 and 10 s. During Leg 204, MS was routinely measured at a spacing of 2.5 cm, with the average of three 1-s data acquisitions being recorded for each sample location, unless otherwise stated. The instrument automatically zeroes and records a free-air value for MS at the start and end of each section run. Instrument drift during a section run is then accommodated by subtraction of a linear interpolation between the first and last free-air readings. Drift-corrected MS data were archived as raw instrument units (SI) and not corrected for changes in sediment volume. Therefore, the data is reported as "uncorrected volume susceptibility."

Gamma Ray Attenuation Density

GRA density was determined using the GRA densitometer. This sensor system measures the attenuation (mainly by Compton scattering) of a gamma beam caused by the average electron density in the gamma path. A well-collimated gamma beam (primary photon energy of 662 keV) is produced from a small (370 MBq; ~1994) ^{137}Cs source (half-life = 30.2 yr) and passes through an assumed known thickness of sediment (internal diameter of core liner). At the start of Leg 204, we discovered that the energy counting window was incorrectly set, as it was counting a significant number of low-energy photons (Compton scattered). For the most accurate results, it is important to only count the unattenuated photons (662 keV); hence, the window should be set evenly

around the ^{137}Cs peak but beginning at the base of the "Compton trough."

The measurements are most empirically related to the bulk density of the material, and hence, the data are often referred to as "wet bulk density." However, we believe this to be slightly confusing and prefer to refer to this data set as "gamma density," or GRA density, which we then compare to wet bulk density measured by MAD gravimetric techniques. Although the empirical calibration procedure for GRA is based on bulk density measurements (i.e., of a known graduated aluminum and water standard), the measurements will vary from true gravimetric bulk density because of variations in mineralogy. Gamma attenuation coefficients for different materials vary as a function of atomic number. Fortuitously, most earth-forming minerals have similar and low atomic numbers (similar to aluminum). Consequently, the correlation of GRA density and bulk density is usually very good. In summary, GRA density should be considered as the density of sediment and rocks as determined from GRA measurements using aluminum and water as reference materials.

The gamma source collimator is 5 mm, which produces an effective downcore spatial resolution of ~1 cm. Following our detailed setup and calibration procedure, we logged the graduated aluminum and water standard as a check to confirm accurate calibration. These data indicate an excellent calibration and illustrate the downcore spatial resolution (Fig. **F12**). The minimum integration time for a statistically significant GRA density measurement is 1 s. During many ODP legs, a count time of 2 s is used. However, we considered this count period to be too short and used a 5-s count time throughout Leg 204 in order to improve precision. A freshwater control was run with each section to measure instrument drift. GRA data are of highest quality when measured on nongassy APC cores because the liner is generally completely filled with sediment. In XCB cores, GRA measurements can often be unreliable (unless the sample points are very carefully chosen) because of the disturbance caused by the mixing of drilling slurry and core biscuits.

F12. GRA profile, p. 79.

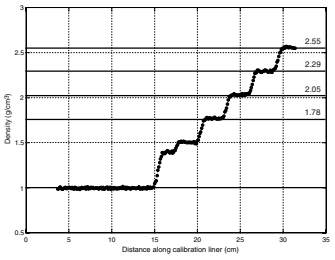

Non Contact Resistivity System

Electrical resistivity of sediment cores has been measured during a number of ODP legs in an ad hoc manner on split cores. This has usually been done by inserting electrodes into the split core or by placing an array of electrode pads on the open surface of split cores. It has long been recognized that resistivity measurements provide important information that can be used to further understand sediment facies and geochemical processes. Combination logs of resistivity and density provide pertinent lithologic information (grain size/permeability/tortuosity) that cannot be achieved with other nondestructive measurements. Pore water salinity also influences the resistivity of sediments; hence, resistivity is valuable as a continuous log for geochemical purposes. However, it has proved a difficult parameter to measure in a fully automated, nonintrusive, and routine manner. The relatively new Geotek NCR system, which overcomes these difficulties, was installed for trial purposes during Leg 204 to test the possible value of this new sensor system.

Measurement of sediment resistivity using the NCR system can be made rapidly on a whole core in the plastic liner and, hence, is an ideal additional component to the MST. Consequently, during the first part of Leg 204, it was installed as an integral component of the MST for test

purposes. It was not available for routine measurements until Hole 1251B but was then used at a number of sites during the remainder of the leg. The NCR technique operates by inducing a high-frequency magnetic field in the core from a transmitter coil, which in turn induces electrical currents in the core that are inversely proportional to the resistivity. A receiver coil measures very small magnetic fields that are regenerated by the electrical current. To measure these very small magnetic fields accurately, a difference technique has been developed that compares the readings generated from the measuring coils to the readings from an identical set of coils operating in air. This technique provides the accuracy and stability required. Resistivities between 0.1 and 10 Ωm can be measured at spatial resolutions along the core of ~2–4 cm. As with other parameters, the measurements are sensitive to core temperature and should be obtained in a stable temperature environment for best results.

Calibration was achieved by filling short lengths (~25 cm each) of core liner core with water containing known concentrations of NaCl. This provides a series of calibration samples with known resistivities that are then placed on the MST and logged. The logged results are illustrated in Figure **F13A**, which shows the raw output data in millivolts decreasing with decreasing salinity. The drop in output between the calibration sections illustrates the effect of having complete insulating gaps between the samples. Averaged values in each salinity are then plotted against the theoretical resistivity in Figure **F13B,** which provides a power-law calibration equation.

F13. Calibration plots for the NCR system, p. 80.

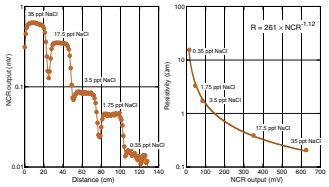

Compressional Wave Velocity

Transverse V_P was measured on the MST track with the *P*-wave logger (PWL) for all cores at a routine sample interval of 2.5 cm. The PWL transmits a 500-kHz *P*-wave pulse through the core at a specified repetition rate (50 pulses per second). The transmitting and receiving ultrasonic transducers are aligned so that wave propagation is perpendicular to the core axis. Core diameter is measured using two displacement transducers that are mechanically linked to the ultrasonic transducers. The recorded velocity is the average of the user-defined number of acquisitions per location (10 during Leg 204). Calibrations of the displacement transducers and measurement of electronic delay within the PWL circuitry were conducted using a series of acrylic blocks of known thickness and *P*-wave traveltime. Repeated measurements of V_P through a core liner filled with distilled water at a known temperature were used to check calibration validity. The Hamilton Frame discrete method of measuring velocity (PWS3) on the split track was used to occasionally check the MST values. In fact, we discovered a significant PWS3 measurement error (50 m/s), caused by a worn displacement transducer, which was corrected by adjusting the transducer to a new location.

The PWL was generally not used when cores were taken with the XCB, as the poor core quality precluded reliable velocity measurements. Normally, the undisturbed biscuits of primary sediments are surrounded by lower-velocity drilling slurry. Consequently, in XCB cores, we attempted to obtain velocity measurements by extracting undisturbed fragments of material and trimming them for use in the split-core PSW3 velocity system (see below).

Compressional Wave Velocity (PWS1, PWS2, and PWS3)

Sediment V_P was also measured on the split liner with the ODP standard Hamilton Frame PWS3 system, which is composed of two transducer pairs that take measurements transversely through the core liner or directly on sediment fragments ("chunks"). The system determines V_P based on the traveltime of a 500-kHz wave between a pair of piezoelectric crystals separated by a variable distance (measured using displacement transducers). System accuracy was checked by measuring the velocity of acrylic samples. In addition, the PWS1 and PWS2 velocity sensors were used on selected cores to determine velocity anisotropy in the upper 10 mbsf, where gas expansion effects least affected the sediment quality.

Routine sampling frequency and location for *P*-wave measurements were generally coincident with the discrete MAD samples. Note that the velocity data stored in the Janus database are uncorrected for in situ temperature and pressure. These corrections can be made using the relationships outlined in Wyllie et al. (1956), Wilson (1960), and Mackenzie (1981). Poor core quality in deeper sections (generally in XCB cores) and abundant gas-expansion cracks and voids inhibited reliable measurements throughout Leg 204.

Thermal Conductivity

Thermal conductivity measurements on whole-core samples were made using the TK04 (Teka Bolin) system described by Blum (1997). Measurements were generally made once per core (generally within Section 3) but were increased to three per core where downhole temperature measurements were taken. The measurement system employs a single needle probe (von Herzen and Maxwell, 1959) heated continuously in "full-space configuration." At the beginning of each measurement, temperatures in the samples were monitored automatically, without applying a heater current, until the background thermal drift was <0.04°C/min. Once the samples were equilibrated, the heater circuit was closed and the temperature rise in the probe was recorded. The needle probe contains a heater wire and calibrated thermistor. The probe is assumed to be a perfect conductor because of its high conductance relative to the core sediments. With this assumption, the temperature of the superconductive probe has a linear relationship with the natural logarithm of the time after the initiation of heating,

$$T(t) = (q/4k)\ln(t) \pm Cz, \quad (6)$$

where

T = temperature,
q = heat input per unit length per unit time,
k = thermal conductivity,
t = time after the initiation of the heat, and
C = constant.

The thermal conductivity (k) was determined, using equation 6, by fitting the temperatures measured during the first 150 s of each heating experiment (for details see Kristiansen, 1982; Blum, 1997).

The reported thermal conductivity value for each sample is the average of three repeated measurements. Data are reported in W/(m·K), with measurement errors of 5%–10% in high-quality cores.

Moisture and Density Analysis

MAD parameters were determined from wet mass, dry mass, and dry volume measurements of split core sediments after method C of Blum (1997). Push-core samples of ~10 cm^3 were placed in 10-mL glass beakers. In stiffer sediments drilled with the XCB where no push-core samples could be retrieved, samples were taken in small biscuits. Care was taken to sample undisturbed parts of the core and to avoid drilling slurry. Immediately after the samples were collected, wet sediment mass (M_{wet}) was measured. Alternatively, the sample was temporarily covered with parafilm to prevent any moisture loss prior to weighing. Dry mass and volume were measured after samples were heated in an oven at 105°C for 24 hr and allowed to cool in a desiccator. Sample mass was determined to a precision of 0.01 g using two Scientech 202 electronic balances and a computer averaging system to compensate for the ship's motion. The reference mass was always set to be within a 5-g margin of the actual sample weight. Sample volumes were determined using a helium-displacement Quantachrome penta-pycnometer with a precision of 0.02 cm^3. Volume measurements were repeated five times, until the last two measurements exhibited <0.01% standard deviation. A reference volume was used to calibrate the pycnometer and to check for instrument drift and systematic error. After a calibration run for all five cells, two runs of measurements of five samples each were conducted before repeated calibration. The time required to run 10 samples, including a calibration, was ~2.5 hr. Sampling frequency was typically one per section, but it was decreased if uniform lithology was encountered throughout the core.

Moisture content, grain density, bulk density, and porosity were calculated from the measured wet mass, dry mass, and dry volume as described by Blum (1997). Corrections were made for the mass and volume of evaporated seawater using a seawater density of 1.024 g/cm^3 and a salt density of 2.20 g/cm^3.

Torvane Shear Strength Measurements

Shear strength measurements are extremely difficult to obtain in the gas hydrate–bearing sediments encountered during this leg. Gas expansion and the presence of hydrate destroy the sediment fabric and do not allow for reliable shear strength measurements. Consequently, the automated shear vane equipment was not used except on selected cores, normally at shallow depth above 10 mbsf. However, we measured shear strengths using a handheld Torvane wherever the sediment conditions permitted. The device is quick to use and comes with three vane sizes: small, medium, and large (19, 25, and 48 mm diameter), providing maximum shear strength measurements up to 250, 100, and 20 kPa, respectively.

Gas Expansion Effects

Most of the cores recovered during Leg 204 suffered significant disturbance caused by gas-expansion effects. Expansion of free gas, exsolu-

tion of dissolved gas, and dissociation of hydrate can cause gas expansion effects. It is worth noting here that a unit volume of free gas at 1000 m below the sea surface will expand by a factor of 100 by the time it reaches the surface (ignoring any temperature expansion or further exsolution). Another way of visualizing the expansion of gas during the core recovery process is to consider that a 0.1-mm-diameter free gas bubble in the sediment matrix at a depth of 1000 m will become a 4.5-mm-diameter gas bubble at the sea surface. When relatively low volumes of gas exsolve from pore fluids during core recovery, small bubbles will form in the sediment matrix with only minor amounts of core-volume expansion. As the gas volumes become greater, the sediment structure begins to fracture and a large amount of core expansion occurs, forming a series of large gas voids in the core. This process takes some time but is readily visible on the catwalk. When core expansion occurred, the core was generally pushed back together prior to sectioning, but inevitably these fractures remain in the core and affect the physical property measurements to some extent.

MS measurements are probably the least affected by core expansion, as these measurements depend only on the sediment/mineral volume. After the core has been pushed back together, the overall mineral volume changes over a 4-cm interval (the approximate spatial resolution of the sensor) is fairly small; therefore, significant effects are only seen where there are still clear gas gaps (greater than ~1 cm).

GRA measurements can be significantly affected by gas voids and sediment cracks. The downcore spatial resolution is ~1 cm, and hence, all cracks, no matter how minor, will show up in the GRA density profile. With significant degassing in many cores, this effect shows up as a very "noisy" data set. These data are, in fact, quite accurately representing the state of the core but of course do not represent the in situ condition. The closest representation of the in situ condition is achieved by taking the upper values of the GRA data envelope. However, even these values are often lower than the in situ densities because of gas in the matrix. The reader should see the data summaries and comparisons with downhole logs.

Gas expansion has the largest effect on the measurement of ultrasonic V_P. Even very small amounts of free gas in the sediment matrix (<1%) will cause a significant decrease in velocity. More importantly, the very high attenuation of *P*-waves at ultrasonic frequencies in sediments with even very low volumes of free gas makes the measurement of velocity all but impossible. During Leg 204, we generally encountered gas-rich sediments in which V_P measurements were possible only in the upper few meters. In practice, we observed that V_P was generally only measurable above the sulfate/methane interface (SMI). Below the SMI, the gas exsolved generally prevented the acquisition of reliable data.

Gas expansion has little, if any, effect on the gravimetric determination of bulk density if the samples are carefully chosen. Small gas bubbles that form in the sediment matrix will not cause any effect on the wet-weight measurement or the dry-volume measurement and, hence, on the calculated bulk density and porosity values. The only time that gas expansion will have an effect on these measurements is when cracks in the sediment have caused premature drying. Even this effect is negated if the sampling is carried out promptly after core splitting.

Nearly all of the above effects of core disturbance caused by gas expansion do not occur when the physical property measurements are

made at in situ pressures. This is one of the primary reasons for collecting pressure cores and analyzing them in the V-MSCL (see "Downhole Tools and Pressure Coring," p. 34, for information about the use of the systems of pressure coring and to the appropriate site chapter where results are described in detail). Where comparisons between different data sets are appropriate, they are included in the site chapters.

To illustrate the pervasive nature of gas expansion throughout Leg 204, even in cores that did not apparently expand on the catwalk, we imaged an APC section through the liner before it was split. Figure F14 shows the nature of this cracking in a typical APC core (Section 204-1251G-1H-6). The image was obtained with the Geotek XY-DIS using a procedure known as "virtual slabbing." This is achieved by calibrating the camera on a white sheet of paper wrapped around the core rather than the flat white tile. A white calibration is achieved that compensates for the changes in illumination across the curved surface, providing a flat looking "slabbed" final image.

F14. Gas expansion cracks, p. 81.

DOWNHOLE TOOLS AND PRESSURE CORING

During Leg 204, a suite of downhole tools was employed to measure in situ temperature and pore pressure, to retrieve cores under pressure, and to estimate the in situ concentration of methane and other natural gases. Temperature, pressure, and gas composition and concentration are the critical factors for determining the extent of the GHSZ and whether gas hydrate can form in that zone. In addition, temperature effects rates of sediment diagenesis and microbial activity. Pore pressure is important because fluid flow occurs if the pressure gradient differs from hydrostatic, thus transporting natural gas into the GHSZ, providing nutrients for microbes, and modifying the temperature and pressure field.

In situ sediment thermal measurements were made during Leg 204 using the APC temperature (APCT) tool and the Davis-Villinger Temperature Probe (DVTP) (Davis et al., 1997). Temperatures and pressures were measured using a DVTP modified to include a pressure port and sensor (Davis-Villinger Temperature-Pressure Probe [DVTPP]) that was previously used during Legs 190 and 201. Pressure was also measured during a trial run of the Fugro-McClelland piezoprobe, which operates on similar principles as the DVTPP.

Retrieval of cores at in situ pressure was a high priority during Leg 204. Natural gas in deep sediment may be present in three phases. If the concentration (molality) of gas in pore water is less than the solubility, the gas is dissolved. If the concentration of gas is greater than its solubility, gas is present as a free phase (bubbles) below the GHSZ and as solid hydrate within the GHSZ. Knowledge of the gas concentration in deep sediment is critical for understanding the dynamics of hydrate formation and the effect hydrates have on the physical properties of the sediment. However, reliable data on gas concentration are difficult to obtain. Because gas solubility decreases as pressure decreases and temperature increases, cores recovered from great depth often release a large volume of gas during recovery (Wallace et al., 2000; Paull and Ussler, 2001). The only way to determine true in situ concentrations of natural gas in the subseafloor is to retrieve cores in an autoclave that maintains in situ conditions. The original ODP pressure core sampler (PCS) has proven to be an essential tool that is very effective for estimating in situ gas concentrations (Dickens et al., 1997, 2000b) and was used extensively during Leg 204. However, it is less effective for studies

of physical properties of gas hydrate–bearing sediments at in situ conditions.

The HYACINTH (deployment of Hydrate Autoclave Coring Equipment [HYACE] tools in new tests on hydrates) program, funded by the European Union (EU), is developing the next generation of pressure corers. Both HYACE coring systems were used during Leg 204. The Fugro Pressure Corer (FPC) is designed for sediments that are normally cored with the APC and XCB, and the HYACE Rotary Corer (HRC) is designed to drill more lithified sediments and rocks normally cored with the XCB and RCB. These pressure cores are contained in an inner plastic liner that can be transferred (under full pressure) from the autoclave into other pressure chambers. When transferred into a logging chamber, the pressurized cores can be logged using the V-MSCL. This was used to make measurements on cores collected by the HYACE coring tools and on standard ODP cores repressurized to in situ pressures. By measuring V_P, *P*-wave attenuation, and GRA density at in situ pressures and by pressure cycling, we anticipated being able to distinguish between hydrate and free gas while also measuring some in situ properties that would help to constrain models of hydrate and free gas distribution.

In Situ Temperature and Pressure

Advanced Piston Corer Temperature Tool

The APCT tool fits directly into the cutting shoe on the APC and can, therefore, be used to measure sediment temperatures during regular piston coring. The tool consists of electronic components, including battery packs, a data logger, and a platinum resistance–temperature device calibrated over a temperature range of 0°–30°C. Descriptions of the tool and of the principles behind analysis of the data it acquires can be found in Pribnow et al. (2000) and Graber et al. (2002) and the references therein. The thermal time constant of the cutting shoe assembly where the APCT tool is inserted is ~2–3 min. The only modification to normal APC procedures required to obtain temperature measurements is to hold the corer in place for ~10 min after cutting the core. During this time, the APCT tool logs temperature data on a microprocessor contained within the instrument as it approaches equilibrium with the in situ temperature of the sediments. Following deployment, the data are downloaded for processing. The tool can be preprogrammed to record temperatures at a range of sampling rates. Sampling rates of 10 s were used during Leg 204. A typical APCT measurement consists of a mudline temperature record lasting 10 min for the first deployment at each borehole and 2 min on subsequent runs. This is followed by a pulse of frictional heating when the piston is fired, a period of thermal decay that is monitored for 10 min or more, and a frictional pulse upon removal of the corer.

A second source of uncertainty in these data is possible temporal change of the bottom-water temperature resulting from tides, seasons, and longer-term climate change. Evidence for short-term changes in this region is seen in data from a near-bottom current meter that was deployed for 6 months at a water depth of 800 m in the saddle between the northern and southern summits of Hydrate Ridge (R. Collier, pers. comm., 2000). These data show peak-to-peak tidal variations of up to 0.3°C, a superimposed variation with a timescale of 2 months and peak-to-peak amplitude of 0.04°C, and an apparent seasonal variation of

0.3°C. These multiple sources of bottom-water temperature variation, which occur on a timescale that will not be felt at subseafloor depths greater than a few meters lead to significant temporal variability in the mudline temperature. Because of these observations, it may, in general, be inappropriate to include the mudline temperature when determining the subsurface temperature gradient from downhole temperature data. Mudline temperatures, however, are reported in the data tables because they can provide a useful data point for postcruise studies.

Davis-Villinger Temperature Probe

The temperature measurement aspects of the DVTP are described in detail by Davis et al. (1997) and summarized by Pribnow et al. (2000) and Graber et al. (2002). The probe is conical and has two thermistors; the first is located 1 cm from the tip of the probe and the other 12 cm above the tip. A third thermistor, referred to as the internal thermistor, is in the electronics package. Thermistor sensitivity is 1 mK in an operating range of –5° to 20°C, and the total operating range is –5° to 100°C. The thermistors were calibrated at the factory and on the laboratory bench before installation in the probe. In addition to the thermistors, the probe contains an accelerometer sensitive to 0.98 m/s². Both peak and mean acceleration are recorded by the logger. The accelerometer data are used to track disturbances to the instrument package during the equilibration interval. In a DVTP deployment, mudline temperatures (within the drill pipe) are measured for 10 min during the first run within each hole and for 2 min during subsequent runs, before descent into the hole for a 10-min equilibration time series at the measurement depth in the subseafloor. The time constants for the sensors are ~1 min for the probe-tip thermistor and ~2 min for the thermistor 12 cm from the tip. Only data from the probe tip thermistor were used for estimation of in situ temperatures.

In Situ Temperature Data Reduction

The transient thermal-decay curves for sediment thermal probes are a function of the geometry of the probes and the thermal properties of the probe and sediments (Bullard, 1954; Horai and von Herzen, 1985). Data analysis requires fitting the measurements to predicted temperature decay curves calculated based on tool geometry and the thermal properties of the sediment. Pribnow et al. (2000) discuss data analysis procedures and uncertainties. For the APCT tool, the software program TFIT, developed by K. Becker and J. Craig, was used. The DVTP and DVTPP data can be analyzed using the software program CONEFIT, developed by Davis et al. (1997).

However, during Leg 204, DVTP and DVTPP data were generally noisy and CONEFIT did not yield stable solutions. In some cases, we assumed that the temperature had reached equilibrium. In other cases, no estimate of in situ temperatures was attempted on board.

Figure F15A shows a typical temperature history recorded by the APCT tool. Various stages in the tool-deployment history are marked. Mudline temperature is determined from the time the tool is held near the seafloor prior to penetration of the APC. Initial APC penetration is marked by a temperature pulse resulting from friction. A second pulse is observed when the tool is extracted from the sediment. The best fitting time of penetration and in situ temperature are calculated from data delimited by three points that are picked by the shipboard analyst. The

F15. Typical APCT tool and DVTPP runs, p. 82.

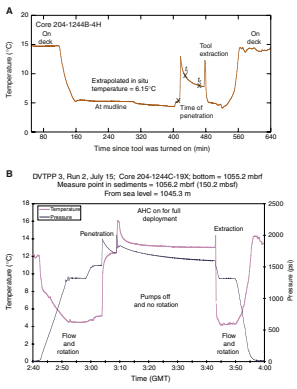

thermal conductivity of the sediment must also be specified. Thermal conductivities measured from the core interval closest to the APCT measurement were used (see **"Physical Properties,"** p. 22). The estimated uncertainty of the derived in situ temperature for good-quality measurements is 0.1°C (Pribnow et al., 2000), although the uncertainty may be considerably larger for poor-quality measurements. Because of problems with instrument calibration that became evident during the leg (see **"Downhole Tools and Pressure Coring,"** p. 29, in the "Site 1244" chapter), temperature gradients may be better resolved than absolute values of temperature, provided the same tool was used to make all measurements at a given site. Additional analysis will be performed postcruise to decrease uncertainty resulting from instrument calibration.

Davis-Villinger Temperature-Pressure Probe

Simultaneous measurement of formation temperature and pressure was achieved using a modified DVTP. The probe has a tip that incorporates both a single thermistor in an oil-filled needle and ports to allow hydraulic transmission of formation fluid pressures to a precision Paroscientific pressure gauge inside. A standard data logger was modified to accept the pressure signal instead of the second thermistor signal in the normal DVTP described above. Thermistor sensitivity of the modified tool is reduced to 0.02 K in an operating range of –5° to 20°C. A typical deployment of the tool is shown in Figure **F15B.** It consists of lowering the tool by wireline to the mudline where there is a 10-min pause to collect data. Subsequently, it is lowered to the base of the hole and latched in at the bottom of the drill string, with the end of the tool extending 1.1 m below the drill bit. The extended probe is pushed into the sediment below the bottom of the hole and pressure is recorded for ~40 min. If smooth pressure decay curves are recorded after penetration, then theoretical extrapolations to in situ pore pressures are possible.

Temperature data from the DVTPP were treated as discussed for the DVTP. For both the DVTPP and the piezoprobe (discussed below), the pressure response is qualitatively similar to, but slower, than the thermal response. The decay time is a function of the sediment permeability and the magnitude of the initial pulse, which is a function of the taper angle and diameter of the tool (Whittle et al., 2001; Heeseman, 2002). Analysis of in situ pressure will be done postcruise.

Fugro-McClelland Piezoprobe

In April 2001, a proposal was submitted to the U.S. Department of Energy to modify and implement the use of the Fugro-McClelland piezoprobe tool on the *JOIDES Resolution* during ODP Leg 204. The piezoprobe has been tested and proven (e.g., Ostermeier et al., 2000; Whittle et al., 2001) on numerous geotechnical cruises that measured pressure and temperature, but it had not been adapted for ODP until Leg 204. To adapt it on the *JOIDES Resolution* for testing and use with the APC/XCB bottom-hole assembly (BHA) required modifications prior to the leg. The modifications made by Fugro-McClelland and ODP were designed to (1) adapt the piezoprobe for a Schlumberger wireline, (2) increase the landing ring size, (3) implement a stabilizer sleeve to prevent bending, (4) shorten the bit to minimize risk of bending, and (5) extend pawls for the four-cone APC bit used on the *JOIDES Resolution.*

The piezoprobe works within the borehole and measures pressure through a transducer at its tip, which is similar to the pop-up pore pressure instrument (PUPPI) (see Schultheiss and McPhail, 1986). The probe is lowered through the drill pipe, measures hydrostatic pressure, and is pushed into the sediment ~1 m beyond the base of the borehole, where pressure is again measured. The resultant pressure vs. time curves for multiple experiments provide estimates of in situ pressure as a function of depth. The pressure decay can be used to evaluate the permeability and coefficient of consolidation (e.g., Elsworth et al., 1998; Schnaid et al., 1997), two parameters that are necessary to describe fluid flow and deformation within the shallow subsurface. The narrow taper of the piezoprobe allows a pressure decay to be measured in low-permeability sediments within an hour, a time frame that is reasonable for use on the *JOIDES Resolution*. The piezoprobe also records temperature data during each measurement. Similar to the APCT tool and the DVTP tool, the temperature decay can be used to estimate in situ temperature.

During Leg 204, the piezoprobe was deployed twice, with the second run being successful (see **"Downhole Tools and Pressure Coring,"** p. 29, in the "Site 1244" chapter).

Comparison between the Piezoprobe and the Davis-Villinger Temperature-Pressure Probe

The DVTPP and the piezoprobe both provide the ability to make estimates of in situ temperature and pressure in low-permeability strata at a relatively quick rate (i.e., multiple measurements per hole and dozens of measurements per cruise). The basic operational procedure for each is similar to that for the temperature tools: (1) insert probe at the base of the borehole, (2) monitor pressure disturbance from probe insertion, and (3) record pressure decay and extrapolate out to infinite time for estimate of in situ pressure. The decay time is a function of the sediment permeability and the size of the initial pulse. The magnitude of the pressure pulse is a function of the taper angle and diameter of the tool (Whittle et al., 2001). The piezoprobe has a narrower diameter (6.4 mm) and smaller taper angle (<2°) than the DVTPP (diameter = 8 mm and taper = 2.5°) and therefore produces a smaller pressure disturbance. Whittle et al. (2001) have demonstrated that it is beneficial to monitor the pressure decay long enough so that a significant proportion of the pulse has dissipated before recovery of the tool; with the piezoprobe, this takes ~2 hr in low-permeability strata (Whittle et al., 2001), longer than is generally allowed for the DVTPP during ODP legs.

Pressure Core Sampler

The PCS is a downhole tool designed to recover a 1-m-long sediment core with a diameter of 4.32 cm at in situ pressure up to a maximum of 10,000 psi (Pettigrew, 1992; Graber et al., 2002). It consists of the inner core barrel and a detachable sample chamber (Fig. **F16**). When its valves seal properly, controlled release of pressure from the PCS through a manifold permits collection of gases that would otherwise escape on the wireline trip. The PCS currently provides the only proven means to determine in situ gas abundance in deep-sea sediments where gas concentrations at depth exceed saturation at atmospheric pressure and room temperature (Dickens et al., 1997). The analysis of recorded data (e.g., time series of pressure and the volume of released gas) may also

F16. PCS depressurization experiment, p. 83.

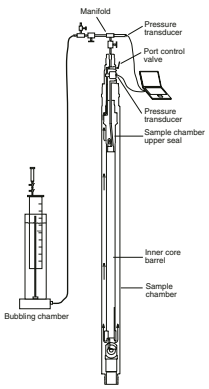

help to determine if gas hydrate is present in the cored interval (Dickens et al., 2000b).

After retrieval, the PCS is placed into an ice bath to keep the inside temperature at ~0°C. A manifold is connected to the PCS to decrease pressure by releasing gas under manual control. Only a small volume of gas (~100–150 mL) should be collected during the first gas release. This is because it has been empirically determined that the first gas sample thus obtained is contaminated by air. Additional gas releases should lead to immediate pressure drops. Ideally, the pressure in the PCS should then increase with time as gas exsolves from pore water or from decomposing gas hydrate. Gas should be released when pressure does not increase significantly over a 10- to 15-min time interval, and the process should be repeated. Sometimes gas may be released before the pressure has built up because of constraints with operational logistics. At the end of the experiment, ice should be removed from around the PCS and the PCS should be warmed up to release all gas remaining in the core. Splits of gases are collected into a 1-L bubbling chamber that consists of an inverted graduated cylinder placed in a plexiglass tube filled with a saturated NaCl solution. After measuring the volume of collected gas, gas aliquots are sampled from a valve at the top of the cylinder using a syringe.

Prior to Leg 204, the PCS was successfully used to study in situ gases during ODP Leg 164 on the gas hydrate–bearing Blake Ridge (Paull, Matsumoto, Wallace, et al., 1996; Dickens et al., 1997) and during Leg 201 at sites along the gas-rich Peru margin (Dickens et al., 2003). One of the objectives of PCS use during Leg 201 was to test the coring capabilities in a variety of lithologic conditions. Several modifications to the PCS were made prior to Leg 201 (Dickens et al., 2003), including the addition of an optional cutting shoe for rotary coring and the construction of a new gas manifold (see "Downhole Tools" in Dickens et al., 2003). The PCS was deployed 17 times during Leg 201. Dickens et al. (2003) concluded that (1) the tool performed better during Leg 201 than on Leg 164, (2) the PCS can operate successfully in a variety of submarine environments, and (3) cores collected at shallow sediment depth can be degassed to generate gas concentration profiles.

Two significant modifications were made between Legs 201 and 204 in order to better address the scientific objectives of Leg 204. First, a methane tool was installed inside the PCS to measure temperature, pressure, and conductivity during the PCS recovery (see below). Second, pressure transducers that permit continuous monitoring of pressure both on the manifold and inside the PCS were installed. Pressure is recorded on a personal computer every 5 s and is presented as a graph during the experiment. An ASCII file of the data is preserved at the end of the experiment. These modifications should permit better monitoring of pressure and temperature inside the PCS after the core is retrieved from the subsurface.

Methane Tools (Advanced Piston Corer Methane Tool and Pressure Core Sampler Methane Tool)

The APCM and the PCS methane tool (PCSM) continuously record the temperature, pressure, and electrical conductivity changes in the core headspace from the time the core is cut through its ascent to the rig floor. The APCM sensors are mounted in a special piston head on the standard ODP APC piston, and the data acquisition electronics are embedded within the piston. The PCSM is a slimmed-down version of

the APCM, which is mounted on the top of the PCS manifold mandrel. Both tools operate passively and require little shipboard attention. Variations in the relative amounts of gas stored in different types of sediment can be determined by establishing families of ascent curves composed of data from successive cores. Models indicate that these data will also provide information on whether gas hydrate was present in the sediment before core retrieval. The methane tools are being developed jointly by ODP and Monterrey Bay Aquarium Research Institute (MBARI). They are derivatives of MBARI's Temperature-Pressure-Conductivity (TPC) tool.

Both tools are very similar in construction, the only difference being that the APCM replaces the piston-rod snubber in the APC coring system and therefore has a seal package on its exterior. The tools consist of an instrumented sensor head with the electronics and battery pack housed in a sealed case. The three sensors (temperature, pressure, and conductivity) and a data port are packaged in the face of the $2^3/_8$-in-diameter sensor head. The temperature sensor is a ±0.05°C accuracy thermistor installed in a $^3/_{16}$-in-diameter × ¼-in-long probe. The pressure sensor is a 0- to 10,000-psi "Downhole Series" transducer with a ±0.15% full-scale accuracy that is especially designed for temperature stability. The electrical conductivity sensor is a three-pin bulkhead connector with an inconel body and gold-plated 0.040-in-diameter Kovar pins. The data port is a three-pin keyed bulkhead connector for RS-232 communication. The electronics consists of two boards, an analog to digital (A/D) board and a commercial microcontroller board. The microcontroller board plugs directly into the A/D board, and the A/D board is mounted on an aluminum backbone. The microcontroller includes a Motorola 68338 processor, a DOS-like operating system, and 48 MB of flash memory. The A/D board is an ODP/MBARI-designed board with one A/D device for the pressure transducer and one for the thermistor and conductivity sensors. The battery pack consists of an assembly of two double-C lithium/thionyl chloride batteries in series and an integral hard-mounted nine-pin connector. The 1-in-diameter × 9-in-long battery pack provides 7.3 V, with a 100-mA rating. The APCM is installed on the APC piston after the APC piston-rod snubber and pistonhead body is removed from the lower piston rod. The connection at the lower piston rod consists of a threaded connection with a transverse spring pin running through the thread relief. The spring pin prevents the connection from unscrewing as a result of vibration. After the spring pin is punched out, the piston-rod snubber is removed and replaced with the APCM. This swap-out operation takes <3 min. The PCSM replaces the accumulator on the PCS and threads onto the top of the PCS manifold mandrel.

The APCM and PCSM tools were successfully deployed 107 times during Leg 204 (see Table **T3,** p. 73, in the "Leg 204 Summary" chapter), but all data analysis was deferred until postcruise. Data and results will be presented in the Leg 204 *Scientific Results* volume.

HYACINTH Coring Equipment

Background

Although the PCS was successful during Leg 164, there were a number of aspects worthy of improvement as described by Dickens et al. (2000a). A proposal submitted to the EU resulted in HYACE, which was a 3-yr project aimed at developing new wireline pressure coring tools

that would address a wide range of scientific problems. The HYACE project resulted in the development of two new pressure coring tools. These tools underwent only limited testing on land and at sea during ODP Legs 194 and 201 (Leg 201 was after the end of the HYACE project and at the beginning of the HYACINTH project). The current HYACINTH project is a continuation of the HYACE project and is also funded by the EU. It is designed to bring these new coring tools into operational use and to develop new techniques of subsampling and analyzing cores under pressure. Leg 204 provided the opportunity for further testing and use of these new coring tools. Other important objectives of Leg 204 were to test and use the HYACINTH family of pressure chambers and the core-transfer mechanisms and to measure the physical properties of cores at in situ pressures.

The design and operation of the HYACE tools differs in two significant respects from that of the existing PCS. First, the HYACE tools penetrate the seabed using downhole driving mechanisms powered by fluid circulation rather than by top-driven rotation with the drill string. This allows the drill string to hang stationary in the hole while core is being cut, which should improve core quality and recovery. Second, the HYACE tools recover lined cores, which enables them to be transferred under pressure into a family of chambers, allowing cores to be preserved and studied under pressure.

Two different coring tools have been developed in order to accommodate a wide range of lithologies, a "percussion" corer and a "rotary" corer. Both tools have been designed for use with the same ODP BHA as the PCS (i.e., the APC/XCB BHA). The FPC is designed for recovering unlithified sediment ranging from clay to sand and gravel. When used in a gas hydrate–bearing environment, it is considered to be most applicable where any hydrate present has not significantly cemented the sedimentary particles. The core barrel is driven into the sediment by a hammer mechanism that is driven by fluid circulation. In soft sediments, the core barrel strokes out quickly so that in these lithologies the FPC essentially behaves like a push core.

The HRC is designed to cut a rotary core in more lithified sediment formations and incorporates a downhole mud motor. A dry auger-type of bit, extending beyond the reach of the circulating seawater, is used to cut the core, providing as contamination-free a core as is possible with rotary coring. It is designed, primarily, to recover cores in well-lithified sediments and rocks that can be obtained with the XCB and RCB. The phase II PCS development proposed by Pettigrew (1992) is similar to the approach used in the HRC. However, this was not pursued by ODP because of insufficient funds.

Both the FPC and the HRC use specially designed but different flapper valves to seal the tool's pressure chamber (autoclave), where the core is contained on recovery. This enables larger cores to be cut than with the PCS, which uses a ball valve as the sealing mechanism. The FPC cuts a 58-mm-diameter core, and the HRC cuts a 50-mm-diameter core. Like the PCS, both cores are ~1 m in length. Pressures up to 250 kbar (3625 psi) can be maintained in the present design.

After initial testing on land, the FPC and HRC underwent their first sea trials on the *JOIDES Resolution* at the start of ODP Leg 194. The FPC had limited success in recovering a core under pressure, whereas the HRC encountered significant problems because of its failure to latch properly in the BHA (Rack, 2001). A core was finally cut but was not retrieved under pressure. The FPC had further trials during Leg 201, but hole conditions are thought to have been unfavorable, which pre-

vented the recovery of a pressure core. Valuable lessons were learned during both of these engineering trials of the FPC and the HRC (Rack, 2001), and a number of significant modifications were made to the tools and to the handling procedures prior to the start of Leg 204.

Tool Operations

Both the HRC and the FPC were prepared and assembled on tool trestles located on the port side of the piperacker. Stands of drill pipe normally used from the port side were moved to the starboard side to prevent disruption to the tool preparations as much as possible. The only time the piperacker could not be used was when we added pipe stands during drilling, tripping pipe, and wireline logging. This was particularly helpful in ensuring that the operations went as efficiently as practically possible. The space afforded by using the piperacker was particularly important in view of the fact that the three PCS tools and logging tools were being assembled above the core tech shop.

For deployment, both tools followed similar operational procedures on the rig floor. They were initially transferred from the piperacker working area, where they had been prepared on trestles, into the vertical position. To do this, a tugger line from the derrick was attached to the upper end of the tool while the base of the tool was lowered onto the piperacker skate using the port side racker crane. The tool was then hauled into a vertical position using the tugger line and lowered into the rig floor shuck as the strongbacks were removed. A tugger line supported the heavier strongbacks on the HRC. The tool was deployed in the open drill string and the Drill String Acceleration (DSA) tool was fitted above. When the drill string was closed, the tools were lowered on the wireline while pumping and rotating.

On retrieval from the pipe, both the FPC and the HRC followed a reverse procedure back to the trestles on the piperacker, including replacing the strongbacks. During an early deployment, a problem was encountered whereby the HRC was split into the three main subassemblies as it was removed from the drill string in the vertical position. Although this alleviated the need to reattach the strongbacks when placing the tool subassemblies back to the horizontal position, it took significantly longer and, hence, was subsequently avoided. After disassembly on the trestles, the autoclave was carried to the platform outside the downhole tools laboratory for examination and connection to the pressure transfer system.

Logging Cores at In Situ Pressure

The other components that make up the HYACINTH system used during Leg 204 are the transfer system, the shear mechanism, and the pressure chambers that are used to store and log the cores under pressure. The HYACE transfer mechanism, which consists of a manipulator chamber and a shear mechanism, is used to extract the core under pressure from either the HRC or FPC autoclave and then transfer it into a storage chamber or logging chamber. The shear mechanism cuts the core at the top, removing the “technical part” of the core (piston assembly, etc.) from the core liner containing the sample prior to inserting it into the other chambers. The manipulator can be used to subsequently transfer the core between the logging and storage chambers if and when required.

The specially adapted Geotek V-MSCL was used to measure gamma density and *P*-wave parameters while the cores were under pressure in the HYACINTH logging chambers. It was also used to log regular APC cores that had been repressurized in specially designed logging chambers. The cores were logged vertically to help control the process of degassing during pressure cycling and final pressure release.

As with the PCS, gases exsolved from solution or released by dissociation of gas hydrate were collected into a 1-L bubbling chamber to determine the in situ abundance of gas in the cores. An analysis of the data recorded during the degassing process should help to determine the relative amounts of free gas and gas hydrate present in the cored interval.

Pressurized core logging is unlike normal core logging with the ODP MST or a standard Geotek Multi Sensor Core Logger (MSCL) in that there are two core liners to consider: (1) the thin plastic core liner (the inner liner) and (2) the thicker glass-reinforced plastic (GRP) pressure tube (the outer liner). To calibrate for measurements of V_P and gamma density, similar techniques are used to those developed for the MST and MSCL, which use distilled water and aluminum as standards. In this mode of operation, the inner liner is assumed to have a constant diameter because it cannot be directly measured under pressure. The outer GRP liner was accurately calibrated to account for small variations in diameter and wall thickness along its length. The manufacturing technique necessitates that a change in the internal diameter of ~1 mm occurs along the 1.5 m length. To ensure consistency, the outer liner was always oriented to ensure that the small circumferential variations were effectively negated.

To calibrate V_P, the variations in the total *P*-wave traveltime along the length of the GRP tube were measured when both the inner liner and the GRP were filled with water of known velocity. All data are subsequently corrected as a function of position in the GRP tube. Changes in traveltime as a function of pressure were also measured (up to 200 bar). The measured variation in V_P with pressure is close to the theoretical variation for water. We therefore conclude that the traveltimes in the liner material are essentially constant with changing pressure. In practice, however, *P*-wave data for sediment cores were much harder to interpret than initially thought because of the interference of ultrasonic signals that propagate around the cylindrical GRP liner.

To calibrate the gamma density system, we used the same type of "standard section" as is used with the MST (see **"Physical Properties," p. 22**). During this step, graduated aluminum and water standards are placed in the GRP tube and logged at 2-mm intervals along the core. Consideration is given to the variation in GRP tube diameter by logging the complete tube filled with water and filled with air. We confirmed that there are no pressure effects on the measurements by repeating the experiment at pressures up to 200 bar.

DOWNHOLE LOGGING

The downhole logging program during Leg 204 was specifically designed to obtain the data needed to assess the presence and concentration of gas hydrates on Hydrate Ridge. Several LWD and wireline logging devices were deployed, as described below. Not all tool strings were run in each hole; refer to individual site chapters for details of tool strings deployed at each site.

Logging While Drilling

During Leg 204, four Anadrill LWD and measurement-while-drilling (MWD) tools were deployed at eight of the nine sites cored and drilled on southern Hydrate Ridge. These tools were provided by Schlumberger-Anadrill services under contract with the Lamont-Doherty Earth Observatory Borehole Research Group (LDEO-BRG). LWD surveys were successfully conducted during seven previous ODP legs: Leg 156 (Shipley, Ogawa, Blum, et al., 1995), Leg 170 (Kimura, Silver, Blum, et al., 1997), Leg 171A (Moore, Klaus, et al., 1998), Leg 174A (Austin, Christie-Blick, Malone, et al., 1998), Leg 188 (O'Brien, Cooper, Richter, et al., 2001), Leg 193 (Binns, Barriga, Miller, et al., 2002), and Leg 196 (Mikada, Becker, Moore, Klaus, et al., 2002).

LWD and MWD tools measure different parameters. LWD tools measure in situ formation properties with instruments that are located in the drill collars immediately above the drill bit. MWD tools are also located in the drill collars and measure downhole drilling parameters (e.g., weight on bit, torque, etc.). The difference between LWD and MWD tools is that LWD data are recorded into downhole computer memory and retrieved when the tools reach the surface, whereas MWD data are transmitted through the drilling fluid within the drill pipe by means of a modulated pressure wave, or "mud pulsing," and monitored in real time (see below). MWD tools enable both LWD and MWD data to be transmitted uphole when the tools are used in conjunction. The term LWD is often used more generically to cover both LWD- and MWD-type measurements.

The LWD and MWD tools used during Leg 204 include the resistivity-at-the-bit (RAB) tool, the power pulse MWD tool, the Nuclear Magnetic Resonance (NMR-MRP) tool, and the Vision Neutron Density (VND) tool. This was the first time the NMR-MRP tool was used during an ODP leg. Figure **F17** shows the configuration of the LWD/MWD BHA, and Tables **T4** and **T5** list the set of measurements recorded.

LWD measurements are made shortly after the hole is drilled and before the adverse effects of continued drilling or coring operations. Fluid invasion into the borehole wall is also reduced relative to wireline logging because of the shorter elapsed time between drilling and taking measurements.

The LWD equipment is battery powered and uses erasable/programmable read-only memory chips to store logging data until they are downloaded. The LWD tools take measurements at evenly spaced time intervals and are synchronized with a system on the drilling rig that monitors time and drilling depth. After drilling, the LWD tools are retrieved and the data downloaded from each tool through an RS232 serial link to a laptop computer. Synchronization of the uphole and downhole clocks allows merging of the time-depth data (from the surface system) and the downhole time-measurement data (from the tools) into depth-measurement data files. The resulting depth-measurement data are transferred to the processing systems in the downhole measurements laboratory (DHML) on board the *JOIDES Resolution* for reduction and interpretation.

Depth Tracking Systems

Unlike wireline tools which record data vs. depth, LWD tools record data vs. time. The Anadrill Integrated Drilling and Logging (IDEAL) system records the time and the depth of the drill string below the rig

F17. Drill string used for LWD operations, p. 84.

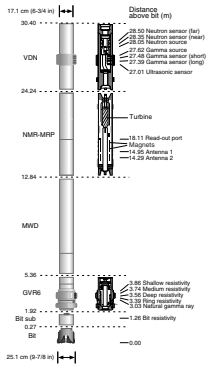

T4. Measurements for LWD and MWD tools, p. 98.

T5. Estimated GVR measurement correction factors, p. 99.

floor. LWD operations aboard the *JOIDES Resolution* require accurate and precise depth tracking and the ability to independently measure and evaluate the movement of the following (Fig. F18):

1. Position of the traveling block in the derrick,
2. Heave of the vessel by the action of waves/swells and tides, and
3. Action of the motion compensator.

F18. Rig instrumentation, p. 85.

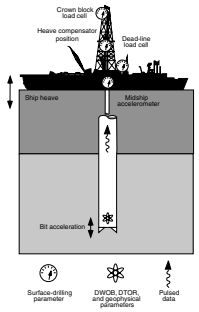

Motion Compensator and Drawworks Encoders

The length of the drill string (combined lengths of the BHA and the drill pipe) and the position of the top drive in the derrick is used to determine the exact depth of the drill bit and rate of penetration. The system configuration is illustrated in Figure F18 and is further described below:

1. Drilling line is spooled on the drawworks. From the drawworks, the drilling line extends to the crown blocks, which are located at the very top of the derrick, and then down to the traveling block. The drilling line is passed several times, usually six or eight times, between the traveling blocks and the crown blocks and then fastened to a fixed point called the dead-man anchor. From the driller's console, the driller controls the operation of the drawworks, which, via the pulley system described above, controls the position of the traveling block in the derrick.
2. On the *JOIDES Resolution,* the heave motion compensator is suspended from the traveling block. The top drive is then attached to the motion compensator. The motion compensator uses pistons that are pressure charged and are thus able to provide a buffer against the waves and swell. As the vessel rises, the pressure on the pistons increases and they extend to keep the bit on bottom, whereas when the vessel drops, the pistons retract and diffuse any extra weight from being stacked on the bit.
3. The drill string is connected to the top drive; therefore, movement of the top drive needs to be measured to provide the drill string depth.

To measure the movement of the traveling blocks a drawworks encoder (DWE) is mounted on the shaft of the drawworks. One revolution of the drawworks will pay out a certain amount of drilling line and, in turn, move the traveling blocks a certain distance. Calibration of the movement of the traveling block to the revolutions of the drawworks is required.

Hookload Sensor

A hookload sensor is used to measure the weight of the load on the drill string and can be used to detect whether the drill string is disconnected from the traveling block and held fast at the rig floor ("in-slips") or not. When drilling ahead, the string is "out-of-slips." When the drill string is in-slips, motion from the blocks or motion compensator will not have any effect on the depth of the bit (i.e., it will remain stationary) and the DWE information does not augment the recorded bit depth. When the drill string is out-of-slips, the DWE information augments the recorded bit depth. The difference in hookload weight between in-slips and out-of-slips is very distinguishable. The heave of the

ship will still continue to affect the bit depth whether the drill string is in-slips or out-of-slips.

Heave Motion Sensors

On the *JOIDES Resolution,* the ability to measure the vessel's heave is addressed in two ways. The rig instrumentation system used by the driller measures and records the heave of the ship and the motion of the cylinder of the active compensator, among many other parameters, at the rig floor. The motion compensator cylinder either extends or retracts to compensate for ship heave that is detected by fixed accelerometers. Both the heave value and cylinder position measurement are transmitted to the Anadrill recording system via the Wellsite Information Transfer System (WITS) line. Software filtering may be used to smooth the time-depth file by applying a weighted average to the time-depth data based on the observed amplitude and period of ship heave. The depth-filtering technique has significantly improved the quality of RAB image logs from previous ODP holes.

Resistivity-at-the-Bit Tools

RAB tools provide resistivity measurements of the formation and electrical images of the borehole wall, similar to the Formation MicroScanner but with complete coverage of the borehole walls and lower vertical and horizontal resolution. In addition, the RAB tool contains a scintillation counter that provides a total gamma ray measurement (Fig. **F19**). Because a caliper log is not available without other LWD measurements, the influence of the shape of the borehole on the log responses cannot be directly estimated.

The RAB tools are connected directly above the drill bit, and they use the lower portion of the tool and the bit as a measuring electrode. This allows the tool to provide a bit resistivity measurement with a vertical resolution just a few inches longer than the length of the bit. A 1-in (2.5 cm) electrode is located 3 ft (91 cm) from the bottom of the tool and provides a focused lateral resistivity measurement (R_{RING}) with a vertical resolution of 2 in (5 cm). The characteristics of R_{RING} are independent of where the RAB tool is placed in the BHA, and its depth of investigation is ~7 in (18 cm). In addition, button electrodes provide shallow-, medium-, and deep-focused resistivity measurements as well as azimuthally oriented images. These images can then reveal information about formation structure and lithologic contacts. The button electrodes are ~1 in (2.5 cm) in diameter and reside on a clamp-on sleeve. The buttons are longitudinally spaced along the RAB tool to render staggered depths of investigation of ~1, 3, and 5 in (2.5, 7.6, and 12.7 cm). The tool's orientation system uses the Earth's magnetic field as a reference to determine the tool position with respect to the borehole as the drill string rotates, thus allowing both azimuthal resistivity and gamma ray measurements. Furthermore, these measurements are acquired with an ~6° resolution as the RAB tool rotates. The vertical resolution for each resistivity measurement is shown in Table **T4.**

Two RAB tool-collar configurations that were designed for use during Leg 204 give slightly different resistivity responses depending on the size of the measuring button sleeve and the hole diameter. The RAB tool used in series in the 6¾-in LWD/MWD BHA is called the GeoVision Resistivity (GVR), the most recent upgrade of the tool (Fig. **F19**). The di-

F19. The RAB tool, p. 86.

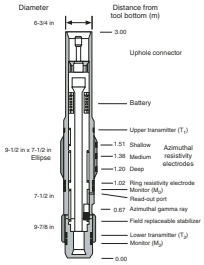

ameter of its measuring button sleeve is 23.3 cm ($9^1/_8$ in), and the diameter of the three-cone rotary bit used during Leg 204 is 25 cm ($9^7/_8$ in). This results in a 1.7-cm gap, or "standoff," between the resistivity buttons and the formation. The standoff causes the formation resistivity to be underestimated slightly, depending on the ratio between the formation and borehole fluid resistivity. For a resistivity ratio of <100, as expected for all Leg 204 sites, a resistivity correction factor of up to 4% may be applied to each of the GVR measurements. Estimated correction factors for the GVR tool are given in Table **T5** (Schlumberger, 2001, unpubl. data). Because of its limited depth of penetration into the formation (see below), the correction factor for the shallow button resistivity is greatest.

A RAB-8 tool collar configuration for use with a larger 8-in-diameter BHA was specially designed for ODP. The U.S. Department of Energy provided partial funding support for the modified RAB-8 tool deployment during Leg 204. The design is intended to be run in conjunction with a modified motor-driven core barrel core-liner system, thus allowing for RAB measurements to be made while coring (Fig. **F20**).

F20. The RAB-8 tool, p. 87.

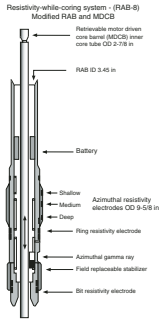

ODP Leg 204 represents the first ever attempt to core and record LWD data simultaneously. The RAB-8 tool is deployed alone in the BHA, and the standard 25 cm ($9^7/_8$ in) diameter rotary bit is used. The diameter of the measuring button sleeve for the RAB-8 tool is 24.1 cm (9½ in); thus, the standoff is half that for the RAB-6 and the resistivity correction factors are negligible for all of the RAB-8 measurements, including the shallow button resistivity.

Resistivity-at-the-Bit Programming

All logging data are collected at a minimum vertical density of 15 cm whenever possible; hence, a balance must be determined between the rate of penetration (ROP) and the sampling rate. This relationship depends on the recording rate, the number of data channels to record, and the memory capacity (46 MB) of the LWD tool. During Leg 204, we used a data acquisition sampling rate of 5 s for high-resolution GVR images. The RAB-8 tool was programmed with a sampling rate of 10 s for data acquisition. The maximum ROP allowed to produce one sample per 6-in interval is given by the equation

$$\text{ROP (in meters per hour)} = 548/\text{sample rate}. \quad (7)$$

This relationship gives 110 m/hr maximum ROP for the GVR and 55 m/hr for the RAB-8 tool.

For Leg 204, the target ROP was 25–50 m/hr, roughly 25%–50% of the maximum allowable for the GVR and RAB-8 tools. These reduced rates improve the vertical resolution of the resistivity images to 5–10 cm per rotation. Under this configuration, the GVR tool has enough memory to record up to 80 hr of data and the RAB-8 tool can record as long as 30 hr. This would be sufficient, under normal operating conditions, to complete the scheduled LWD operations at the Leg 204 drill sites.

Bit Resistivity Measurements

For the bit resistivity measurements, a lower transmitter (T_2) produces a current and a monitoring electrode (M_0) located directly below

the ring electrode measures the current returning to the collar (Fig. F19). When connected directly to the bit, the GVR tool uses the lower few inches of the tool as well as the bit as a measurement electrode. The resultant resistivity measurement is termed RBIT, and its depth of investigation is ~12 in (30.48 cm).

Ring Resistivity Measurements

The upper and lower transmitters (T_1 and T_2) produce currents in the collar that meet at the ring electrode. The sum of these currents is then focused radially into the formation. These current patterns can become distorted depending on the strength of the fields produced by the transmitters and the formation around the collar. Therefore, the GVR tool uses a cylindrical focusing technique that takes measurements in the central (M_0) and lower (M_2) monitor coils to reduce distortion and create an improved ring response. The ring electrode is held at the same potential as the collar to prevent interference with the current pattern. The current required for maintaining the ring at the required potential is then measured and related to the resistivity of the formation. Because the ring electrode is narrow (~4 cm), the result is a measurement (R_{RING}) with 5-cm vertical resolution.

Button Resistivity Measurements

The button electrodes function the same way as the ring electrode. Each button is electrically isolated from the body of the collar but is maintained at the same potential to avoid interference with the current field. The amount of current required to maintain the button at the same potential is related to the resistivity of the mud and formation. The buttons are 4 cm in diameter, and the measurements (R_{BUTTON}) can be acquired azimuthally as the tool rotates within 56 sectors to produce a borehole image.

Measurement-While-Drilling Tool

During Leg 204, Anadrill's MWD tool was deployed in combination with the LWD tools (Fig. F17). The MWD tool had previously been deployed during Leg 188 (O'Brien, Cooper, Richter, et al., 2001) and Leg 196 (Mikada, Becker, Moore, Klaus, et al., 2002). During Leg 204, the MWD tool was deployed with the LWD tools at all sites, except on the test run with the RAB coring tool. MWD tools measure downhole drilling parameters and consist of sensors located in the drill collar, immediately above the RAB tool in the BHA (Fig. F17).

The MWD data are transmitted by means of a pressure wave (mud pulsing) through the fluid within the drill pipe. The 6-in (17 cm) power-pulse MWD tool operates by generating a continuous mud-wave transmission within the drilling fluid and by changing the phase of this signal (frequency modulation) to transmit relevant bit words representing information from various sensors. Figure F21 illustrates the MWD mud pulse system and a representative pressure wave. Two pressure sensors attached to standpipe on the rig floor and on the gooseneck on the crown block are used to measure the pressure wave acting on the drilling fluid when information is transmitted up the drill pipe by the MWD tool. With the MWD mud pulsing systems, pulse rates range

F21. The MWD tool, p. 88.

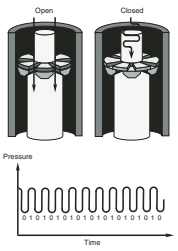

from 1 to 6 bps, depending primarily on water depth and mud density. Pulse rates of 6 bps were achieved during Leg 204.

The drilling parameters transmitted by mud pulse to the Anadrill surface recording system during Leg 204 include downhole weight on bit (DWOB), downhole torque on bit (DTOR), bit bounce, and tool stick slip. These measurements are made using paired strain gauges near the base of the MWD collar. Table T6 lists the set of measurements recorded using the MWD tool, which are transmitted to the surface. DWOB and DTOR information are also transmitted to the driller via the surface rig instrumentation system transmission protocol using the WITS standard. The comparison of MWD drilling parameter data, rig instrumentation system data, and ship-heave information recorded synchronously during Leg 204 was used to improve drilling control and to assess the quality of the recorded LWD data.

In addition to the drilling parameters listed in Table T6, the mud pulse system also transmitted some geophysical data from LWD tools to the surface. Measurement parameters from each LWD collar are updated at rates corresponding to 15-cm to 1.5-m depth intervals, depending on the initialized values and ROP of the tool. These parameters are used to verify the operational status of each tool downhole and provide real-time logs. In contrast to these real-time data, the downhole memory in the LWD tools is set to record data at a minimum rate of one sample per 15 cm.

T6. Acronyms and units for LWD and MWD tools, p. 100.

Nuclear Magnetic Resonance Tool

The U.S. Department of Energy provided funding support to deploy Anadrill's NMR-MRP tool during Leg 204. The basic technology behind this tool is similar to modern wireline nuclear magnetic resonance technology (e.g., Kleinberg et al., 2003; Horkowitz et al., 2002), which is based on measurement of the relaxation time of the magnetically induced precession of polarized protons. A combination of bar magnets and directional antennas are used to focus a pulsed polarizing field into the formation (Fig. F22). The NMR-MRP tool measures the relaxation time of polarized molecules in the formation, which provides information related to the formation porosity. By exploiting the nature of the chemical bonds within pore fluids, for hydrogen in particular, the NMR-MRP tool can provide estimates of the total porosity and bound fluid volume and thus be useful to determine whether water, gas, or gas hydrates are present in the formation.

F22. The NMR-MRP tool, p. 89.

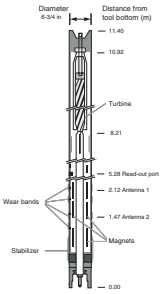

During Leg 204, the NMR-MRP tool acquired formation and engineering information in memory and transmitted some data to the surface via MWD. The relaxation-time spectra were recorded downhole, and total porosity estimates were transmitted to the surface in real time. These spectra were stacked in postprocessing to improve the measurement precision. The signal investigates a 15-cm cylindrical volume of the borehole, and for a $9^7/_8$-in bit size, the depth of investigation of the measurement is ~5 cm into the formation. Lateral tool motion may reduce NMR-MRP data quality in some circumstances. Therefore, accelerometers and magnetometers contained in the downhole tool are used to evaluate data quality and determine the maximum relaxation times that can be resolved. Data were also acquired while sliding (not rotating) the tool over short intervals to compare measurements with and without the effect of lateral vibration while drilling. Both real-time and memory data from the NMR-MRP tool were transmitted to LDEO-BRG

and Schlumberger via Inmarsat B for reprocessing and data-quality assessment.

Vision Neutron Density Tool

The VND tool is similar in principle to the Azimuthal Density Neutron (ADN) tool (Anadrill-Schlumberger, 1993; Mikada, Becker, Moore, Klaus, et al., 2002). The density section of the tool uses a 1.7-Ci ^{137}Cs gamma ray source in conjunction with two gain-stabilized scintillation detectors to provide a borehole-compensated density measurement. The detectors are located 5 and 12 in (12.7 and 30.48 cm) below the source (Fig. **F23**). The number of Compton scattering collisions (change in gamma ray energy by interaction with the formation electrons) is related to the formation density. Returns of low-energy gamma rays are converted to a photoelectric effect value, measured in barns per electron. The photoelectric effect value depends on electron density and hence responds to bulk density and lithology (Anadrill-Schlumberger, 1993). It is particularly sensitive to low-density, high-porosity zones.

The gamma ray source and detectors are positioned behind holes in the fin of a full gauge 9-in (25.08 cm) clamp-on stabilizer (Fig. **F23**). This geometry forces the sensors against the borehole wall, thereby reducing the effects of borehole irregularities and drilling. The vertical resolution of the density and photoelectric effect measurements is ~15 and 5 cm, respectively. For measurement of tool standoff and estimated borehole size, a 670-kHz ultrasonic caliper is available on the VND tool. The ultrasonic sensor is aligned with and located just below the density detectors. In this position, the sensor can also be used as a quality control for the density measurements. Neutron porosity measurements are obtained using fast neutrons emitted from a 10-Ci americium oxide–beryllium (AmBe) source. Hydrogen quantities in the formation largely control the rate at which the neutrons slow down to epithermal and thermal energies. The energy of the detected neutrons has an epithermal component because much of the incoming thermal neutron flux is absorbed as it passes through the 1-in drill collar. Neutrons are detected in near- and far-spacing detector banks, located 12 and 24 in (30.48 and 60.96 cm), respectively, above the source. The vertical resolution of the tool under optimum conditions is ~34 cm. The neutron logs are affected to some extent by the lithology of the matrix rock because the neutron porosity unit is calibrated for a 100% limestone environment. Neutron porosity logs are processed to eliminate the effects of borehole diameter, tool size, temperature, drilling mud hydrogen index (dependent on mud weight, pressure, and temperature), and mud. Formation salinities, lithology, and other environmental factors will also affect neutron porosities, and these parameters must be estimated for each borehole during neutron log processing (Schlumberger, 1994).

In near-vertical drill holes, the VND tool does not collect quadrant azimuthal data. Data output from the VND tool includes apparent neutron porosity (i.e., the tool does not distinguish between pore water and lattice-bound water), formation bulk density, and photoelectric effect (PEF). The density logs graphically presented here have been "rotationally processed" to show the average density that the tool reads while it is rotating. In addition, the VND tool outputs a differential caliper record based on the standard deviation of density measurements made at high sampling rates around the circumference of the borehole. The measured standard deviation is compared with that of an in-gauge borehole, and the difference is converted to the amount of borehole en-

F23. The VND tool, p. 90.

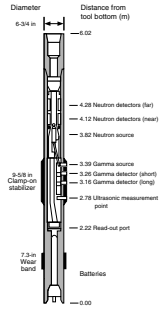

largement (Anadrill-Schlumberger, 1993). A standoff of <1 in between the tool and the borehole wall indicates good borehole conditions, for which the density log values are considered to be accurate to ±0.015 g/cm³ (Anadrill-Schlumberger, 1993).

Logging-While-Drilling Data Flow

Figure F24 shows onboard flow of the LWD/MWD data during Leg 204. Surface drilling parameters and MWD data were directly transmitted to the Schlumberger IDEAL system. A laptop personal computer was used to download and transfer the LWD data from all the tools on the rig floor to the IDEAL system for depth-time correlation. The log data were then distributed to the shipboard party via the workstation in the DHML. RAB image data were processed and converted to graphic format using GeoFrame (see "Logging Data Flow and Processing," p. 57) and custom codes on the DHML workstation prior to distribution to the shipboard party.

F24. LWD data flow, p. 91.

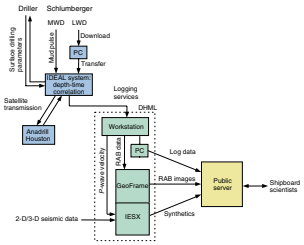

Core Barrel Measurements

Drill String Acceleration Tool

To evaluate downhole motion and pressure during coring, a device was designed by the LDEO-BRG to measure acceleration on various coring tools used by ODP (Guerin and Goldberg, 2002a). The DSA is a memory probe that records pressure and three-component acceleration and is attached to the top of a core barrel (Fig. F25). The true vertical displacement at the bit may be estimated by time integration of the acceleration data. In addition, drilling vibration data and downhole pipe motion data, information about core barrel landing, pressure up, and other operational events are recorded by the DSA tool. To date, the DSA tool has been used with the APC, RCB, FPC, and HRC.

F25. The DSA tool, p. 92.

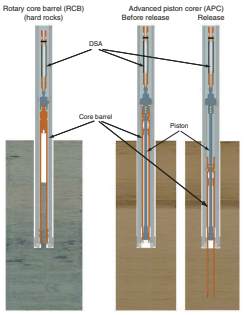

Specifications and Operations

The principal components of the DSA tool are a pressure sensor and two accelerometers. The pressure sensor measures pressure in the drill pipe every second, which is used to trigger the recording of acceleration data at a preprogrammed depth. One accelerometer is a vertical-component high-sensitivity transducer, recording motion along the axis of the drill string. The other is a high-frequency, three-axis transducer to record bit vibrations. The DSA tool runs as a self-contained memory device with a battery life allowing 9 hr of operations and enough memory to record ~1.5 hr of data at a 100-Hz sampling frequency. Before deployment, the DSA tool is connected through a serial port to a data acquisition PC for initialization and the initial recording depth, typically 200 m above coring depth, is defined by the LDEO logging staff scientist. After recovery, the DSA tool is reconnected to a PC and the data are downloaded in ASCII files ready for immediate analysis. The first processing step is the conversion of the raw data into acceleration, using calibration coefficients provided by the accelerometer manufacturers. The sensors, electronics board, memory, and batteries are enclosed in a 1.2-m-long stainless steel pressure case and can operate under temperature and pressure up to 85°C and 75 MPa, respectively.

Continuous coring in ODP holes is performed by recovering the core barrel at regular intervals, typically every 9.5 m. The procedure is the

same for the APC in soft sediments and for the RCB in harder formations (Fig. F25). The empty core barrel is lowered with a wireline or allowed to fall freely to the bottom of the drill string, advances 9.5 m during coring, and then is retrieved by a wireline that latches to the top of the core barrel. After reaching the rig floor, the core is removed for analysis and an empty core barrel is dropped in the drill string to continue the coring process. The DSA tool was designed to minimize any impact on coring operations. The initialized tool is attached by threaded collars to the top of the core barrel (Fig. F25), and the DSA tool/core barrel assembly is lowered to the bottom of the drill string. The top of the DSA tool can receive the normal core retrieval tool, and the entire assembly is recovered together. Only a few minutes are required to connect and disassemble the DSA tool/core barrel connection, which usually do not add to the net time on the rig floor for core retrieval. DSA data are typically available to assess the coring process and characterize formation attributes before cores have degassed and reached thermal equilibrium.

Wireline Logging Tools

Procedures and Data

Downhole logs reveal the physical, chemical, and structural properties of formations penetrated by a borehole. A variety of geophysical tools make rapid, continuous, in situ measurements as a function of depth after the hole has been drilled that can be used to interpret the lithology of the penetrated formation. Where core recovery is good, core data are used to calibrate the geophysical signature of the rocks. In intervals of low core recovery or disturbed cores, log data may provide the only way to characterize the borehole section. Geophysical well logs can aid in characterizing sedimentary sequences and integrating core and seismic reflection data. Individual logging tools are joined together into tool strings (Fig. F26) so that several measurements can be made during each logging run (Table T7). The tool strings are lowered to the bottom of the borehole on a wireline cable, and data are logged as the tool string is pulled back up the hole. Repeat runs are made to improve coverage and confirm the accuracy of log data. Not all tool strings are run in each hole; refer to individual site chapters for details of logging strings deployed at each site.

Logging Tools and Tool Strings

During ODP Leg 204, the following four different logging strings were deployed (Fig. F26; Table T7):

1. The triple combination (triple combo) string (resistivity, density, and porosity measurements), which consists of the Hostile Environment Gamma Ray Sonde (HNGS), the phasor dual induction–spherically focused resistivity (DIT-SFR) tool, the Hostile Environment Litho-Density Tool (HLDT), and the Accelerator Porosity Sonde (APS). The LDEO high-resolution Temperature/Acceleration/Pressure (TAP) tool was attached at the bottom of this tool string and the Inline Checkshot Tool (QSST) was added at the top.
2. The FMS-sonic tool string, which consists of the FMS, General Purpose Inclinometer Tool (GPIT), and Scintillation Gamma Ray (SGT) Tool, and the Dipole Sonic Imager (DSI).

F26. Tool strings used for wireline logging operations, p. 93.

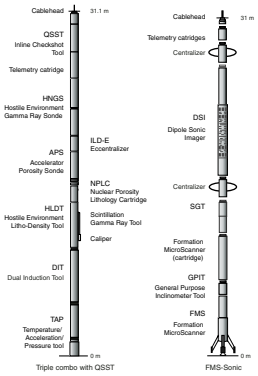

T7. Measurements made by wireline tool strings, p. 101.

3. The Well Seismic Tool (WST).
4. The Vertical Seismic Imager (VSI).

Leg 204 was the first time the QSST and the VSI have been run during an ODP leg.

Principles and Uses of the Logging Tools

The parameters measured by each tool, the sample intervals used, and the vertical resolution are summarized in Table T7. Explanations of tool name acronyms and their measurement units are summarized in Table T8. More detailed descriptions of individual logging tools and their geological applications can be found in Ellis (1987), Goldberg (1997), Rider (1996), Schlumberger (1989, 1994), Serra (1984, 1986, 1989), and the LDEO-BRG Wireline Logging Services Guide (2001).

T8. Acronyms and units used for wireline logging tools, p. 102.

Hostile Environment Spectral Gamma Ray Sonde and Scintillation Gamma Ray Tool

The HNGS measures the natural gamma radiation from isotopes of potassium, thorium, and uranium and uses a five-window spectroscopic analysis to determine concentrations of radioactive K (in weight percent), Th (in parts per million), and U (in parts per million). The HNGS uses two bismuth germanate scintillation detectors for gamma ray detection with full spectral processing. The spectral analysis filters out gamma ray energies below 500 keV, eliminating sensitivity to bentonite or KCl in the drilling mud and improving measurement accuracy. The HNGS also provides a measure of the total gamma ray emission (American Petroleum Institute units [gAPI]), and the uranium-free or computed gamma ray emission (CGR) (in gAPI units). The HNGS response is influenced by the borehole diameter and the weight and concentration of bentonite or KCl present in the drilling mud. KCl may be added to the drilling mud to prevent freshwater clays from swelling and forming obstructions. All of these effects are corrected for during processing of HNGS data at LDEO-BRG.

The SGT tool uses a sodium iodide scintillation detector to measure the total natural gamma ray emission, combining the spectral contributions of K, U, and Th concentrations in the formation. The SGT tool is not a spectral tool but provides high-resolution total gamma ray data for depth correlation between logging strings. It is included in all tool strings (except the triple combo, where the HNGS is used) to provide a reference log to correlate and depth between different logging runs. With the FMS-DSI tool string, the SGT tool is placed between the two tools, providing correlation data to a deeper level in the hole.

Hostile Environment Litho-Density Tool

The HLDT consists of a radioactive cesium (^{137}Cs) gamma ray source (622 keV) and far and near gamma ray detectors mounted on a shielded skid, which is pressed against the borehole wall by a hydraulically activated eccentralizing arm. Gamma rays emitted by the source experience both Compton scattering and photoelectric absorption. Compton scattering involves the ricochet of gamma rays off electrons in the formation via elastic collision, transferring energy to the electron in the process. The number of scattered gamma rays that reach the detectors is directly related to the number of electrons in the formation, which is

related to bulk density. Porosity may also be derived from this bulk density if the matrix density is known.

The HLDT also measures the PEF caused by absorption of low-energy gamma rays. Photoelectric absorption occurs when gamma rays reach <150 keV after being repeatedly scattered by electrons in the formation. As the PEF depends on the atomic number of the elements in the formation, it is essentially independent of porosity. Thus, the PEF varies according to the chemical composition of the sediment. Some examples of PEF values are pure calcite = 5.08, illite = 3.03, quartz = 1.81, and kaolinite = 1.49 b/e^-. The PEF values can be used in combination with HNGS curves to identify different types of clay minerals. Coupling between the tool and borehole wall is essential for good HLDT logs. Poor contact results in underestimation of density values. Both density correction and caliper measurement of the hole are used to check the contact quality.

Accelerator Porosity Sonde

The APS consists of a minitron neutron generator that produces fast neutrons (14.4 MeV) and five neutron detectors (four epithermal and one thermal) positioned at different spacings along the tool. The tool is pressed against the borehole wall by an eccentralizing bow-spring. Emitted high-energy (fast) neutrons are slowed down by collisions with atoms. The amount of energy lost per collision depends on the relative mass of the nucleus with which the neutron collides. The largest energy loss occurs when the neutron strikes a nucleus of equal mass, such as hydrogen, which is mainly present in pore water. Once neutrons degrade to thermal energies (0.025 eV), they may be captured by the nuclei of silicon, chlorine, and boron and other elements, with the associated emission of a gamma ray. The neutron detectors record both the numbers of neutrons arriving at various distances from the source and the neutron arrival times, which act as a measure of formation porosity. However, hydrogen bound in minerals such as clays or in hydrocarbons also contributes to the measurement, so the raw porosity value is often an overestimate.

Phasor Dual Induction–Spherically Focused Resistivity Tool

The DIT-SFR tool provides three different measurements of electrical resistivities, each with a different depth of penetration into the formation. Two induction devices (deep and medium resistivity) transmit high-frequency alternating currents through transmitter coils, creating magnetic fields that induce secondary (Foucault) currents in the formation. These ground-loop currents produce new inductive signals, proportional to the conductivity of the formation, which are measured by the receiving coils. The measured conductivities are then converted to resistivity. A third device, a spherically focused resistivity instrument that gives higher vertical resolution, measures the current necessary to maintain a constant voltage drop across a fixed interval.

High-Resolution Temperature/Acceleration/Pressure Tool

The TAP tool is a "dual application" logging tool (i.e., it can operate either as a wireline tool or as a memory tool using the same sensors). Data acquisition electronics are dependent on the purpose and required precision of logging data. During Leg 204, the TAP tool was deployed as

a memory tool in low-resolution mode; data were stored in the tool and downloaded after the logging run was completed. Temperatures determined using the TAP tool do not necessarily represent in situ formation temperatures because water circulation during drilling will have disturbed temperature conditions in the borehole. However, from the spatial temperature gradient, abrupt temperature changes can be identified that may correspond to contrasts in permeability at lithologic boundaries or may represent localized fluid flow into the borehole, indicating fluid pathways and fracturing.

Dipole Sonic Imager

The DSI employs a combination of monopole and dipole transducers to make accurate measurements of sonic wave propagation in a wide variety of formations. In addition to a robust and high-quality measurement of V_P, the DSI uses the dipole source to generate a flexural mode in the borehole that can be used to estimate shear (*S*-) wave velocity even in highly unconsolidated formations. When the formation shear velocity is less than the sonic velocity of the borehole fluid, particularly in unconsolidated sediments, the flexural wave travels at the *S*-wave velocity and is the most reliable way to estimate a shear velocity log. Meanwhile, the monopole source generates *P*-, *S*-, and Stoneley waves into hard formations. The configuration of the DSI also allows recording of cross-dipole waveforms. In many cases, the dipole sources can also provide estimates of *S*-wave velocity in hard rocks better than or equivalent to the monopole source. These combined modes can be used to estimate *S*-wave splitting caused by preferred mineral and/or structural orientation in consolidated formations. A low-frequency (80 Hz) source enables Stoneley waveforms to be acquired as well.

The DSI measures the transit times between sonic transmitters and an array of eight receiver groups with 15-cm spacing, each consisting of four orthogonal elements that are aligned with the dipole transmitters. During acquisition, the output from these 32 individual elements are differenced or summed appropriately to produce in-line and cross-line dipole signals or monopole-equivalent (*P*- and Stoneley) waveforms, depending on the operation modes. The detailed description of tool configuration and data processing are described in the Leg 174B *Initial Reports* volume (Shipboard Scientific Party, 1998). The velocity data from the DSI together with the formation density can be used to generate a synthetic seismogram.

Formation MicroScanner Tool

The FMS produces high-resolution images of borehole wall microresistivity that can be used for detailed sedimentologic or structural interpretation. This tool has four orthogonally oriented pads, each with 16 button electrodes that are pressed against the borehole walls. Good contact with the borehole wall is necessary for acquiring good-quality data. Approximately 30% of a borehole with a diameter of 25 cm is imaged during a single pass. Coverage may be increased by a second run. The vertical resolution of FMS images is ~5 mm, allowing features such as burrows, thin beds, fractures, veins, and vesicles to be imaged. The resistivity measurements are converted to color or grayscale images for display. In site chapters in this volume, local contrasts in FMS images were improved by applying dynamic normalization to the FMS data. A linear gain is applied, which keeps a constant mean and standard devia-

tion within a sliding window of 1 m. FMS images are oriented to magnetic north using the GPIT (see below). This allows the dip and strike of geological features intersecting the hole to be measured from processed FMS images. FMS images can be used to visually compare logs with the core to ascertain the orientations of bedding, fracture patterns, and sedimentary structures and to identify stacking patterns. FMS images have proved particularly valuable in interpreting sedimentary structures, and they have been used to identify cyclical stacking patterns in carbonates, turbidite deposits, and facies changes (Serra, 1989).

General Purpose Inclinometer Tool

The GPIT is included in the FMS-sonic tool string to calculate tool acceleration and orientation during logging. The GPIT contains a triple-axis accelerometer and a triple-axis magnetometer. The GPIT records the orientation of the FMS images and allows more precise determination of log depths than can be determined from cable length, as the accelerometer data can be used to correct for cable stretching and/or ship heave.

Vertical Seismic Imager

The VSI is a borehole seismic wireline tool optimized for vertical seismic profiles (VSPs) and walkaway vertical seismic profiles (W-VSPs) in both cased and open hole and vertical and deviated wells. The VSI consists of multiple three-axis geophones in series separated by "hard wired" acoustically isolating spacers. A schematic illustration of the tool is given in Figure **F27.** The tool diameter is $3^3/_8$ in, with temperature and pressure ratings to175°C and 20,000 psi, respectively.

F27. The VSI, p. 94.

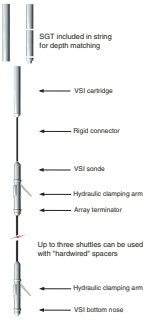

During Leg 204, the VSI was nominally configured using three shuttles (each containing three geophones) spaced 15.12 m apart and combined with the SGT tool. In practice, after problems using three shuttles simultaneously, only one shuttle was used at a time. For vertical incidence VSP operations, the shuttles were mechanically clamped against the borehole wall and sources (e.g., generator-injector [GI] guns) on the *JOIDES Resolution* were fired between 5 and 15 times by control hardware in the Schlumberger multi-tasking acquisition and imaging system (MAXI)S unit. For constant-offset and W-VSP operations, sources were fired on another ship (e.g., *Maurice Ewing*) by Macha radio control from the Schlumberger MAXIS unit. The VSI tool was then unclamped and pulled uphole. Although a 7.5-m spacing had been planned, problems clamping the sensors resulted in variable station spacing. The VSI records the full seismic waveform for each firing. These waveform data are stacked by the MAXIS recording software and may be output in LDF (internal Schlumberger format) or SEG-Y formats.

Three types of VSP experiments (vertical incidence, constant-offset, and/or walkaway) were conducted during Leg 204 using the VSI and GI gun sources located on the *JOIDES Resolution* and the *Maurice Ewing*. The vertical incidence and constant offset surveys were conducted by alternating source firings between the *JOIDES Resolution* and the *Maurice Ewing* at each VSI depth station. These were followed by walkaway VSP experiments in which sources were fired from the *Maurice Ewing* alone as it moved along two crossing lines intersecting near the drill site. The U.S. Department of Energy provided partial funding support for this tool deployment during Leg 204.

Inline Checkshot Tool

The Schlumberger QSST is a single-axis seismic checkshot tool that runs in-line with the triple combo tool string (Fig. F26). The QSST consists of a single hydrophone and does not utilize a clamping arm like the WST to force it into contact with the borehole wall. Seismic coupling is achieved by setting the tool on the hole bottom and allowing the tool to lean against the borehole wall, coupling passively to the formation. The QSST then records the vertically incident signals at the bottom of the hole that are generated by a seismic source on the *JOIDES Resolution* (e.g., GI guns) positioned just below the sea surface. The recorded signals enable a one-way traveltime to be determined from the surface to total depth, providing a check of V_P vs. depth for calibration of seismic profiles and correction of sonic logs. Off-bottom stations are not possible using the QSST. The rig time required to run this single-point checkshot survey is negligible since the QSST may be included during the triple combo logging run. Data from the QSST are provided by the Schlumberger multi-tasking acquisition and imaging system (MAXIS) unit in SEG-Y.

Logging Data Flow and Processing

Data for each wireline logging run were recorded and stored digitally and monitored in real time using the Schlumberger MAXIS 500 system. After logging was completed in each hole, data were transferred to the shipboard DHML for preliminary processing and interpretation. FMS image data were interpreted using Schlumberger's GeoFrame 3.8 software package. Well seismic, sonic, and density data were used for calculation of synthetic seismograms with GeoQuest's IESX software package to establish the seismic to borehole tie.

Logging data were also transmitted to LDEO-BRG using a FFASTEST satellite high-speed data link for processing soon after each hole was logged. Data processing at LDEO-BRG consists of (1) depth-shifting all logs relative to a common datum (i.e., in mbsf), (2) corrections specific to individual tools, and (3) quality control and rejection of unrealistic or spurious values. Once processed at LDEO-BRG, log data were transmitted back to the ship, providing near real-time data processing. Processed data were then replotted on board (see the "Logging" section in each site chapter). Further postcruise processing of the log data from the FMS is performed at LDEO-BRG. Postcruise-processed data in ASCII format are available directly from the LDEO-BRG Internet World Wide Web site at **www.ldeo.columbia.edu/BRG/ODP/DATABASE/.** A summary of "logging highlights" is posted on the LDEO-BRG Web site at the end of each leg.

Downhole logging aboard the *JOIDES Resolution* is provided by LDEO-BRG in conjunction with Leicester University Borehole Research, the Laboratoire de Mesures en Forages Montpellier, University of Aachen, University of Tokyo, Schlumberger Well Logging Services, and Schlumberger Measurement While Drilling.

Wireline Logging Data Quality

Logging data quality may be seriously degraded by changes in the hole diameter and in sections where the borehole diameter greatly decreases or is washed out. Deep-investigation measurements such as resistivity and sonic velocity are least sensitive to borehole conditions.

Nuclear measurements (density and neutron porosity) are more sensitive because of their shallower depth of investigation and the effect of drilling fluid volume on neutron and GRA. Corrections can be applied to the original data in order to reduce these effects. Very large washouts, however, cannot be corrected for. HNGS and NGT data provide a depth correlation between logging runs. Logs from different tool strings may, however, still have minor depth mismatches caused by either cable stretch or ship heave during recording. Ship heave is minimized by a hydraulic wireline heave compensator designed to adjust for rig motion during logging operations.

Gas Hydrate Detection and Evaluation with Downhole Logs

With growing interest in natural gas hydrate, it is becoming increasingly important to be able to identify the presence of in situ gas hydrate and accurately assess the volume of gas hydrate and included free gas within gas hydrate accumulations. Numerous publications (Mathews, 1986; Collett, 1993, 1998a, 1998b, 2001; Goldberg, 1997; Guerin et al., 1999; Goldberg et al., 2000; Helgerud et al., 2000) have shown that downhole geophysical logs can yield information about the presence of gas hydrate.

Because gas hydrates are characterized by unique chemical compositions and distinct electrical resistivities, physical, and acoustic properties, it is possible to obtain gas hydrate saturation (percent of pore space occupied by gas hydrate) and sediment porosity data by characterizing the electrical resistivity, acoustic properties, and chemical composition of the pore-filling constituents within gas hydrate–bearing reservoirs. Two of the most difficult reservoir parameters to determine are porosity and the degree of gas hydrate saturation. Downhole logs often serve as a source of porosity and hydrocarbon saturation data. Most of the existing gas hydrate–log evaluation techniques are qualitative in nature and have been developed by the extrapolation of untested petroleum industry log evaluation procedures. To adequately test the utility of standard petroleum log evaluation techniques in gas hydrate–bearing reservoirs would require numerous laboratory and field measurements. However, only a limited number of gas hydrate occurrences have been sampled and surveyed with open-hole logging devices.

Reviewed below are downhole log measurements that together yield useful gas hydrate–reservoir information. The downhole measurements considered include gamma-gamma density, neutron porosity, electrical resistivity, acoustic transit time, and nuclear magnetic resonance. Most of these measurements are converted to porosity; however, because gas hydrate affects each measurement of porosity in a different fashion, the quantity of gas hydrate can be estimated by comparison of porosity measurements made using different techniques.

Gamma-Gamma Density Logs

Gamma density logs are primarily used to assess sediment porosities. The theoretical bulk density of a Structure I methane hydrate is ~0.9 g/cm^3 (Sloan, 1998). Gas hydrate can cause a small but measurable effect on density-derived porosities. At relatively high porosity (>40%) and high gas hydrate saturation (>50%), the density log–derived porosities need to be corrected for the presence of gas hydrate (Collett, 1998b).

Neutron Porosity Logs

Neutron logs are also used to determine sediment porosities. Since Structure I methane hydrate and pure water have similar hydrogen concentrations, it can be generally assumed that neutron porosity logs, which are calibrated to pure water, are not significantly affected by the presence of gas hydrates. At high reservoir porosities, however, the neutron porosity log could overestimate porosities (Collett, 1998b).

Electrical Resistivity

Water content and pore water salinity are the most significant factors controlling the electrical resistivity of a formation. Other factors influencing resistivity of a formation include the concentration of hydrous and metallic minerals, volume of hydrocarbons including gas hydrates, and pore structure geometry. Gas hydrate–bearing sediments exhibit relatively high electrical resistivities in comparison to water-saturated units, which suggests that a downhole resistivity log can be used to identify and assess the concentration of gas hydrates in a sedimentary section. The relation between rock and pore fluid resistivity has been studied in numerous laboratory and field experiments. From these studies, relations among porosity, pore fluid resistivity, and rock resistivity have been found. Among these findings is the empirical relation established by Archie (Archie, 1942), which is used to estimate water saturations in gas-oil-water-matrix systems. Research has shown that the Archie Relation also appears to yield useful gas hydrate saturation data (reviewed by Collett, 2000).

Acoustic Transit Time

The velocity of *P*- and *S*-waves in a solid medium, such as gas hydrate–bearing sediment, is usually significantly greater than the velocity of *P*- and *S*-waves in water or gas-bearing sediments. Studies of downhole acoustic log data from both marine and permafrost associated gas hydrate accumulations have shown that the volume of gas hydrate in sediment can also be estimated by measuring interval velocities (Guerin et al., 1999; Helgerud et al., 2000; Collett, 2000). Analysis of sonic logging waveforms has also shown that the presence of gas hydrate can generate significant energy loss in monopole and dipole waveforms (Guerin and Goldberg, 2002b).

Nuclear Magnetic Resonance Logs

NMR logs use the electromagnetic properties of hydrogen molecules to analyze the nature of the chemical bonds within pore fluids. Relative to other pore-filling constituents, gas hydrates exhibit unique chemical structures and hydrogen concentrations. In theory, therefore, it should be possible to develop NMR well-log evaluation techniques that would yield accurate reservoir porosities and water saturations in gas hydrate–bearing sediments. Because of tool design limitations, gas hydrates cannot be directly detected with today's downhole NMR technology; however, they can be useful to yield very accurate gas hydrate saturation estimates. Because of the short transverse magnetization relaxation times (T2) of the water molecules in the clathrate, gas hydrates are not "seen" by the NMR tool and will be assumed to be part of the solid matrix. Thus, the NMR-calculated total porosity in a gas hydrate–bearing sedi-

ment should be lower than the actual porosity. With an independent source of accurate total porosity, such as density- or neutron-porosity-log measurements, it should be possible to accurately estimate gas hydrate saturations by comparing the apparent NMR-derived porosity to the total density-derived porosity.

Interpreting Structure from Resistivity-at-the-Bit and Formation MicroScanner Images

Structural data were determined from RAB images using Schlumberger's GeoFrame software. GeoFrame presents RAB data as a planar "unwrapped" 360° resistivity image of the borehole with depth. The image orientation is referenced to north, which is measured by the magnetometers inside the tool, and the hole is assumed to be vertical. Horizontal features appear horizontal on the images, whereas planar dipping features are sinusoidal in aspect. Sinusoids are interactively fitted to beds and fractures to determine their dip and azimuth, and the data are exported from GeoFrame for further analysis.

Methods of interpreting structure and bedding differ considerably between core analysis, wireline FMS images, and RAB image analysis. Resolution is considerably lower for RAB image interpretation (5–10 cm at best, compared with millimeters within cores and 0.5 cm for FMS images), and therefore, identified features are likely to be different in scale. For example, microfaults ("small faults;" <1 mm width) and shear bands (1–2 mm; up to 1 cm width) can only be identified in FMS data. This should be considered when directly comparing reports. The RAB tool provides 360° coverage at a lower resolution; the FMS provides higher-resolution data, but coverage is restricted to only ~30% of the borehole wall. Fractures were identified within RAB images by their anomalous resistivity or conductivity and from contrasting dip relative to surrounding bedding trends. Differentiating between fractures and bedding planes can be problematic, particularly if both are steeply dipping and with similar orientations.

Core-Log-Seismic Correlation

We correlated the results of a 3-D seismic survey acquired on the *Thompson* in June and July 2000 with the Leg 204 LWD and wireline log data. The correlation included core physical properties, wireline logs, and two-dimensional and 3-D seismic survey images collected during 14 yr of research at Hydrate Ridge. To ensure accurate correlation of the data, it was important to ascertain the accuracy of the navigation of each of the associated surveys, the hole deviation, the drill string position at the seafloor relative to the sea surface, the accuracy of the depth-converted seismic data, and the vertical and horizontal seismic resolution. Accurate correlation is critical to extend the study of the direct measurements of the subsurface physical properties away from the borehole using the 3-D seismic data.

Seismic Waveform Modeling

In order to correlate the 3-D seismic data with the LWD data, synthetic seismograms were constructed using the best densities and velocities for each site, which included data such as the LWD density, core density, wireline sonic and core *P*-wave velocity. The 256-ms long-source wavelet used at each site was calculated deterministically using

25 traces from the seafloor reflection in the vicinity of Hole 1245A, where the seafloor was reasonably flatlying and smooth.

UNDERWAY GEOPHYSICS

Because Leg 204 followed a high-resolution 3-D seismic reflection and ocean-bottom seismometer site survey, no additional underway geophysical data were acquired during the leg. We did, however, take advantage of the fact that we would be on the southern summit of Hydrate Ridge at Site 1249, where bubble plumes had previously been observed in the water column using 12-kHz echo sounding data (Fig. F3, p. 53, in the "Leg 204 Summary"), to obtain additional 12-kHz data. The objective of this effort was to obtain a time series of changes in bubble-plume intensity over a period of several days. Recording capability, which was restricted to analog paper records displaying nonoverlapping depth scales spanning 750 m, was not ideal for this effort, but we hoped to obtain some qualitative data that would permit us to evaluate whether a more quantitative approach would be fruitful in the future. Data were very noisy because of ship noise, and no unequivocal evidence for bubbles was obtained.

REFERENCES

Anadrill-Schlumberger, 1993. *Logging While Drilling:* Houston (Schlumberger), document SMP-9160.

Archie, G.E., 1942. The electrical resistivity log as an aid in determining some reservoir characteristics. *J. Pet. Technol.,* 5:1–8.

Arsenault, M.A., Trehu, A.M., Bangs, N., and Nakamura, Y., 2001. *P*-wave tomography of Hydrate Ridge, Oregon continental margin. *Eos Trans.,* 82:604. (Abstract).

Austin, J.A., Jr., Christie-Blick, N., Malone, M.J., et al., 1998. *Proc. ODP, Init. Repts.,* 174A: College Station, TX (Ocean Drilling Program).

Balsam, W.L., and Damuth, J.E., 2000. Further investigations of shipboard vs. shore-based spectral data: implications for interpreting Leg 164 sediment composition. *In* Paull, C.K., Matsumoto, R., Wallace, P., and Dillon, W.P. (Eds.), *Proc. ODP, Sci. Results,* 164: College Station, TX (Ocean Drilling Program), 313–324.

Balsam, W.L., Damuth, J.E., and Schneider, R.R., 1997. Comparison of shipboard vs. shore-based spectral data from Amazon-Fan cores: implications for interpreting sediment composition. *In* Flood, R.D., Piper, D.J.W., Klaus, A., and Peterson, L.C. (Eds.), *Proc. ODP, Sci. Results,* 155: College Station, TX (Ocean Drilling Program), 193–215.

Balsam, W.L., Deaton, B.C., and Damuth, J.E., 1998. The effects of water content on diffuse reflectance measurements of deep-sea core samples: an example from ODP Leg 164 sediments. *Mar. Geol.,* 149:177–189.

Barron, J.A., 1992. Neogene diatom datum levels in the equatorial and North Pacific. *In* Ishizaki, K., and Saito, T. (Eds.), *The Centenary of Japanese Micropaleontology:* Tokyo (Terra Sci. Publ.), 413–425.

Barron, J.A., and Gladenkov, A.Y., 1995. Early Miocene to Pleistocene diatom stratigraphy of Leg 145. *In* Rea, D.K., Basov, I.A., Scholl, D.W., and Allan, J.F. (Eds.), *Proc. ODP, Sci. Results,* 145: College Station, TX (Ocean Drilling Program), 3–19.

Berggren, W.A., Hilgen, F.J., Langereis, C.G., Kent, D.V., Obradovich, J.D., Raffi, I., Raymo, M.E., and Shackleton, N.J., 1995a. Late Neogene chronology: new perspectives in high-resolution stratigraphy. *Geol. Soc. Am. Bull.,* 107:1272–1287.

Berggren, W.A., Kent, D.V., Swisher, C.C., III, and Aubry, M.-P., 1995b. A revised Cenozoic geochronology and chronostratigraphy. *In* Berggren, W.A., Kent, D.V., Aubry, M.-P., and Hardenbol, J. (Eds.), *Geochronology, Time Scales and Global Stratigraphic Correlation*. Spec. Publ.—SEPM (Soc. Sediment. Geol.), 54:129–212.

Binns, R.A., Barriga, F.J.A.S., Miller, D.J., et al., 2002. *Proc. ODP, Init. Repts.,* 193 [CD-ROM]. Available from: Ocean Drilling Program, Texas A&M University, College Station TX 77845-9547, USA.

Blum, P., 1997. Physical properties handbook: a guide to the shipboard measurement of physical properties of deep-sea cores. *ODP Tech. Note,* 26 [Online]. Available from World Wide Web: <http://www.odp.tamu.edu/publications/tnotes/tn26/INDEX.HTM>. [Cited 2001-09-02].

Boone, D.R., Johnson, R.L., and Liu, Y., 1989. Diffusion of the interspecies electron carriers H_2 and formate in methanogenic ecosystems and its implications in the measurement of K_m for H_2 or formate uptake. *Appl. Environ. Microbiol.,* 55:1735–1741.

Borowski, W.S., Paull, C.K., and Ussler, W., III, 1996. Marine pore-water sulfate profiles indicate in situ methane flux from underlying gas hydrate. *Geology,* 24:655–658.

Bullard, E.C., 1954. The flow of heat through the floor of the Atlantic Ocean. *Proc. R. Soc. London A,* 222:408-429.

Cande, S.C., and Kent, D.V., 1995. Revised calibration of the geomagnetic polarity timescale for the Late Cretaceous and Cenozoic. *J. Geophys. Res.,* 100:6093–6095.

Cline, J.D., 1969. Spectrophotometric determination of hydrogen sulfide in natural waters. *Limnol. Oceanogr.,* 14:454–458.

Collett, T.S., 1993. Natural gas hydrates of the Prudhoe Bay–Kuparuk River area, North Slope, Alaska. *AAPG Bull.,* 77:793–812.

————, 1998a. Well log characterization of sediment porosities in gas-hydrate-bearing reservoirs [paper presented at Annu. Tech. Conf. Exhib. Soc. Pet. Eng., New Orleans, September 1998], Pap. SPE 49298. Available from: Society of Petroleum Engineers.

————, 1998b. Well log evaluation of gas hydrate saturations. In *Trans. SPWLA 39th Annu. Logging Symp.:* Houston (SPWLA), 39:MM.

————, 2000. A review of well-log analysis techniques used to assess gas-hydrate-bearing reservoirs: *In* Paull, C.K., and Dillon, W.P. (Eds.), *Natural Gas Hydrates: Occurrence, Distribution, and Detection.* Geophys. Monogr., Am. Geophys. Union, 189–210.NCR system

D'Hondt, S.L., Jørgensen, B.B., Miller, D.J., et al., 2003. *Proc. ODP, Init. Repts.,* 201 [CD-ROM]. Available from: Ocean Drilling Program, Texas A&M University, College Station TX 77845-9547, USA.

Davis, E.E., Villinger, H., MacDonald, R.D., Meldrum, R.D., and Grigel, J., 1997. A robust rapid-response probe for measuring bottom-hole temperatures in deep-ocean boreholes. *Mar. Geophys. Res.,* 19:267–281.

Dickens, G.R., Schroeder, D., Hinrichs, K.-U., and the Leg 201 Scientific Party, 2003. The pressure core sampler (PCS) on Ocean Drilling Program Leg 201: general operations and gas release. *In* D'Hondt, S.L., Jørgensen, B.B., Miller, D.J., et al., *Proc. ODP, Init. Repts.,* 201, 1–22 [CD-ROM]. Available from: Ocean Drilling Program, Texas A&M University, College Station TX 77845-9547, USA.

Dickens, G.R., Borowski, W.S., Wehner, H., Paull, C.K., and the ODP Leg 164 Scientific Party, 2000a. Data report: Additional shipboard information for the pressure core sampler (PCS). *In* Paull, C.K., Matsumoto, R., Wallace, P.J., and Dillon, W.P. (Eds.), *Proc. ODP, Sci. Results,* 164: College Station, TX (Ocean Drilling Program), 439–443.

Dickens, G.R., Paull, C.K., Wallace, P., and the ODP Leg 164 Scientific Party, 1997. Direct measurement of in situ methane quantities in a large gas hydrate reservoir. *Nature,* 385: 427–428.

Dickens, G.R., Wallace, P.J., Paull, C.K., and Borowski, W.S., 2000b. Detection of methane gas hydrate in the pressure core sampler (PCS): volume-pressure-time relations during controlled degassing experiments. *In* Paull, C.K., Matsumoto, R., Wallace, P.J., and Dillon, W.P. (Eds.), *Proc. ODP, Sci. Results,* 164: College Station, TX (Ocean Drilling Program), 113–126.

Droser, M.L., and Bottjer, D.J., 1986. A semiquantitative field classification of ichnofabric. *J. Sediment. Petrol.,* 56:558–559.

Ellis, D.V., 1987. *Well Logging for Earth Scientists:* New York (Elsevier).

Elsworth, D., Kondas, A.J., Loureiro, M., and Aggarwal, P.K., 1997. Pore pressure dissipation rates as a discriminant in evaluating permeability distributions from piezocone tests. *In* Robertson, P.K., and Mayne, P.W. (Eds.), *Proc. 1st Int. Conf. Site Characterization:* Rotterdam (A.A. Balkema), 1409–1413.

Froelich, P.N., Kvenvolden, K.A., Torres, M.E., Waseda, A., Didyk, B.M., and Lorenson, T.D., 1995. Geochemical evidence for gas hydrate in sediment near the Chile triple junction. *In* Lewis, S.D., Behrmann, J.H., Musgrave, R.J., and Cande, S.C. (Eds.), *Proc. ODP, Sci. Results,* 141: College Station, TX (Ocean Drilling Program), 279–286.

Gealy, E.L., Winterer, E.L., and Moberly, R., Jr., 1971. Methods, conventions, and general observations. *In* Winterer, E.L., Riedel, W.R., et al., *Init. Repts. DSDP,* 7 (Pt. 1): Washington (U.S. Govt. Printing Office), 9–26.

Gieskes, J.M., Gamo, T., and Brumsack, H., 1991. Chemical methods for interstitial water analysis aboard *JOIDES Resolution. ODP Tech. Note,* 15.

Goldberg, D., 1997. The role of downhole measurements in marine geology and geophysics. *Rev. Geophys.,* 35:315–342.

Goldberg, D., Collett, T.S., and Hyndman, R.D., 2000. Ground truth: in-situ properties of hydrate. *In* Max, M.D. (Ed.), *Natural Gas Hydrate in Oceanic and Permafrost Environments:* The Netherlands (Kluwer Academic Publishers), 295–310.

Graber, K.K., Pollard, E., Jonasson, B., and Schulte, E. (Eds.), 2002. Overview of Ocean Drilling Program Engineering Tools and Hardware. *ODP Tech. Note,* 31 [Online]. Available from World Wide Web: <http://www-odp.tamu.edu/publications/tnotes/tn31/INDEX.HTM>. [Cited 2002-07-03]

Guerin, G., and Goldberg, D., 2002a. Heave compensation and formation strength evaluation from downhole acceleration measurements while coring. *Geo-Mar. Lett.,* 104:10.1007/2002S00367002.

————, 2002b. Sonic attenuation measurements in the Mallik 2L-38 gas hydrates research well, MacKenzie Delta, NWT Canada. *J. Geophys. Res.,* 107:10.1029/2001JB000556.

Guerin, G., Goldberg, D., and Meltser, A., 1999. Characterization of in situ elastic properties of gas-hydrate bearing sediments on the Blake Ridge. *J. Geophys. Res.,* 104:17781–17795.

Heeseman, M., 2002. Modeling and analysis of transient pressure measurements in ODP boreholes for undisturbed formation pressure estimation [Diplomarbeit im Fach Geophysik]. University of Bremen.

Helgerud, M.B., Dvorkin, J., and Nur, A., 2000. Rock physics characterization for gas hydrate reservoirs: elastic properties. *In* Holder, G.D., and Bishnoi, P.R. (Eds.), *Gas Hydrates: Challenges for the Future.* Ann. N.Y. Acad. Sci., 912:116–125.

Hesse, R., 2003. Pore anomalies of submarine gas hydrate zones as tool to assess hydrate abundance and distribution in the subsurface. What have we learned in the past decade? *Earth Sci. Rev.,* 61:149–179.

Hesse, R., and Harrison, W.E., 1981. Gas hydrates (clathrates) causing pore-water freshening and oxygen isotope fractionation in deep-water sedimentary sections of terrigenous continental margins. *Earth Planet. Sci. Lett.,* 55:453–462.

Horai, K., and Von Herzen, R.P., 1985. Measurement of heat flow on Leg 86 of the Deep Sea Drilling Project. *In* Heath, G.R., Burckle, L.H., et al., *Init. Repts. DSDP,* 86: Washington (U.S. Govt. Printing Office), 759–777.

Horkowitz, J., Crary, S., Ganesan, K., Heidler, R., Luong, B., Morley, J., Petricola, M., Prusiecki, C., Speier, P., Poitzsch, M., Scheibal, J.R., and Hashem, M., 2002. Applications of a new magnetic resonance logging-while-drilling tool in a Gulf of Mexico deepwater development well. *Trans. SPWLA Annu. Logging Symp.,* 14.

Kastner, M., Kvenvolden, K.A., Whiticar, M.J., Camerlenghi, A., and Lorenson, T.D., 1995. Relation between pore fluid chemistry and gas hydrates associated with bottom-simulating reflectors at the Cascadia margin, Sites 889 and 892. *In* Carson, B., Westbrook, G.K., Musgrave, R.J., and Suess, E. (Eds.), *Proc. ODP, Sci. Results,* 146 (Pt 1): College Station, TX (Ocean Drilling Program), 175–187.

Kimura, G., Silver, E.A., Blum, P., et al., 1997. *Proc. ODP, Init. Repts.,* 170: College Station, TX (Ocean Drilling Program).

Kleinberg, R., Flaum, C., Straley, C., Brewer, P., Malby, G., Peltzer, E., Freiderich, G., and Yesinowski, J., 2003. Seafloor nuclear magnetic resonance assay of methane hydrate in sediment and rock. *J. Geophys. Res.,* 3:2036.

Koizumi, I., 1992. Diatom biostratigraphy of the Japan Sea: Leg 127. *In* Pisciotto, K.A., Ingle, J.C., Jr., von Breymann, M.T., Barron, J., et al., *Proc. ODP, Sci. Results,* 127/128 (Pt. 1): College Station, TX (Ocean Drilling Program), 249–289.

Koizumi, I., and Tanimura, Y., 1985. Neogene diatom biostratigraphy of the middle latitude western North Pacific, Deep Sea Drilling Project Leg 86. *In* Heath, G.R., Burckle, L.H., et al., *Init. Repts. DSDP,* 86: Washington (U.S. Govt. Printing Office), 269–300.

Kristiansen, J.I., 1982. The transient cylindrical probe method for determination of thermal parameters of earth materials [Ph.D. dissert.]. Aaehus Univ.

Lamont-Doherty Earth Observatory Borehole Research Group, 2001. *ODP Logging Services Electronic Manual,* Version 2.0 [Online]. Available from World Wide Web: <http://www.ldeo.columbia.edu/BRG/ODP/LOGGING/MANUAL/index.html>. [Cited 2003-02-15]

Lovley, D., and Phillips, E.J.P., 1988. Novel mode of microbial energy metabolism: organic carbon oxidation coupled to dissimilatory reduction of iron or manganese. *Appl. Environ. Microbiol.,* 54:1472–1480.

Mackenzie, K.V., 1981. Nine-term equation for sound speed in the oceans. *J. Acoust. Soc. Am.,* 70:807–812.

Manheim, F.T., and Sayles, F.L., 1974. Composition and origin of interstitial waters of marine sediments, based on deep sea drilled cores. *In* Goldberg, E.D. (Ed.), *The Sea* (Vol. 5): *Marine Chemistry: The Sedimentary Cycle:* New York (Wiley), 527–568.

Martini, E., and Müller, C., 1986. Current Tertiary and Quaternary calcareous nannoplankton stratigraphy and correlations. *Newsl. Stratigr.,* 16:99–112.

Mathews, M., 1986. Logging characteristics of methane hydrate. *The Log Analyst,* 27:26–63.

Mayer, L., Pisias, N., Janecek, T., et al., 1992. *Proc. ODP, Init. Repts.,* 138 (Pts. 1 and 2): College Station, TX (Ocean Drilling Program).

Mazzullo, J., and Graham, A.G. (Eds.), 1988. Handbook for shipboard sedimentologists. *ODP Tech. Note,* 8.

Mazzullo, J.M., Meyer, A., and Kidd, R.B., 1988. New sediment classification scheme for the Ocean Drilling Program. *In* Mazzullo, J., and Graham, A.G. (Eds.), *Handbook for Shipboard Sedimentologists. ODP Tech. Note,* 8:45–67.

Mikada, H., Becker, K., Moore, J.C., Klaus, A., et al., 2002. *Proc. ODP, Init. Repts.,* 196 [CD-ROM]. Available from: Ocean Drilling Program, Texas A&M University, College Station TX 77845-9547, USA.

Mix, A.C., Tiedemann, R., Blum, P., et al., 2003. *Proc. ODP, Init. Repts.,* 202 [CD-ROM]. Available from: Ocean Drilling Program, Texas A&M University, College Station TX 77845-9547, USA.

Moore, J.C., Klaus, A., et al., 1998. *Proc. ODP, Init. Repts.,* 171A [CD-ROM]. Available from: Ocean Drilling Program, Texas A&M University, College Station, TX 77845-9547, U.S.A.

Munsell Color Company, Inc., 1975. *Munsell Soil Color Charts:* Baltimore, MD (Munsell).

Murray, R.W., Miller, D.J., and Kryc, K.A., 2000. Analysis of major and trace elements in rocks, sediments, and interstitial waters by inductively coupled plasma–atomic emission spectrometry (ICP-AES). *ODP Tech. Note,* 29 [Online]. Available from World Wide Web: <http://www_odp.tamu.edu/publications/tnotes/tn29/INDEX.HTM>. [Cited 2002-07-03]

O'Brien, P.E., Cooper, A.K., Richter, C., et al., 2001. *Proc. ODP, Init. Repts.,* 188 [CD-ROM]. Available from: Ocean Drilling Program, Texas A&M University, College Station TX 77845-9547, USA.

Ostermeier, R.M., Pelletier, J.H., Winker, C.D., Nicholson, J.W., Rambow, F.H., and Cowan, K.M., 2000. Dealing with shallow-water flow in the deepwater Gulf of Mexico. *Proc. Offshore Tech. Conf.:* Dallas (Offshore Tech. Conf.), 32:75–86.

Paull, C.K., Matsumoto, R., Wallace, P.J., et al., 1996. *Proc. ODP, Init. Repts.,* 146: College Station, TX (Ocean Drilling Program).

Paull, C.K., and Ussler, W., III, 2001. History and significance of gas sampling during the DSDP and ODP. *In* Paull, C.K., and Dillon, W.P. (Eds.), *Natural Gas Hydrates: Occurrence, Distribution, and Detection.* Am. Geophys. Union, Geophys. Monogr. Ser., 124:53–66.

Perch-Nielsen, K., 1985. Cenozoic calcareous nannofossils. *In* Bolli, H.M., Saunders, J.B., and Perch-Nielsen, K. (Eds.), *Plankton Stratigraphy:* Cambridge (Cambridge Univ. Press), 427–554.

Petschick, R., 2000. *MacDiff 4.1.1 Manual* [Online]. Available from World Wide Web: <http://www.geologie.uni-frankfurt.de/Staff/Homepages/Petschick/RainerE.html>. [Revised 2001-05-17]

Pettigrew, T.L., 1992. Design and operation of a wireline pressure core sampler. *ODP Tech Note,* 17.

Pimmel, A., and Claypool, G., 2001. Introduction to shipboard organic geochemistry on the *JOIDES Resolution. ODP Tech. Note,* 30 [Online]. Available from World Wide Web: <http://www-odp.tamu.edu/publications/tnotes/tn30/INDEX.HTM>. [Cited 2002-07-05]

Pribnow, D.F.C., Kinoshita, M., and Stein, C.A., 2000. Thermal data collection and heat flow recalculations for ODP Legs 101–180. Institute for Joint Geoscientific Research, GGA, Hanover, Germany, 0120432. Available from World Wide Web: <http://www-odp.tamu.edu/publications/heatflow/ODPReprt.pdf>. [Cited 2002-07-03]

Rack, F.R., 2001. *Preliminary Evaluation of Existing Pressure/Temperature Coring System:* Washington, D.C. (Joint Oceanographic Institutions).

Rider, M., 1996. *The Geological Interpretation of Well Logs* (2nd ed.): Caithness (Whittles Publishing).

Schlumberger, 1989. *Log Interpretation Principles/Applications:* Houston (Schlumberger Educ. Services), SMP–7017.

————, 1994. *Log Interpretation Charts:* Sugar Land (Schlumberger), SMP-7006.

Schnaid, F., Sills, G.C., Soares, J.M., and Nyirenda, Z., 1997. Predictions of the coefficient of consolidation from piezocone tests. *Can. Geotech. J.,* 34:315–327.

Schultheiss, P.J., and McPhail, S.D., 1986. Direct indication of pore-water advection from pore pressure measurements in Madeira Abyssal Plain sediments. *Nature,* 320:348–350.

Serra, O., 1984. *Fundamentals of Well-Log Interpretation* (Vol. 1): *The Acquisition of Logging Data:* Dev. Pet. Sci., 15A.

————, 1986. *Fundamentals of Well-Log Interpretation* (Vol. 2): *The Interpretation of Logging Data:* Dev. Pet. Sci., 15B.

————, 1989. *Formation MicroScanner Image Interpretation:* Houston (Schlumberger Educ. Services), SMP-7028.

Shepard, F., 1954. Nomenclature based on sand-silt-clay ratios. *J. Sediment. Petrol.,* 24:151–158.

Shipboard Scientific Party, 1998. Introduction. *In* Becker, K., Malone, M.J., et al., *Proc. ODP, Init. Repts.,* 174B: College Station, TX (Ocean Drilling Program), 3–9.

Shipley, T.H., Ogawa, Y., Blum, P., and Bahr, J.M. (Eds.), 1995. *Proc. ODP, Sci. Results,* 156: College Station, TX (Ocean Drilling Program).

Sloan, E.D., 1998. *Clathrate Hydrates of Natural Gases* (2nd ed.): New York (Marcel Dekker).

Smith, D.C., Spivack, A.J., Fisk, M.R., Haveman, S.A., and Staudigel, H., 2000a. Tracer-based estimates of drilling-induced microbial contamination of deep sea crust. *Geomicrobiol. J.,* 17:207–219.

Smith, D.C., Spivack, A.J., Fisk, M.R., Haveman, S.A., Staudigel, H., and ODP Leg 185 Shipboard Scientific Party, 2000b. Methods for quantifying potential microbial contamination during deep ocean coring. *ODP Tech. Note,* 28 [Online]. Available from the World Wide Web: <http://www-odp.tamu.edu/publications/tnotes/tn28/INDEX.HTM>. [Cited 2003-02-16]

Suess, E., von Huene, R., et al., 1988. *Proc. ODP, Init. Repts.,* 112: College Station, TX (Ocean Drilling Program).

Terry, R.D., and Chilingar, G.V., 1955. Summary of "Concerning some additional aids in studying sedimentary formations" by M.S. Shvetsov. *J. Sediment. Petrol.,* 25:229–234.

Tréhu, A.M., and Bangs, N., 2001. 3-D seismic imaging of an active margin hydrate system, Oregon continental margin, report of cruise TTN112. *Oregon State Univ. Data Rpt.,* 182.

von Herzen, R.P., and Maxwell, A.E., 1959. The measurement of thermal conductivity of deep-sea sediments by a needle-probe method. *J. Geophys. Res.,* 64:1557–1563.

Wallace, P.J., Dickens, G.R., Paull, C.K., and Ussler, W., III, 2000. Effects of core retrieval and degassing on the carbon isotope composition of methane in gas hydrate- and free gas-bearing sediments from the Blake Ridge. *In* Paull, C.K., Matsumoto, R., et al., *Proc. ODP, Sci. Results,* 164: College Station, TX (Ocean Drilling Program), 101–112.

Wellsbury, P., Goodman, K., Cragg, B.A., and Parkes, R.J., 2000. The geomicrobiology of deep marine sediments from Blake Ridge containing methane hydrate (Sites 994, 995, and 997). *In* Paull, C.K., Matsumoto, R., Wallace, P.J., and Dillon, W.P. (Eds.), *Proc. ODP, Sci. Results,* 164: College Station, TX (Ocean Drilling Program), 379–391.

Wentworth, C.K., 1922. A scale of grade and class terms of clastic sediments. *J. Geol.,* 30:377–392.

Whittle, A.J., Sutabutr, T., Germaine, J.T., and Varney, A., 2001. Prediction and measurement of pore pressure dissipation for a tapered piezocone. *Geotechnique,* 51:601–617.

Wilson, W.D., 1960. Speed of sound in seawater as a function of temperature, pressure and salinity. *J. Acoust. Soc. Am.,* 32:641–644.

Wyllie, M.R.J., Gregory, A.R., and Gardner, L.W., 1956. Elastic wave velocities in heterogeneous and porous media. *Geophysics,* 21:41–70.

Yanagisawa, Y., and Akiba, F., 1998. Refined Neogene diatom biostratigraphy for the northwest Pacific around Japan, with an introduction of code numbers for selected diatom biohorizons. *J. Geol. Soc. Jpn.,* 104:395–414.

Figure F1. Example of coring and depth intervals.

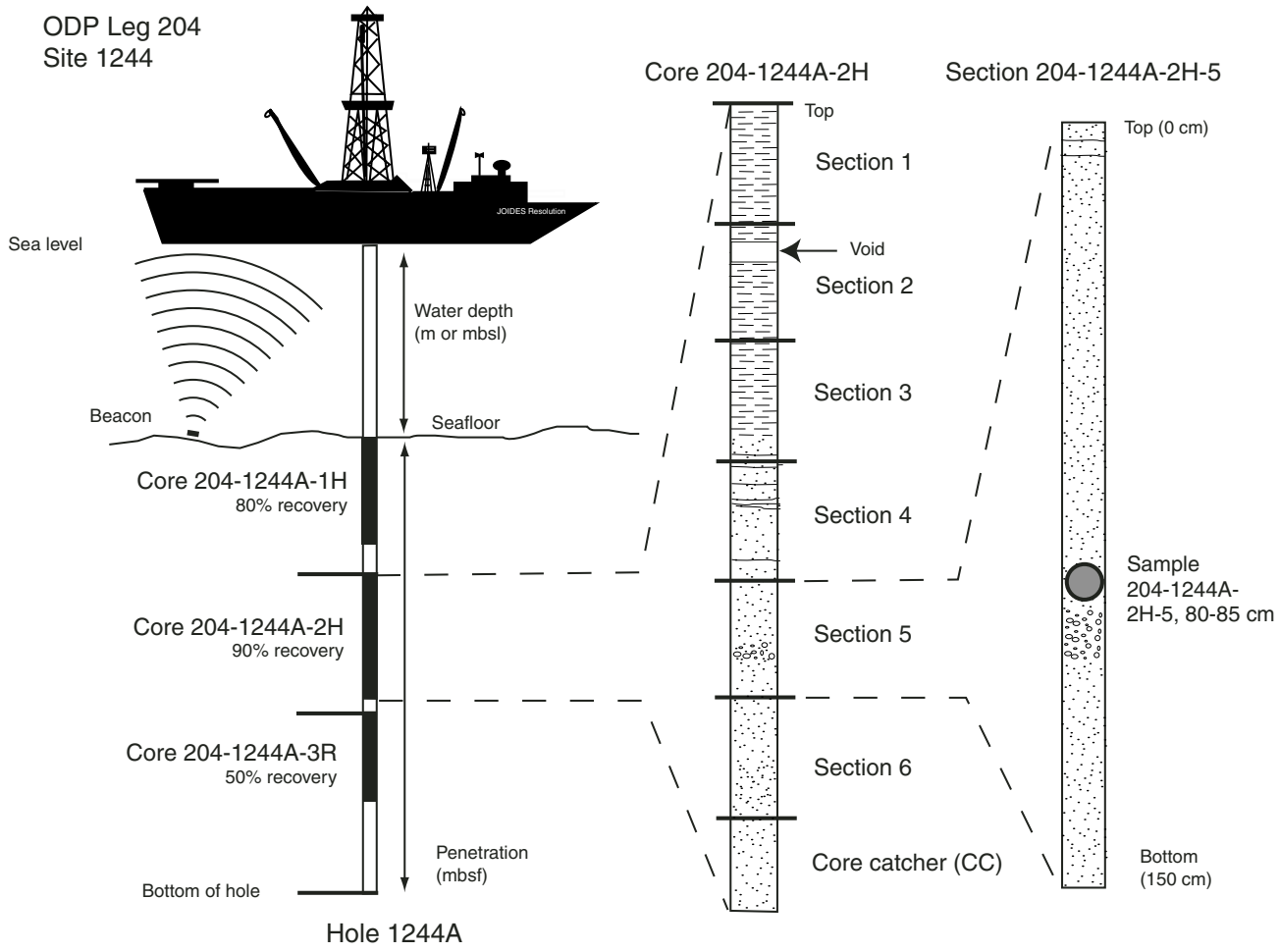

Figure F2. Grain-size classification diagram for siliciclastic sediments. Modified after Wentworth (1922).

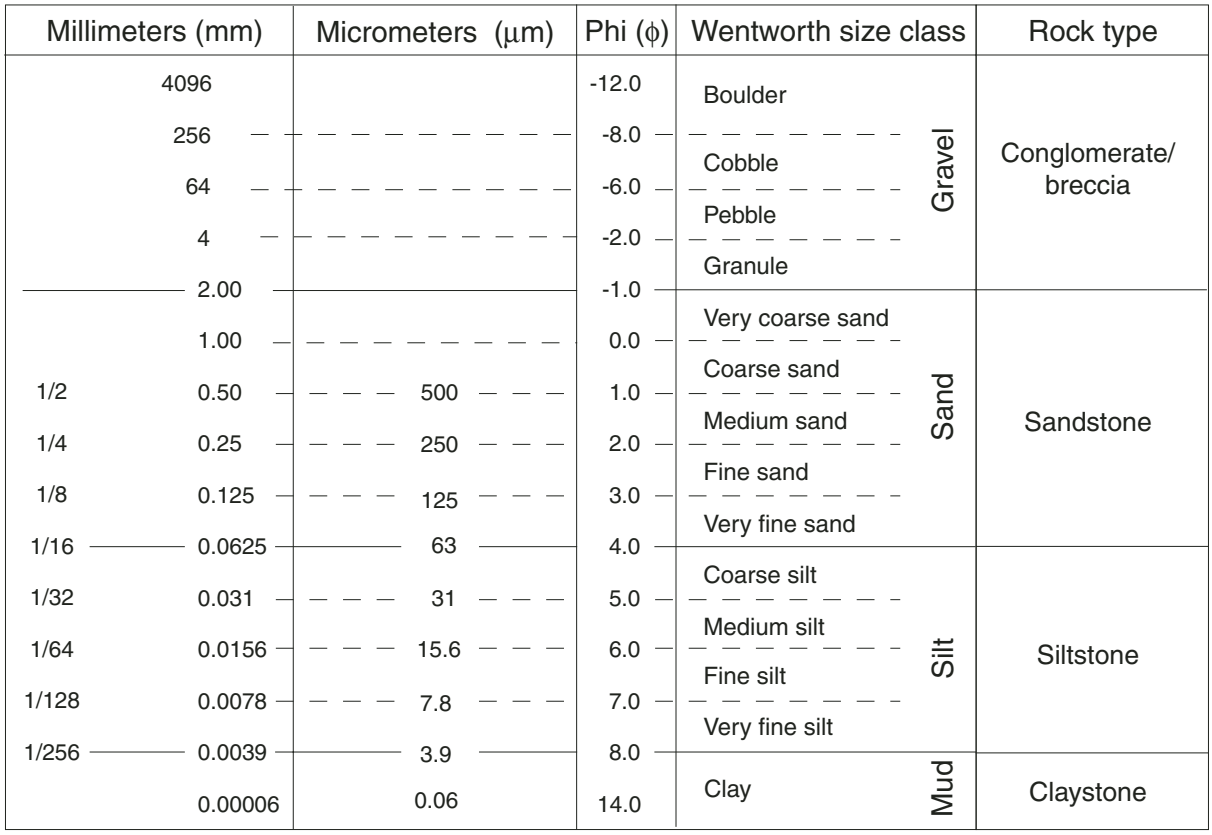

Figure F3. Classification scheme for siliciclastic sediment components (Shepard, 1954).

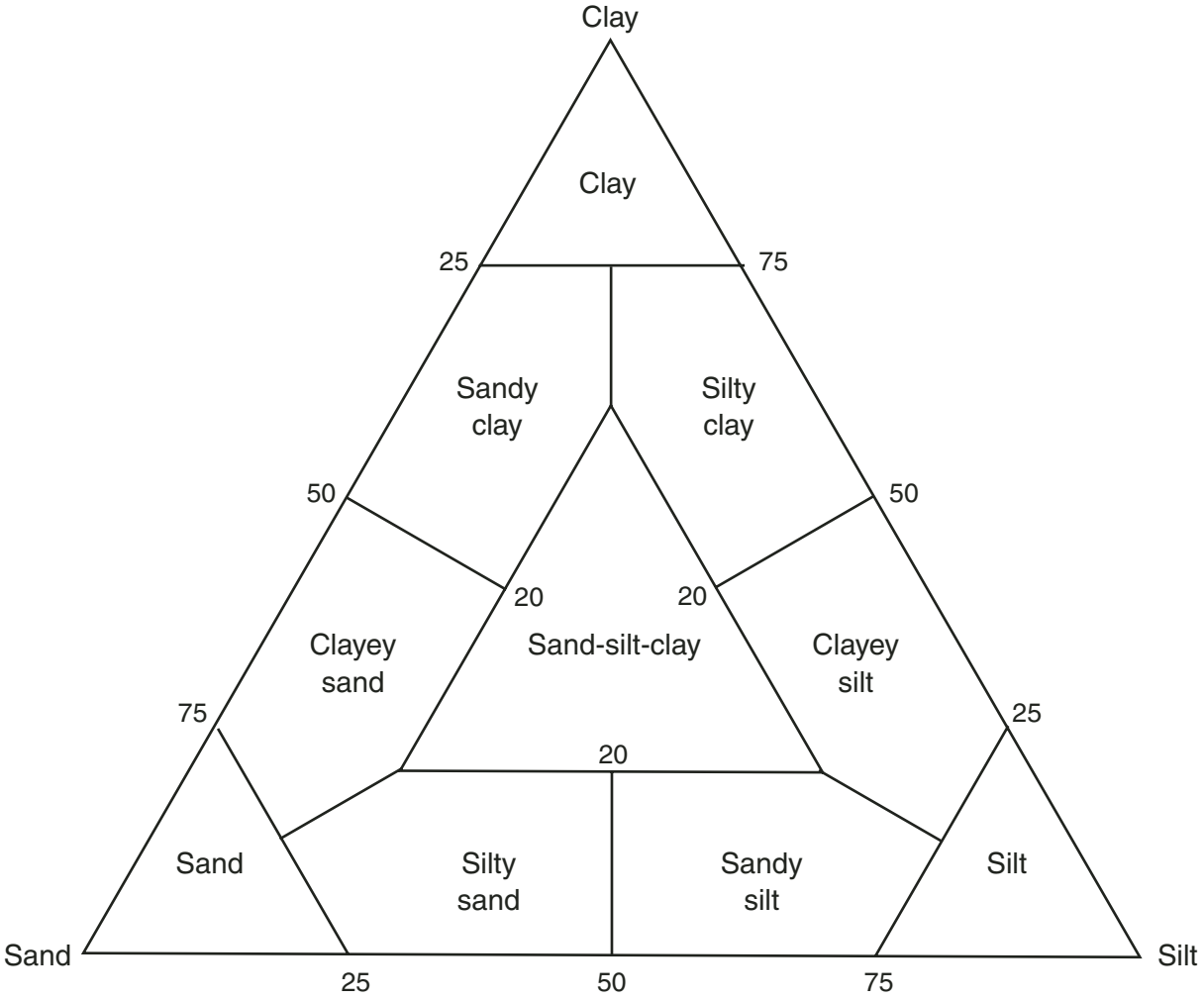

Figure F4. Example of the graphical representation of VCDs (barrel sheets).

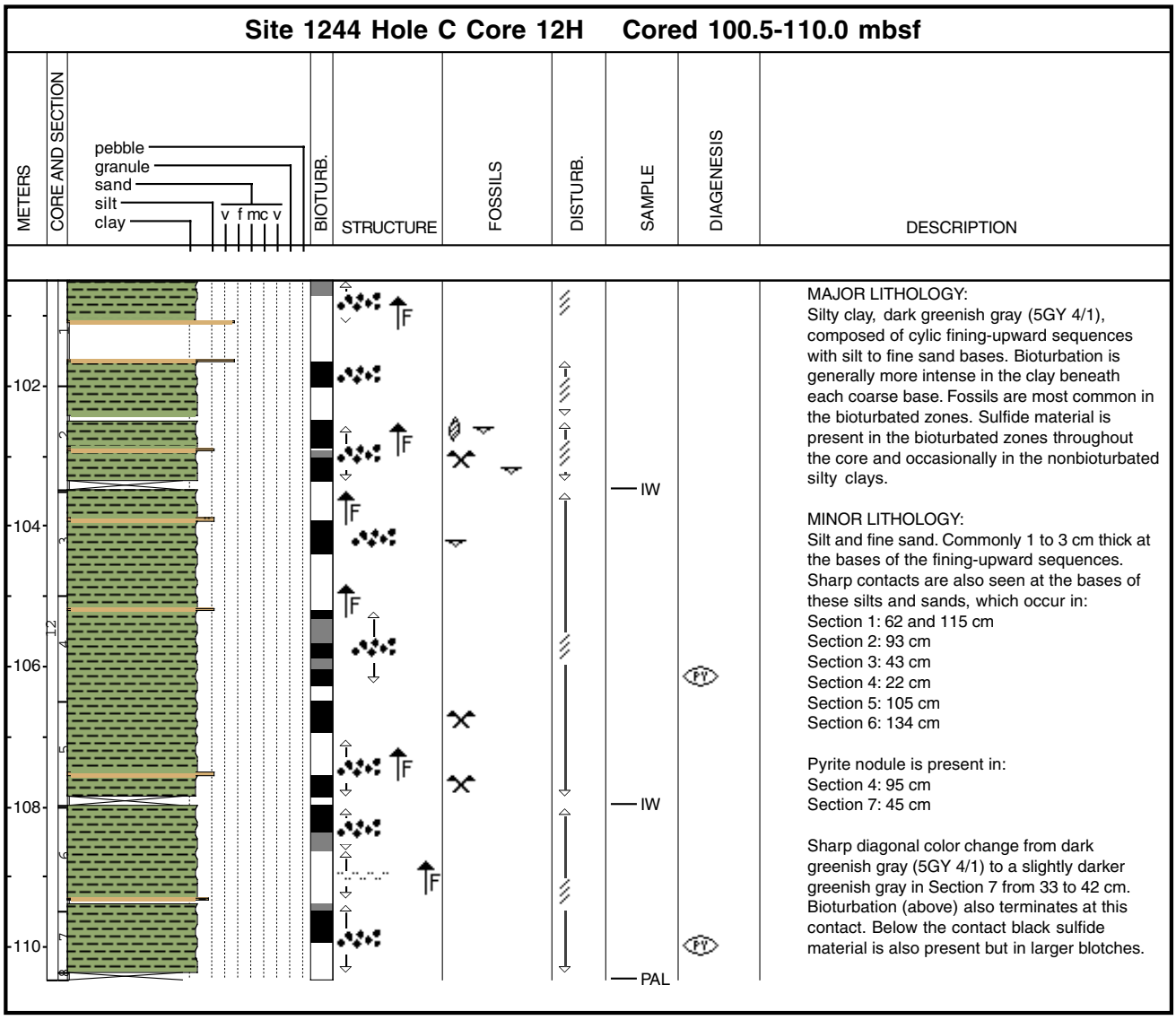

Figure F5. Key to patterns and symbols used in Leg 204 barrel sheets.

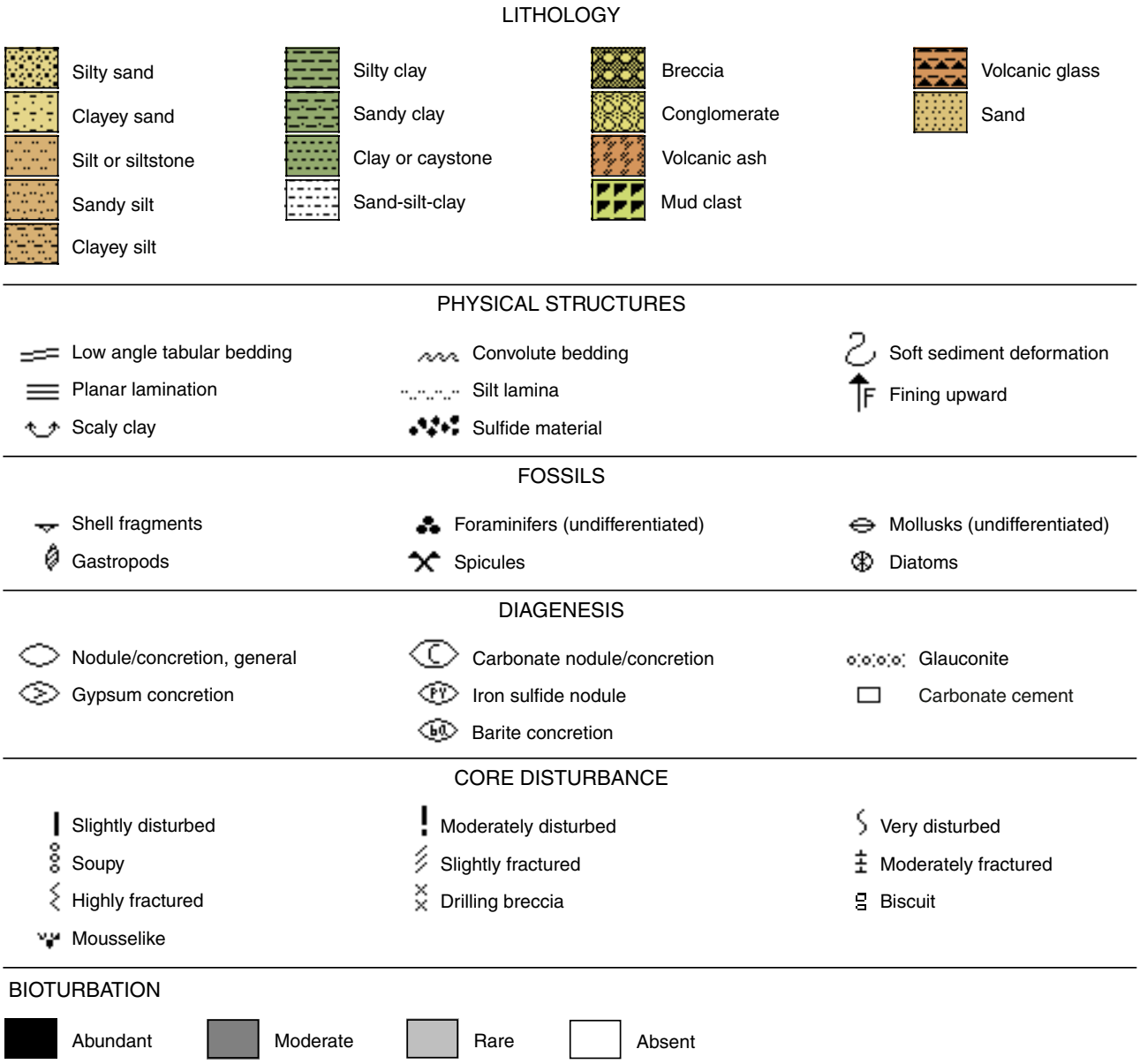

Figure F6. Example of "soupy" sediment texture (interval 204-1248B-1H-2, 70–80 cm).

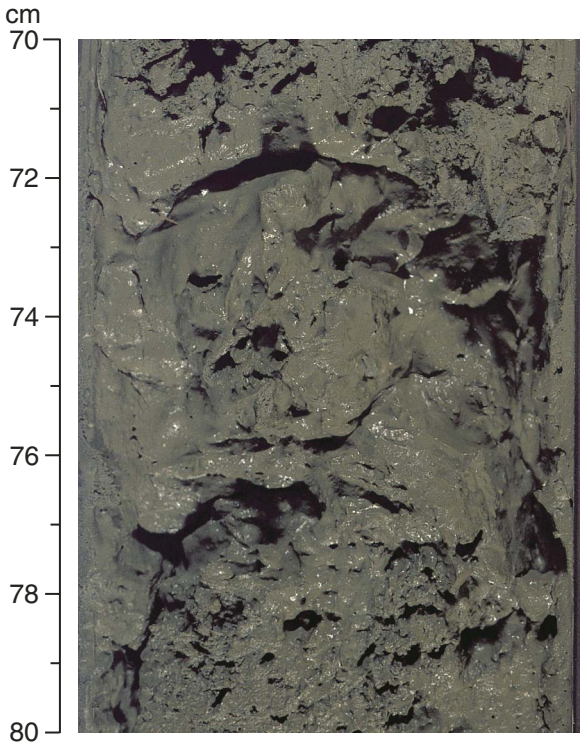

Figure F7. Example of wet, watery, mousselike sediment texture found in soft sediment and associated with hydrate dissociation (interval 204-1249C-4H-3, 19–29 cm).

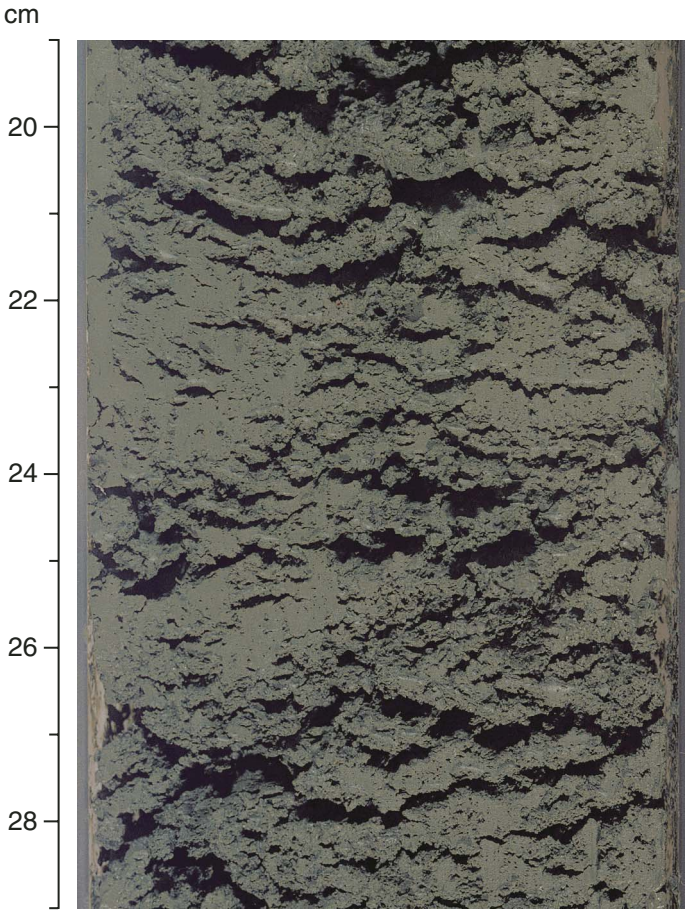

Figure F8. Example of "flaky" mousselike texture found in drier sediment and associated with hydrate dissociation (interval 204-1244C-7H-5, 1–11 cm).

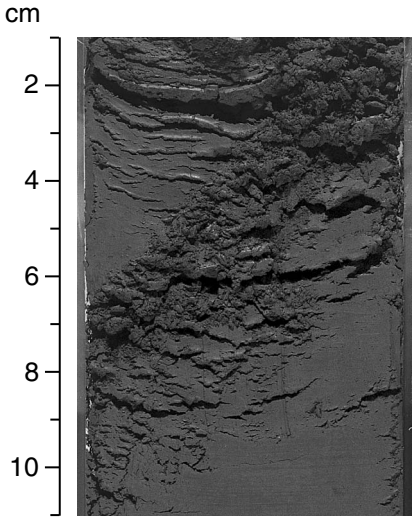

Figure F9. Correlation of the GPTS (Berggren et al., 1995a, 1995b) and the biostratigraphic zonations used during Leg 204. NPD = North Pacific Diatom Zone. FO = first occurrence, LO = last occurrence, N = calcareous nannofossil, D = diatom.

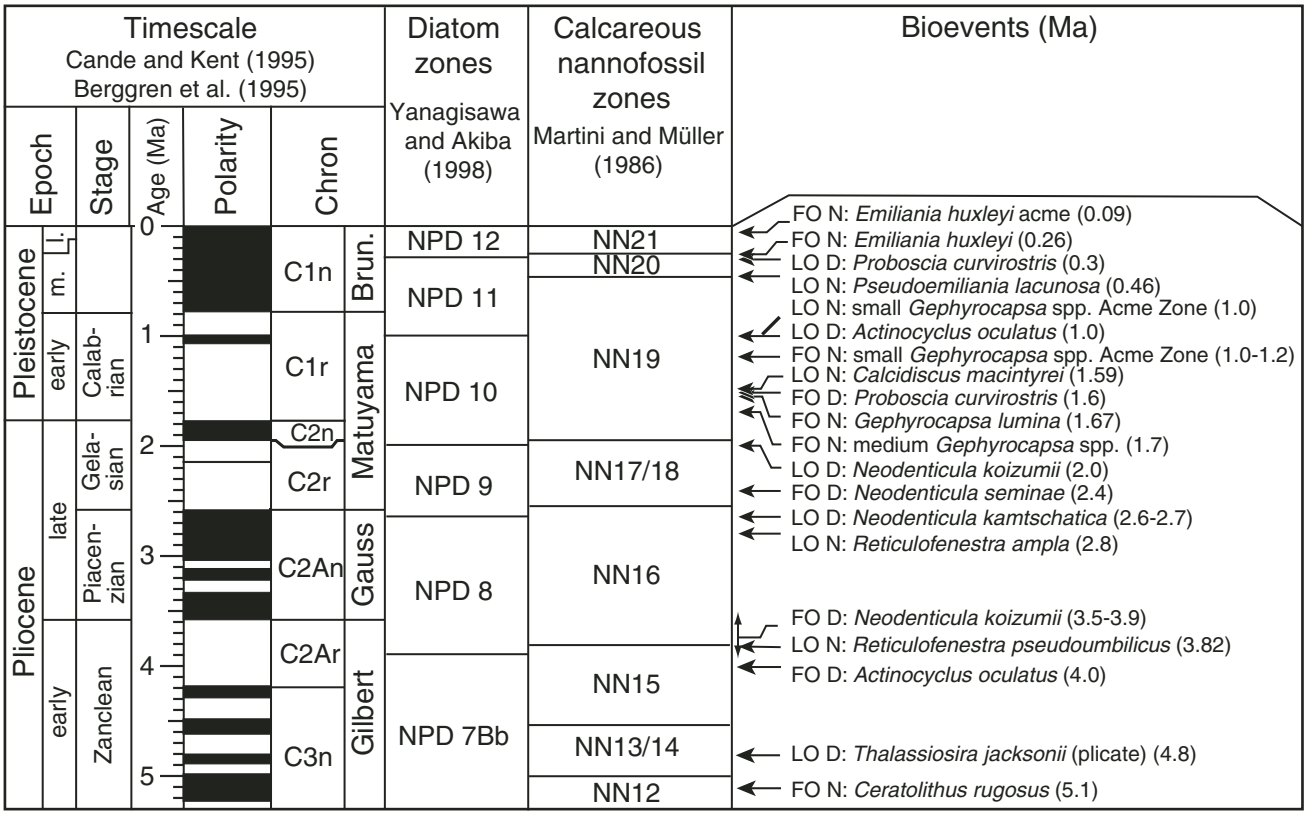

Figure F10. Sedimentologist Jill Weinberger holds a FLIR SC-2000 camera used for IR thermal imaging during Leg 204. The camera was mounted on a track inside a tubular structure designed to reduce extraneous infrared reflections.

Figure F11. Typical gas hydrate shapes observed during Leg 204. **A.** Disseminated gas hydrate (interval 204-1249C-2H-1, 108–140 cm). **B.** Nodular gas hydrate (interval 204-1244C-10H-2, 70–103 cm). **C.** Massive gas hydrate (Section 204-1249C-1H-CC). **D.** Vein gas hydrate (interval 204-204-1244C-8H-1, 47–52 cm). **E.** Veinlet gas hydrate (see Fig. 8C, p. 43, in the "Site 1249" chapter). **F.** Layer gas hydrate (Sample 204-1250C-11H-3, 94–95 cm).

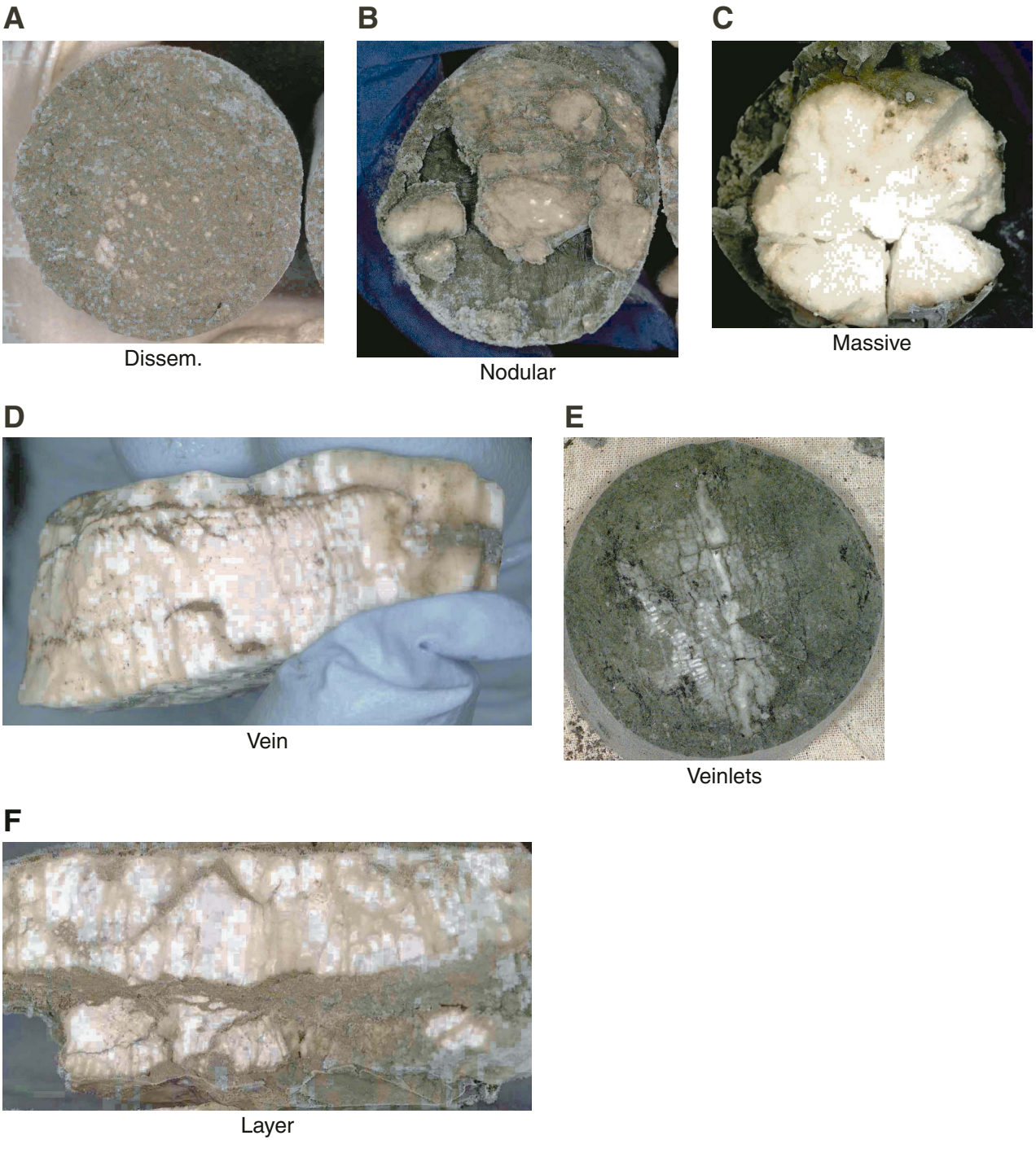

Figure F12. GRA profile of a graduated aluminum and water reference section.

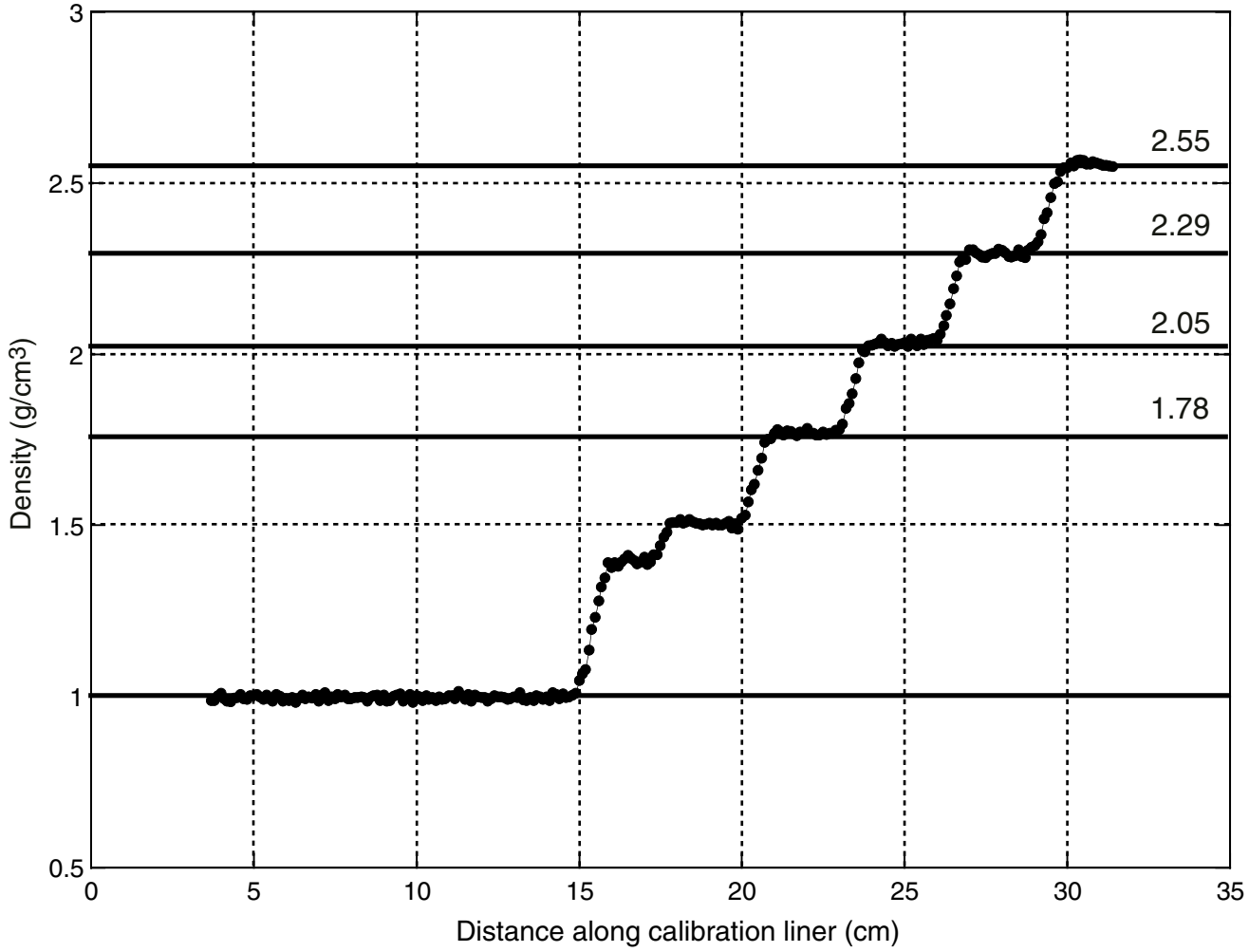

Figure F13. Calibration plots for the Geotek Non Contact Resistivity (NCR) system using 25-cm lengths of core liner filled with filled with NaCl solutions of known concentration. The data were collected automatically by placing the short sections in series on the MST.

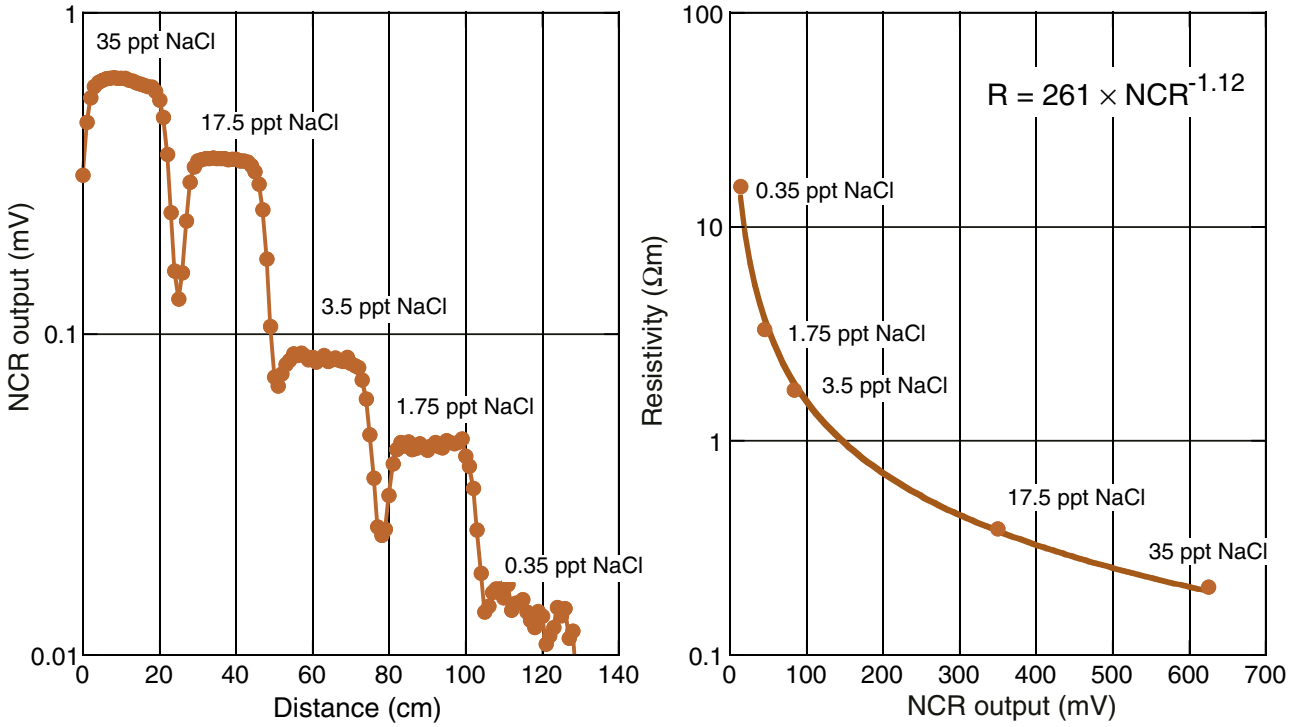

Figure F14. Illustration of gas expansion cracks.

Section 204-1251G-1H-6

Illustration of gas expansion cracks.

Images showing general nature of core cracking that occured throughout Leg 204.

The image was taken from whole core (through the liner) using the Geotek digital imaging system.

The white calibration was performed using white paper wrapped around the core, creating the even illumunation know as "virtual slabbing."

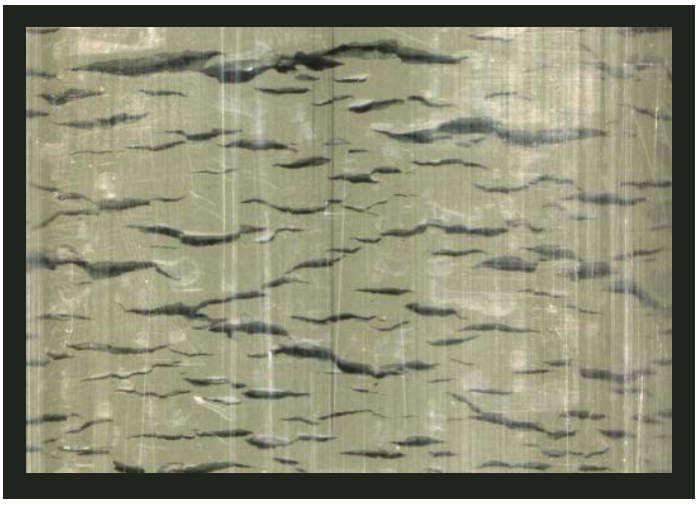

Figure F15. A. Example of data from a typical APCT tool run. Pribnow et al. (2000) discuss uncertainties resulting from subjectivity of analyst picks of t_i and t_r. **B.** Example of a typical Davis-Villinger Temperature-Pressure Probe (DVTPP) run. AHC = active heave compensation, GMT = Greenwich mean time.

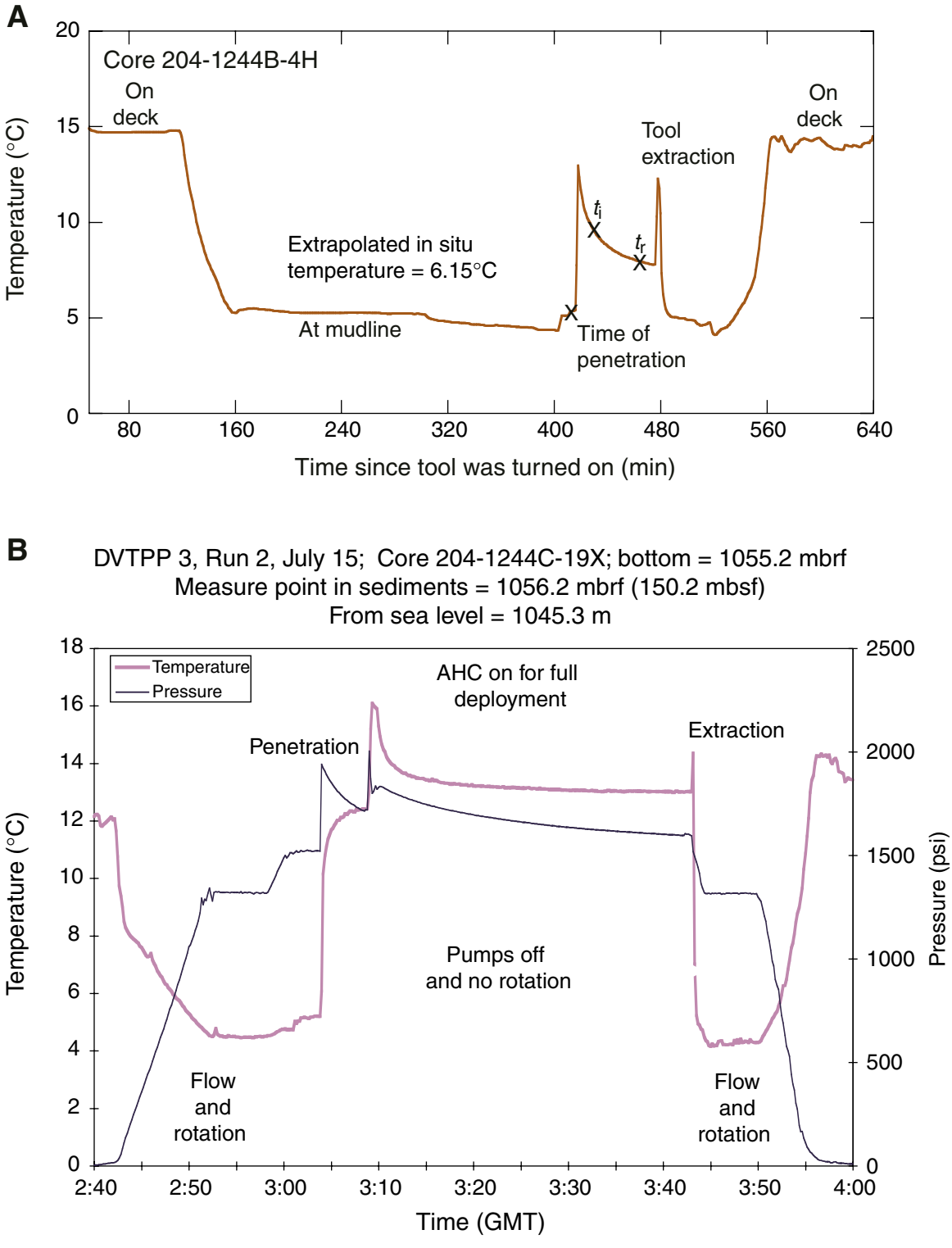

Figure F16. Diagram illustrating the setup during a PCS depressurization experiment. The drawing of the PCS is scaled, and the drawings of the periphery (e.g., bubbling chamber) are not to scale.

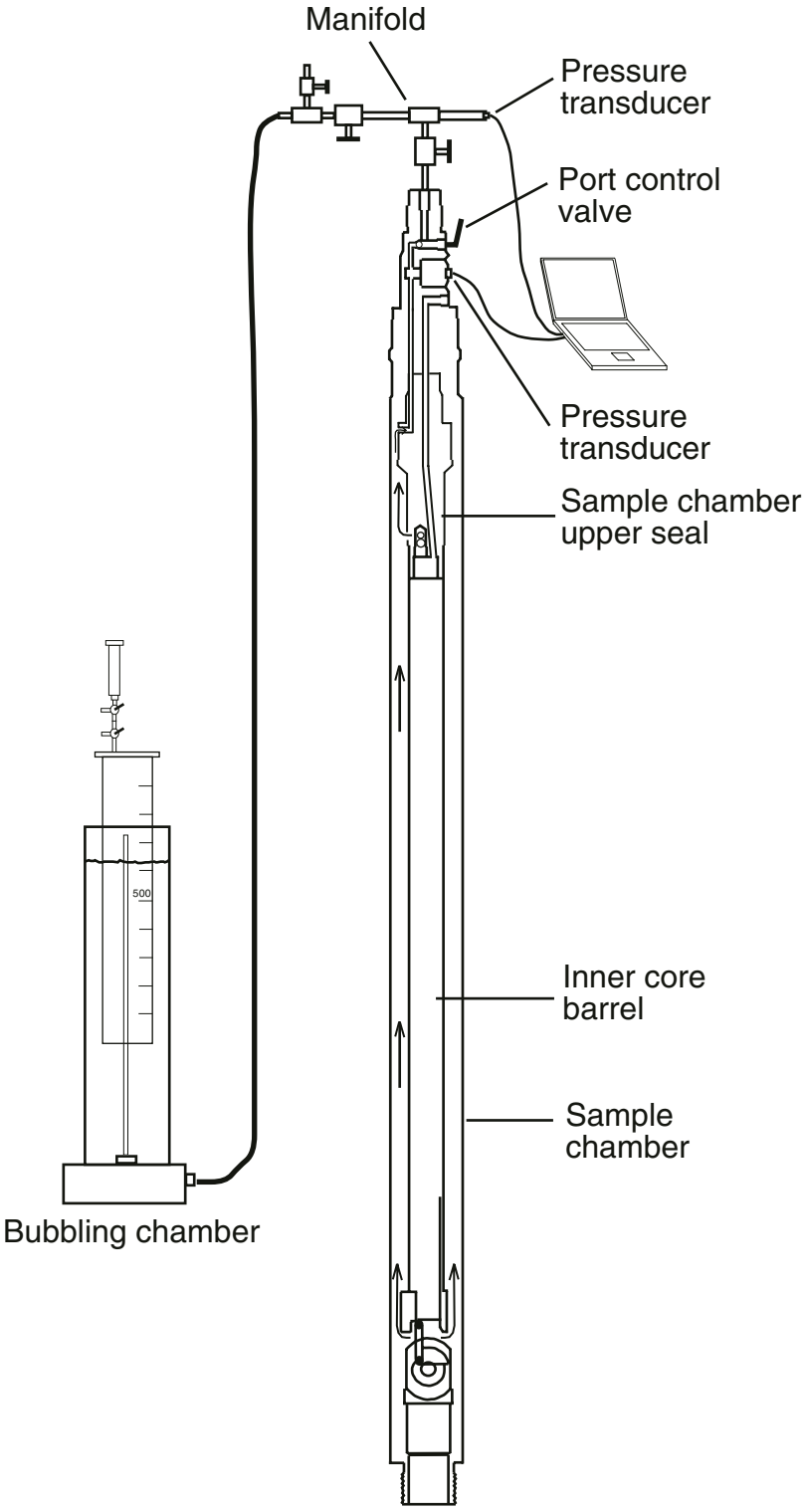

Figure F17. Configuration of the drill string used for logging-while-drilling (LWD) operations. VND = Vision Neutron Density tool; NMR-MRP = Nuclear Magnetic Resonance tool, MWD = Measurement-While-Drilling tool, GVR6 = GeoVision Resistivity tool.

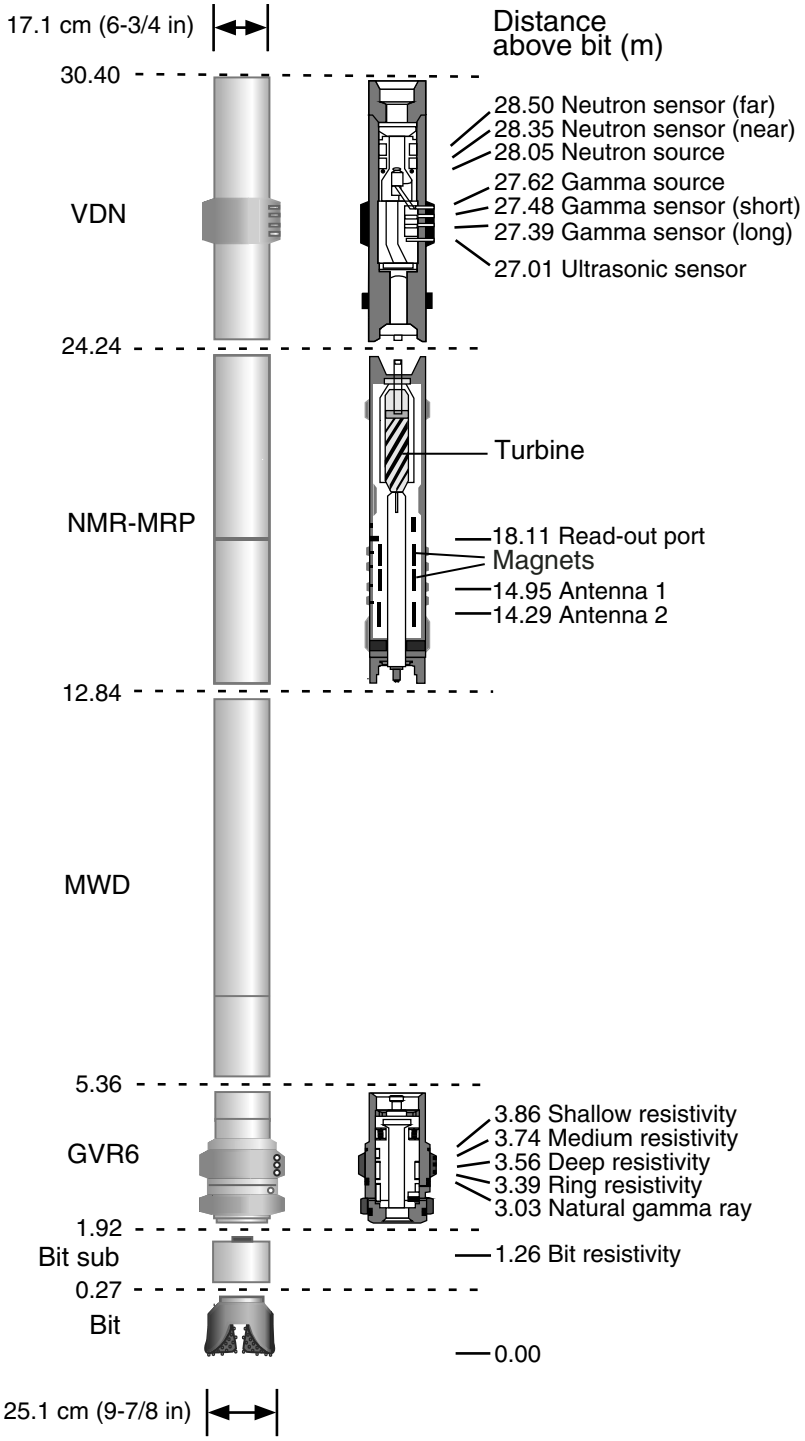

Figure F18. Schematic figure of rig instrumentation. DWOB = downhole weight on bit, DTOR = downhole weight on torque.

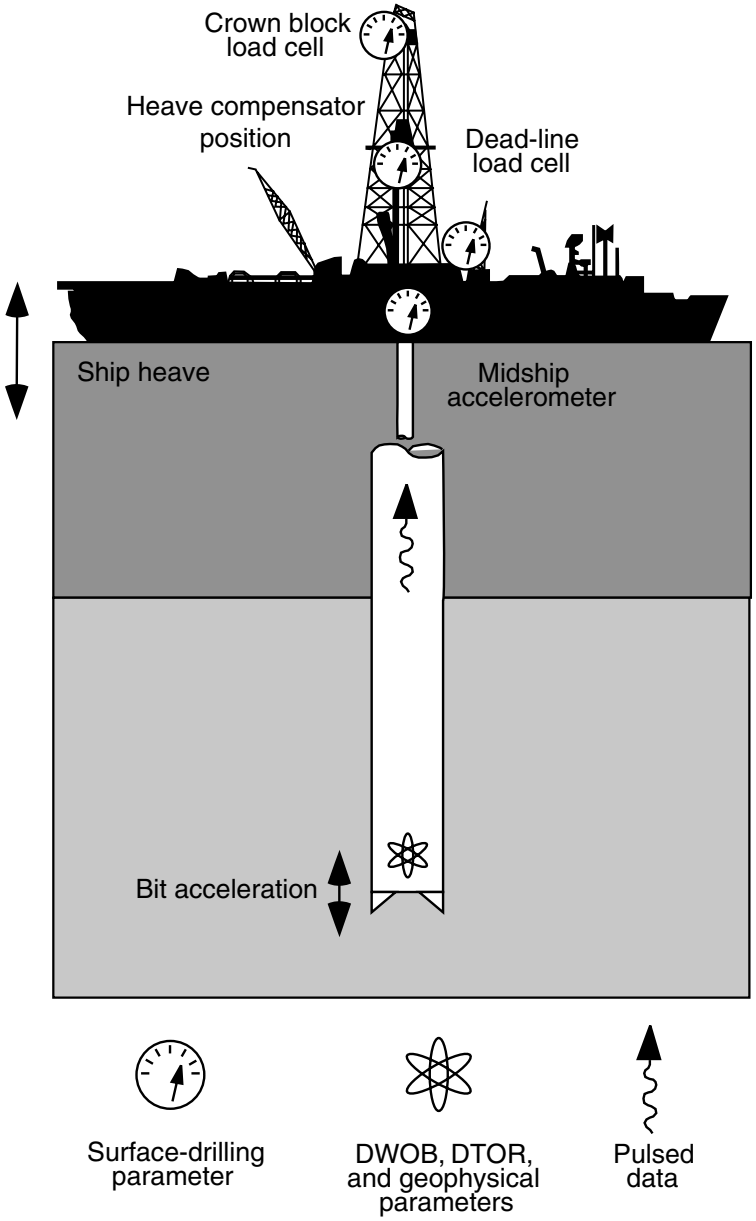

Figure F19. Schematic illustration of the RAB tool.

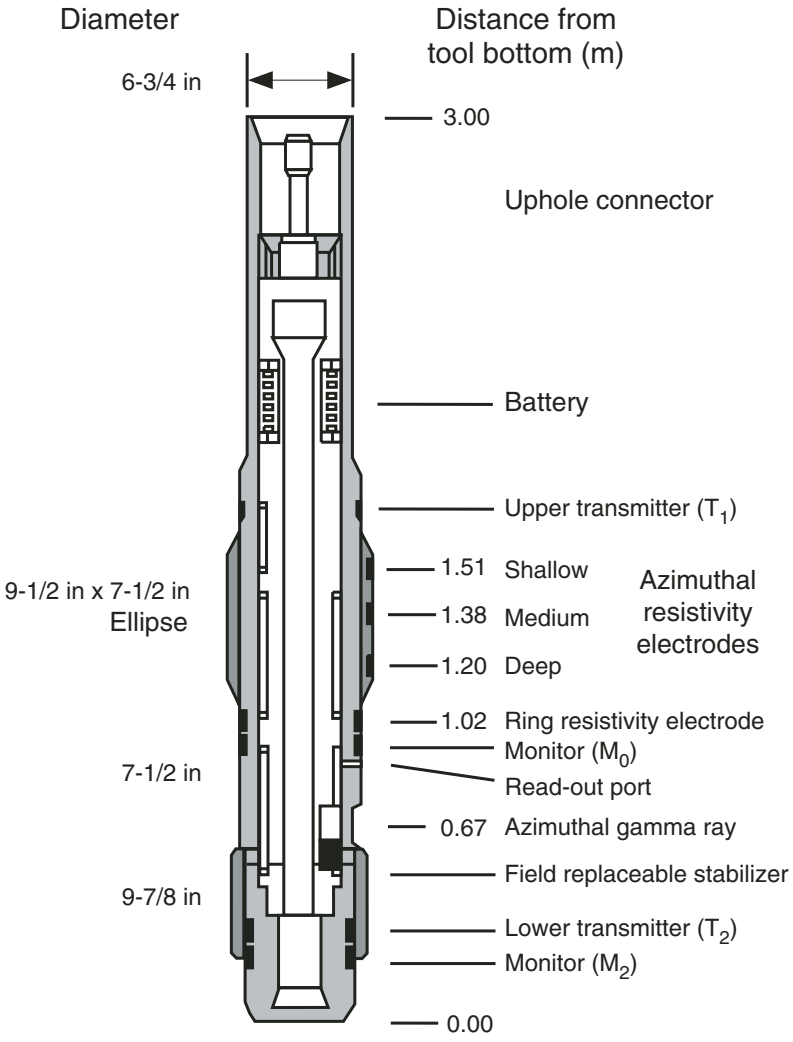

Figure F20. Schematic illustration of the resistivity-at-the-bit (RAB)-8 tool. ID = inner diameter, OD = outside diameter.

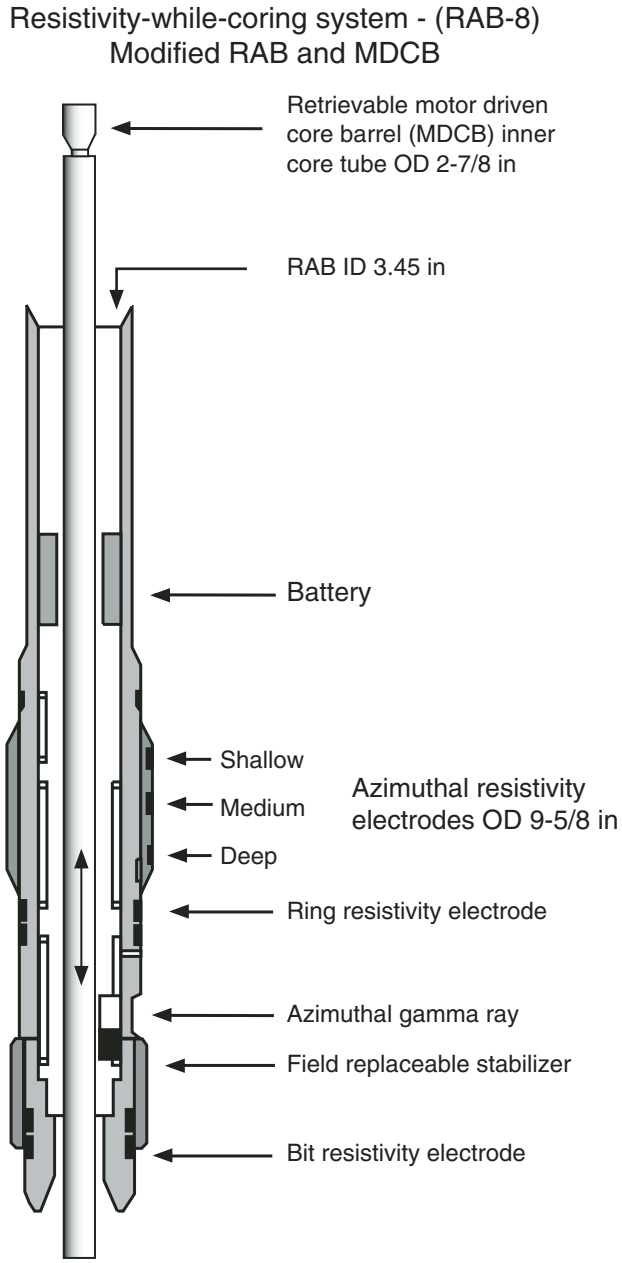

Figure F21. Schematic illustration of the MWD tool. Drilling fluids are constantly pumped down the drill string, and periodic closure of the MWD valve creates pressure pulses that can be detected on the rig floor.

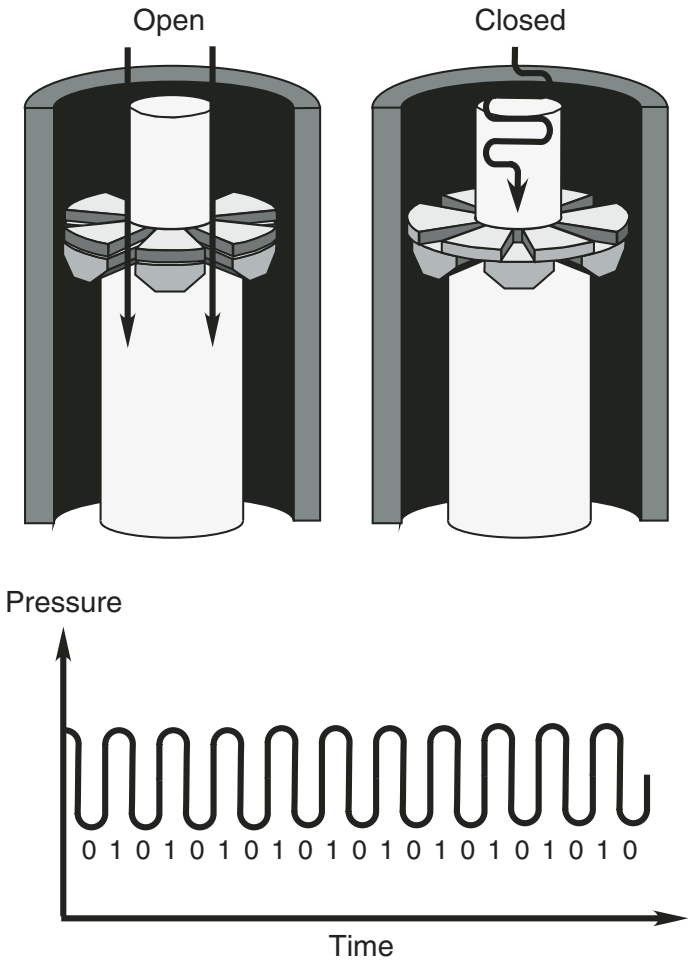

Figure F22. Schematic illustration of the NRM-MRP tool.

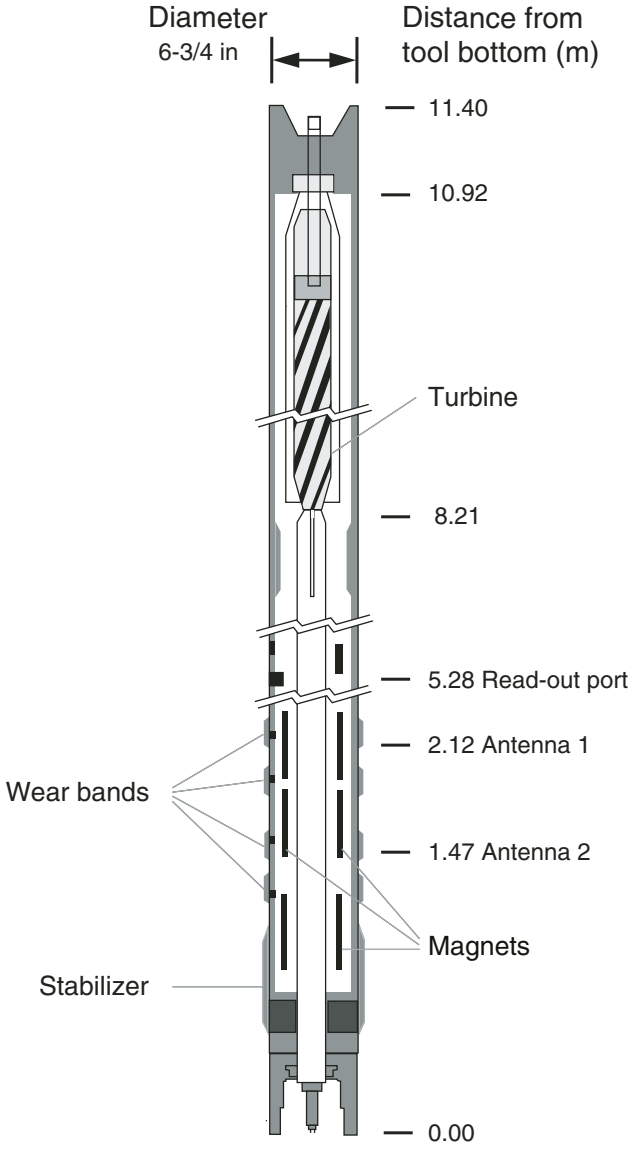

Figure F23. Schematic illustration of the VND tool.

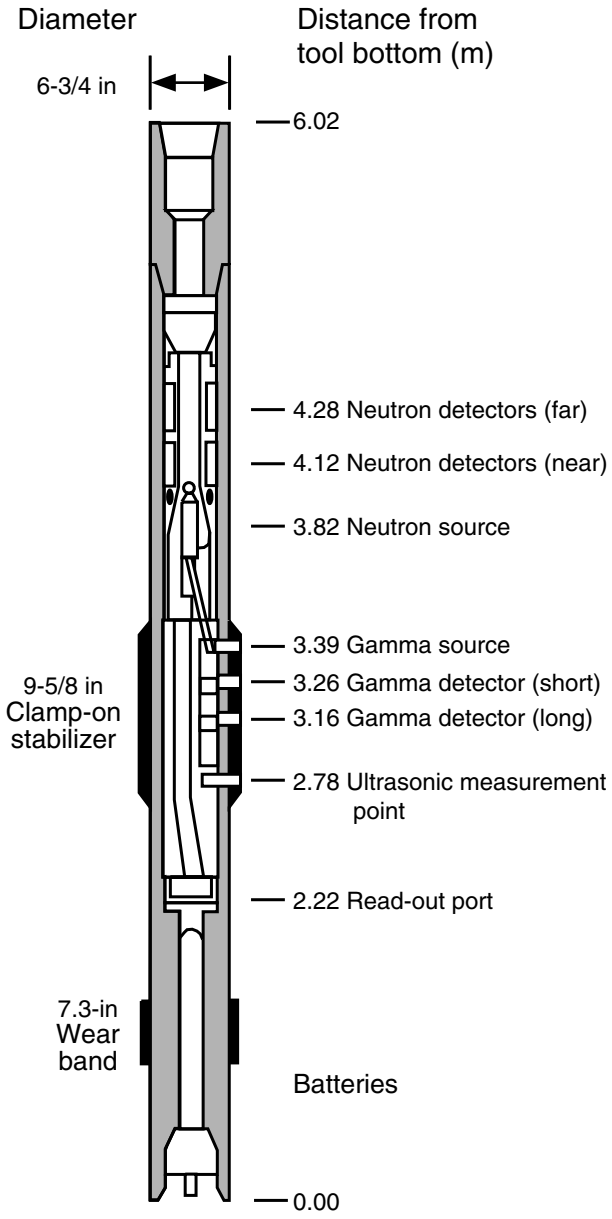

Figure F24. Onboard logging-while-drilling (LWD) data flow. MWD = measurement while drilling. PC = personal computer, IDEAL = integrated drilling and evaluation and logging, DHML = shipboard downhole measurements laboratory, RAB = resistivity at the bit, 2-D = two dimensional, 3-D = three dimensional, IESX = Schlumberger's GeoQuest seismic software.

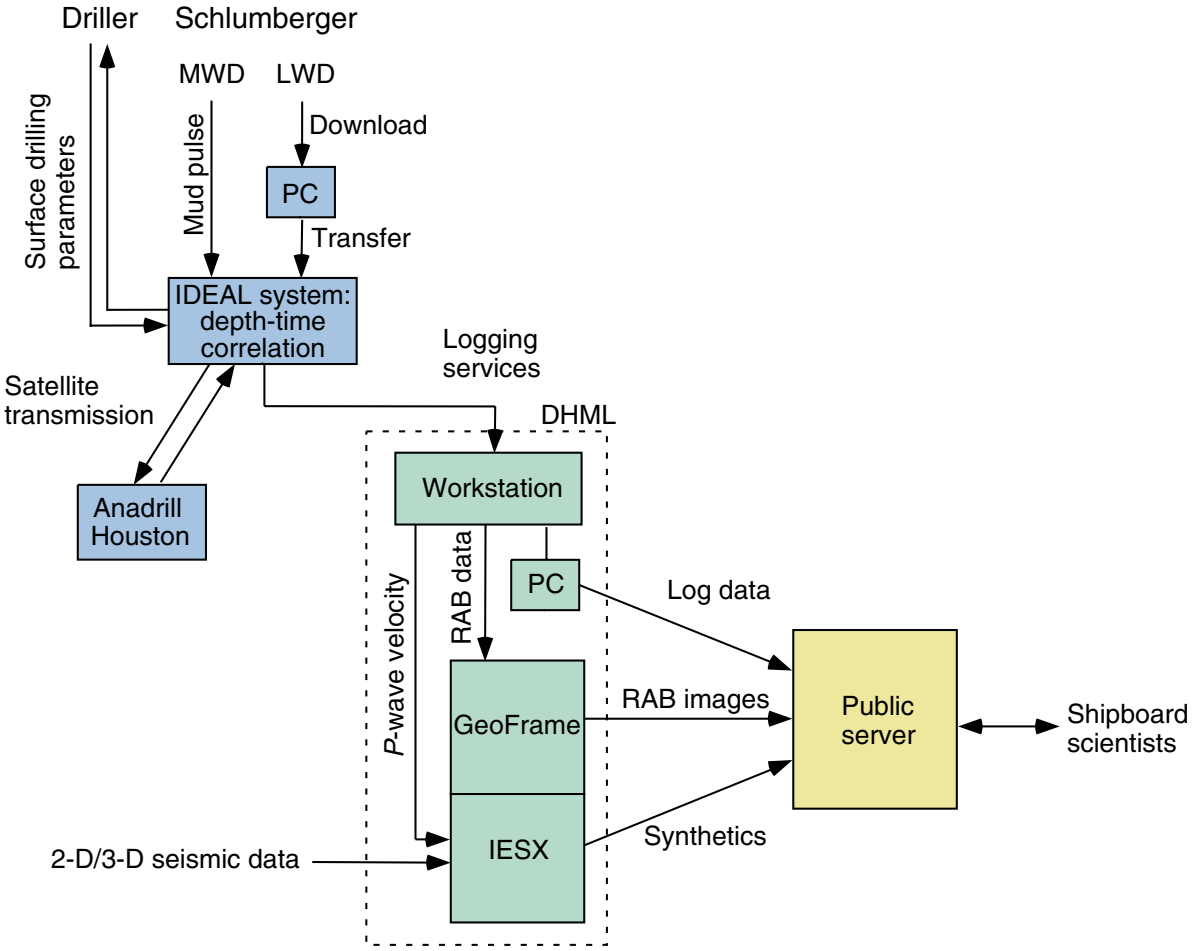

Figure F25. Schematic illustration of the Drill String Acceleration (DSA) tool. NaCl solutions of known concentration. The data were collected automatically by placing the short sections in series on the MST.

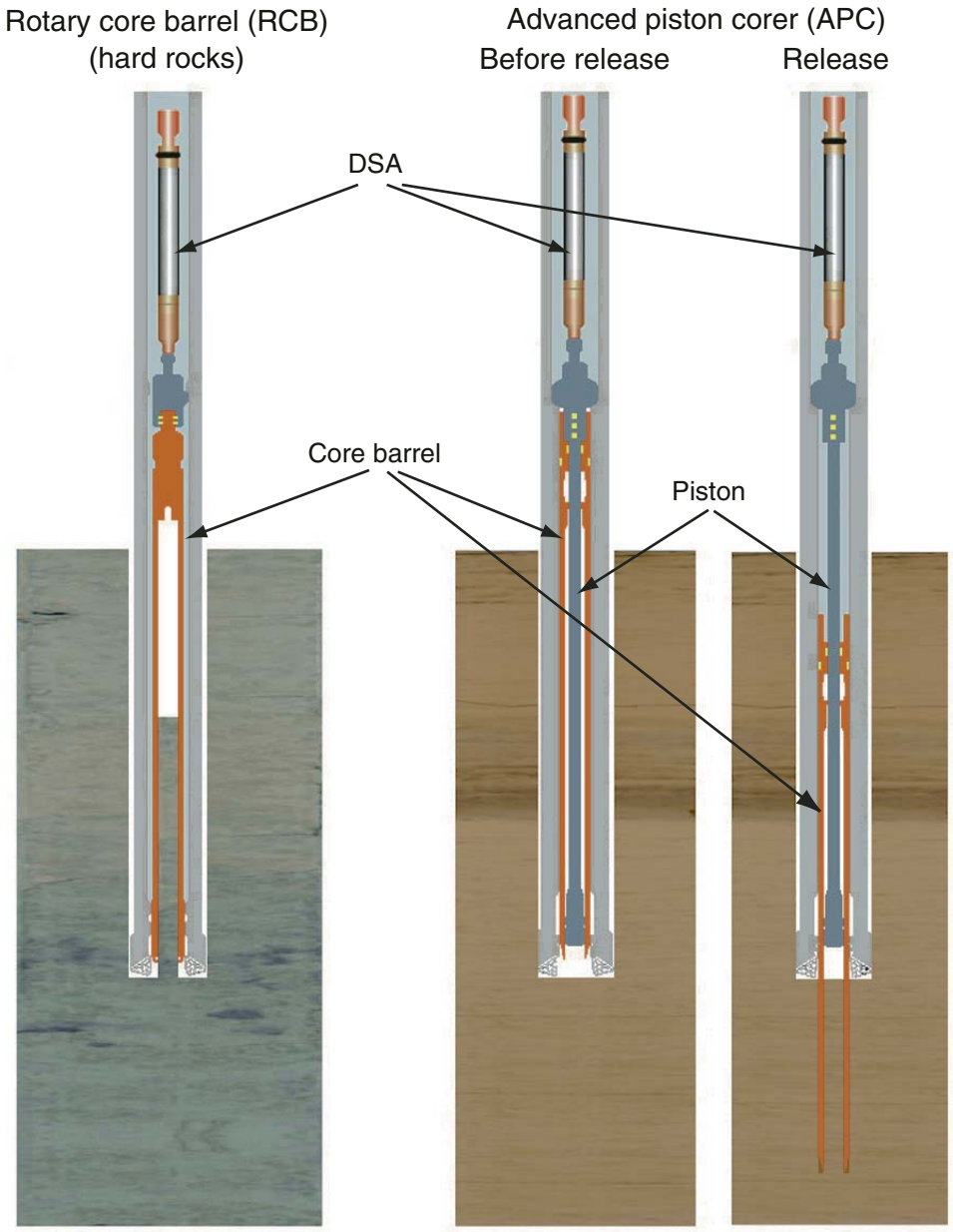

Figure F26. Configuration of the tool strings used for wireline logging operations. For names of tool strings see Tables T7, p. 101, and T8, p. 102.

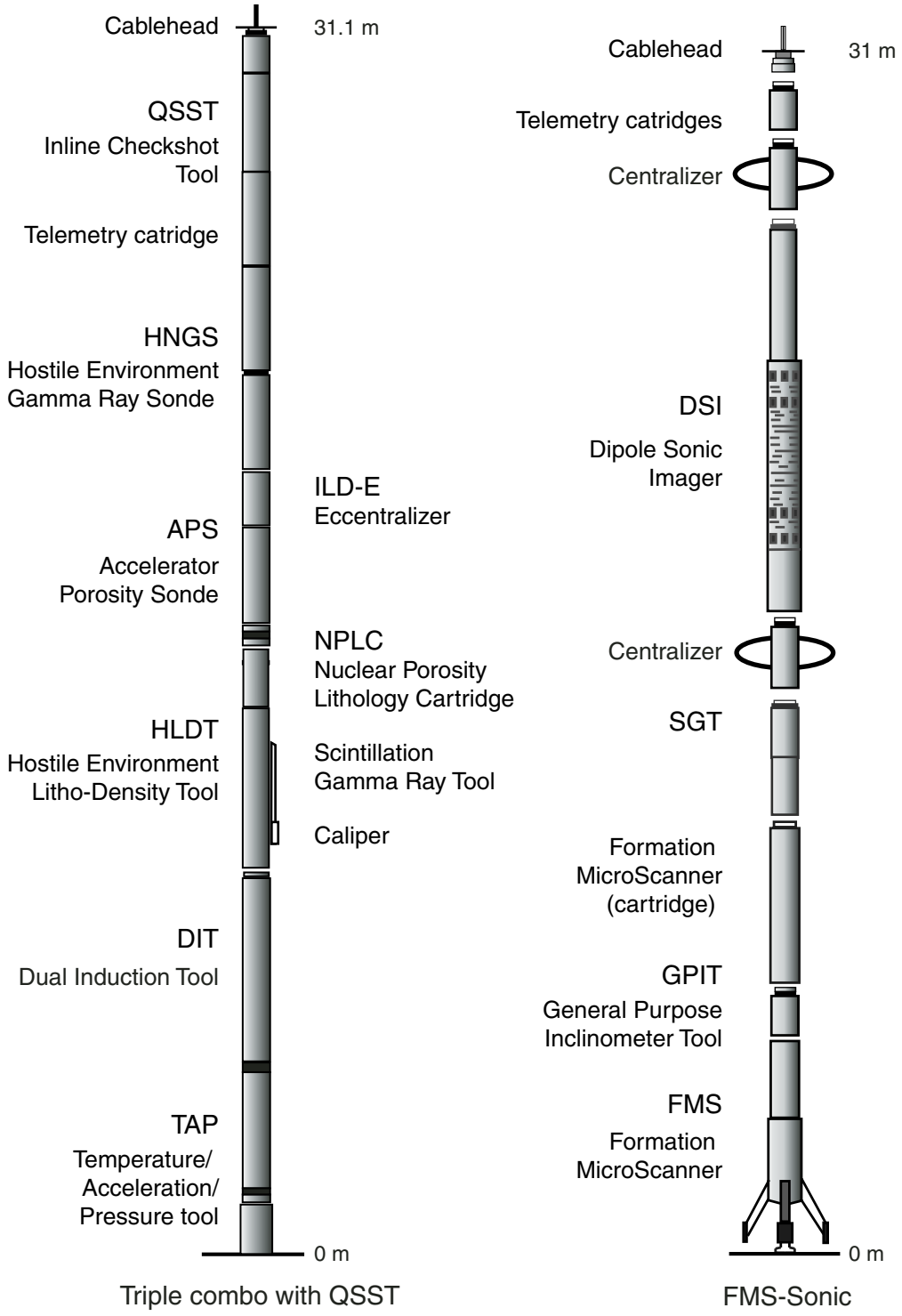

Figure F27. Schematic illustration of the Vertical Seismic Imager (VSI). SGT = Scintillation Gamma Ray Tool.

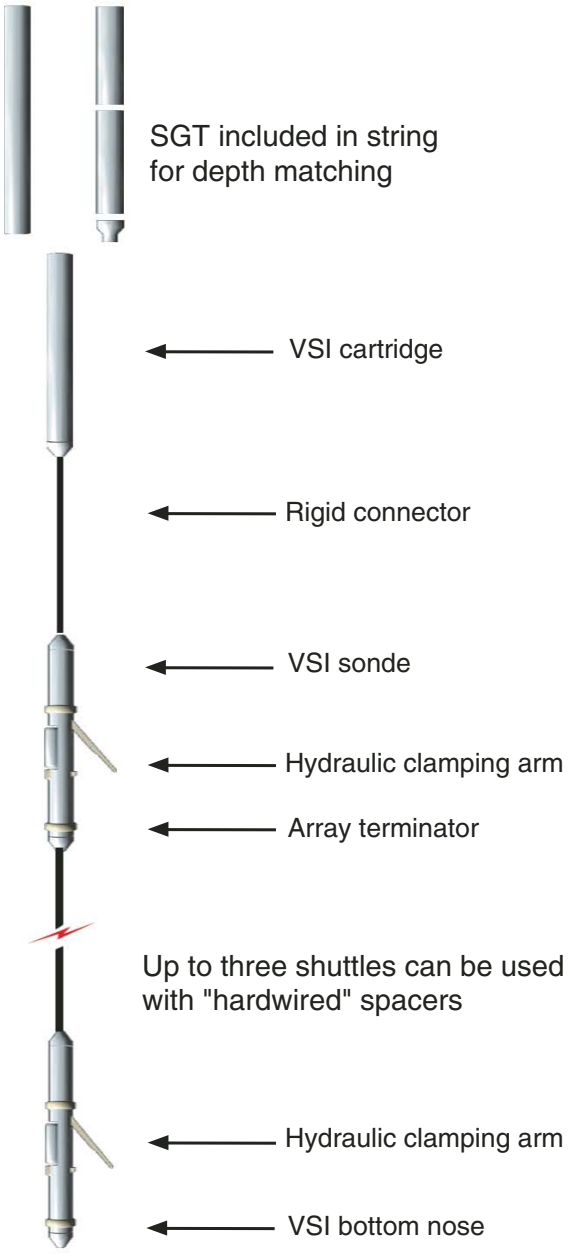

Table T1. Sample spread sheet from SLIDERS used for smear slide and thin section analyses.

		Texture				Mineral										Biogenic						
Sample	Depth (unit)	Lithology	Sand	Silt	Clay	Biotite (22)	Calcite (30)	Carbonate (35)	Feldspar (71)	Glauconite (82)	Muscovite (131)	Opaques (140)	Pyrite (169)	Quartz (172)	Volcanic glass (81)	Carbonaceous shell fragments (267)	Diatoms (58)	Foraminifers (78)	Foraminifers & nannofossils (263)	Nannofossils (132)	Siliceous fossils & spicules (264)	Comments
204-1245B-																						
1H-1, 7	0.07	M	20	60	20			5	10	10		10		15								
1H-3, 60	3.60	M	25	60	15	3		10	5	4	1	3		10			5	40	10			
1H-5, 58	6.58	M	0	10	90			80				5		2								Carbonate nodule?
1H-7, 60	9.10	D	0	25	75	1		5	5			3		10							1	
2H-1, 31	9.81	D	0	20	80			2	5					20								
2H-4, 94	14.94	D	0	20	80					1				20			4					
2H-5, 19	15.69	M	2	8	90			70	1					1			2					Carbonate-rich clay (micritic authigenic)
3H-2, 80	21.30	D	0	15	85			2	2			8		7			3	3			1	
3H-4, 122	24.72	D	0	25	75				5			15		10	1		3				3	
3H-6, 45	26.95	D	0	20	80			5	5			2		5			5	3		3	7	
4H-1, 60	29.10	D	0	15	85							10		30			3					
4H-2, 119	31.19	M	80	20	0			5	5			3		10								Carbonate-bearing sand
4H-4, 50	33.50	D	0	5	95							3		20			1	1				
4H-7, 26	37.76	D		2	98							2		1			2					
5H-1, 65	38.65	D		20	80	2		2				2		5			3					
5H-3, 54	41.54	M	10	70	20	3		4	1	2	1	3		8					7			
5H-4, 120	43.70	M	0	35	65	3		10	2			4		10			2	4	2			Carbonate-rich silty clay
5H-6, 17	45.67	D	0	20	80	2				2		5		8			3		4			
6H-1, 50	48.00	D	0	10	90							5		3			5					
6H-3, 71	51.21	M	90	10	0				1			3		1	30		1				3	Volcanic glass-rich sand
6H-3, 84	51.34	M	95	5	0	1			10					5	15							Volcanic glass-rich sand
6H-5, 47	53.97	M	35	65	0					1		3		5			3	1			1	
6H-6, 36	54.89	D	0	15	85				3			3		10			6				1	
6H-CC, 37	55.50	M	0	10	90							10		2			5				1	
7H-2, 53	58.08	D	8	25	67	3			12		3	2		8			5	1		1	1	
7H-4, 50	60.94	D	0	25	75				12			2		2			8	1		1		
7H-5, 40	61.98	D	8	30	62	6			15		5	4		4			4			1		
7H-6, 6	63.14	D	12	25	63	8			10	1	5	2		10			5					
7H-7, 105	65.63	M	70	20	10	10			25	8		10		40								
8H-1, 30	66.80	D	3	27	70	5			10		5			5			5					
8H-1, 112	67.62	M	70	20	10	12			30	15	5	5		25								
8H-2, 67	68.67	D	3	27	70	3			12					4			8			2	3	
8H-3, 135	70.77	M	60	25	15	5			30	10				25			4	3			2	
8H-6, 67	74.53	D	1	19	80	1			15		1	1		3			3			2		
8H-7, 26	75.62	M	20	20	60	8			20	5		3		15						2		

Note: M = Minor lithology, D = Dominant lithology.

Table T2. Techniques, standards, typical accuracy, and reproducibility for interstitial water analyses.

Analysis	Technique	Standard	Reproducibility (% rsd-1 σ)
Alkalinity	AT	Sodium carbonate solutions	2.1
Cl^-	T	IAPSO	0.3
SO_4^{2-}	IC	IAPSO	1.2
HPO_4^{2-}	S	Solution, weighed	1.0
NH_4^+	S	Solution, weighed	5.9
Na^+	ICP	IAPSO	1.8
K^+	ICP	IAPSO	1.2
Mg^{2+}	ICP-AES	IAPSO	0.9
Ca^{2+}	ICP-AES	IAPSO	0.7
Mn^{2+}	ICP-AES	Dilutions of reference solutions in acidified NaCl matrix	2.1
Fe^{2+}	ICP-AES	Dilutions of reference solutions in acidified NaCl matrix	2.9
B	ICP-AES	Dilutions of reference solutions in acidified NaCl matrix	3.1
Sr^{2+}	ICP-AES	Dilutions of reference solutions in acidified NaCl matrix	2.3
Ba^{2+}	ICP-AES	Dilutions of reference solutions in acidified NaCl matrix	2.0
Li^+	ICP-AES	Dilutions of reference solutions in acidified NaCl matrix	2.2
DOC	TOC	Potassium phthalate standard	1.9

Notes: AT = autotitration, T = titration, IC = ion chromatography, S = spectrophotometry, ICP-AES = inductively coupled plasma–atomic emission spectrophotometry, TOC = total carbon analyzer. rsd-1 σ = one sigma relative standard deviation. IAPSO = International Association for the Physical Sciences of the Ocean.

Table T3. Position of MST sensors.

	MS (cm)	GRA density (cm)	V_P (cm)
Actual	198.5	248.5	267.5
Hole 1251B and before	197.2	247.2	267.2
After Hole 1251B	198	248	268

Notes: MS = magnetic susceptibility, GRA = gamma ray attenuation, V_P = *P*-wave velocity. Hole 1251B was completed at 2235 hr on 29 July 2002.

Table T4. Measurements made by logging-while-drilling and measurement-while-drilling tools.

Tool	Measurement	Approximate vertical resolution (cm)
ADN	Bulk density	15
	Porosity	30
RAB	Resistivity-at-the-bit	5–8
	Gamma ray	46
MWD	Drilling parameters-at-the-bit	NA

Notes: All tool names are trademarks of Schlumberger. See Table **T6,** p. 100, for explanations of acronyms used to describe the tools. For additional information about tool physics and use consult ODP Logging Services at **www.ldeo.columbia.edu/BRG/ODP.** NA = not applicable.

Table T5. Estimated GeoVision Resistivity measurement correction factors.

Measurement	Correction factor (%)
Resistivity-at-the-bit	3
Ring resistivity	1
Deep resistivity	2
Medium resistivity	4
Shallow resistivity	NA

Note: NA = not applicable.

Table T6. Acronyms and units used for logging-while-drilling and measurement-while-drilling tools.

Tool	Output	Tool name/Explanation of output	Unit
ADN		Azimuthal Density Neutron tool	
	TNPH	Thermal neutron porosity	%
	RHOB	Bulk density	g/cm^3
	ROMT	Maximum density total from rotational processing	g/cm^3
	DROR	Correction for rotational density	g/cm^3
	DCAL	Differential caliper	in
NMR		Nuclear Magnetic Resonance	
	MRP	Magnetic resonance porosity	%
RAB		Resistivity-at-the-Bit tool	
	BDAV	Deep resistivity average	Ωm
	BMAV	Medium resistivity average	Ωm
	BSAV	Shallow resistivity average	Ωm
	RING	Ring resistivity	Ωm
	RBIT	Bit resistivity	Ωm
		Spatially oriented resistivity images of borehole wall	Ωm
MWD		Measurement-While-Drilling tool	
	DWOB	Downhole weight on bit	klbf
	DTOR	Downhole torque at bit	kft·lbf
	*	Bit bounce	klbf
	*	Tool stick slip	

Note: * = no acronym.

Table T7. Measurements made by wireline tool strings.

Tool string	Tool	Measurement	Sampling interval (cm)	Approximate vertical resolution (cm)
Triple combination	HNGS	Spectral gamma ray	15	51
	APS	Porosity	5 and 15	43
	HLDS/HLDT	Bulk density	2.5 and 15	38/46
	DIT	Resistivity	15	61
	TAP*	Temperature	1 per s	NA
		Tool acceleration	4 per s	NA
		Pressure	1 per s	NA
	QSST	Inline checkshot		
Formation MicroScanner	SGT	Total gamma ray	15	46
(FMS)-sonic combination	GPIT	Tool orientation	0.25 and 15	NA
	FMS	Microresistivity	0.25	0.5
	DSI/SDT/LSS/BHC	Acoustic velocity	15	107/120/61/61
VSI (stationary measurement)	VSI	Sonic traveltime	Variable	NA
WST (stationary measurement)	WST	Sonic traveltime	Variable	NA

Notes: All tool and tool string names (except the TAP) are trademarks of Schlumberger. For the complete list of acronyms used in the ODP and for additional information about tool physics and use consult ODP Logging Services at **www.ldeo.columbia.edu/BRG/ODP.** See Table **T8,** p. 102, for explanations for acronyms used to describe tool strings and tools. * = not included on every run. NA = not applicable.

Table T8. Acronyms and units used for wireline logging tools.

Tool	Output	Tool name/Explanation of output	Unit
APS		Accelerator Porosity Sonde	
	APLC	Near array porosity (limestone calibrated)	%
	SIGF	Formation capture cross section (Σf)	Capture units
	STOF	Tool standoff (computed distance from borehole wall)	in
DIT		Dual Induction Tool	
	IDPH	Deep induction resistivity	Ωm
	IMPH	Medium induction resistivity	Ωm
	SFLU	Spherically focused resistivity	Ωm
DSI		Dipole Sonic Imager	
	DTCO	Compressional wave delay time (Δ*T*)	ms/ft
	DTSM	Shear wave delay time (Δ*T*)	ms/ft
	DTST	Stoneley wave delay time (Δ*T*)	ms/ft
FMS		Formation MicroScanner	
	C1, C2	Orthogonal hole diameters	in
	P1AZ	Pad 1 azimuth	Degrees
		Spatially oriented resistivity images of borehole wall	
GPIT		General Purpose Inclinometer Tool	
	DEVI	Hole deviation	Degrees
	HAZI	Hole azimuth	Degrees
	F_x, F_y, F_z	Earth's magnetic field (three orthogonal components)	Degrees
	A_x, A_y, A_z	Acceleration (three orthogonal components)	m/s^2
HLDT		Hostile Environment Litho-Density Tool	
	RHOB	Bulk density (corrected)	g/cm^3
	PEF	Photoelectric effect	b/e^-
	CALI	Caliper (measure of borehole diameter)	in
	DRHO	Bulk density correction	g/cm^3
HNGS		Hostile Environment Gamma Ray Sonde	
	HSGR	Standard (total) gamma ray	gAPI
	HCGR	Computed gamma ray (HSGR minus uranium contribution)	gAPI
	HFK	Potassium	wt%
	HTHO	Thorium	ppm
	HURA	Uranium	ppm
QSST		Inline Checkshot Tool	
SGT		Scintillation Gamma Ray Tool	
	ECGR	Environmentally corrected gamma ray	gAPI
TAP		Temperature/Acceleration/Pressure	°C, m/s^2, psi
VSI		Vertical Seismic Imager	
		Acoustic arrival times	ms
WST		Well Seismic Tool	
		Acoustic arrival times	ms